UNIVERSIDAD Ð LA LAGUNA
Departamento de Astrofísica

Universidad de La Laguna

Exploring the UV spectral range to constrain the evolution of massive galaxies in varying environments and varying redshift

Memoria que presenta
Núria Salvador Rusiñol
para optar al grado de
Doctora en Ciencias Físicas.

INSTITUTO Ð ASTROFISICA Ð CANARIAS
San Cristóbal de la Laguna
abril de 2021

Examination date: June, 2021
Thesis supervisor: Alexandre Vazdekis & Michael A. Beasley

ISBN: xx-xxx-xxxx-x
Depósito legal: TF-xxxx/2021
Some of the material included in this document has been already published in *Nature Astronomy* and *The Monthly Notices of the Royal Astronomical Society*.

to my parents

It was the first time that any human had moved away far enough from the Earth to see the whole planet, and this is what they saw, what we all saw: our planet, vulnerable and isolated.
And I remembered very well that first shot. You saw a blue marble, a blue sphere in the blackness and you realized that that was the Earth.
In that one shot, there was the whole of humanity with nothing else, except the person that was in the spacecraft taking that picture, and that completely changed the mindset of the human population of the world.
Our home was not limitless, there was an edge to our existence.
It was a rediscovery of a fundamental truth:
We are ultimately bound by and reliant upon the finite natural world about us.

David Attenborough in *A life on our planet* (2020)

Agradecimientos

This thesis is the result of a thousands of small decisions and events that started many years ago when, by looking at the Orion constellation in the winter nights, I finally decided to study Astrophysics. I understand that it could be seen as a crazy idea, since my previous academic background was not related to science at all. But my family supported me from day one. So I came to Tenerife 10 years ago with only two big luggages to study Physics at the University of La Laguna. I didn't know at that time that I would finally do a PhD. I would repeat it blindly if I could go back in time.

I would like to start with my most sincere gratitude to my supervisors, Alejandro y Mike. No he podido tener más suerte con vosotros. Solo con mirarme ya sabéis lo que pienso. Porque nuestra relación no solamente se ha basado en lo profesional, sino también en lo personal. Horas y horas en la cafetería, hablando de todo lo que se puede hablar con ellos: todo. Ganas de hablar no nos faltan. Gracias por confiar en mi más que yo misma hasta el último segundo y por haber estado cuando lo he necesitado. Alejandro, gracias por transmitirme tu pasión por la ciencia, por hasta hacerme llegar a creer que el paper se escribe en una semana (medido en tiempos de Vazdekis, claro), por compartir nuestra pasión por los dulces (ai, qué ricos son!). Mike, gracias por mostrarme tu apoyo en todo momento y por escucharme siempre en nuestras charlas sobre la vida. Te deseo lo mejor en esta nueva etapa que te espera. Estoy muy agradecida y os voy a echar mucho de menos.

I would like to express my thanks to all the collaborators that have made this thesis possible. A special thank to Francesco La Barbera, for your natural hospitality and for always being so helpful. A l'Anna Ferré Mateu, recordaré sempre la nostra estrella saltimbanqui de Xile. Me gustaría agradecer a Claudio Dalla Vecchia, me ha encantado conocerte a través de Bloko, me dio luz. A big thank to Ignacio Ferreras y Andrea Negri for supporting me during my first long-discussed paper. También a Jesús Falcón que, a pesar de no haber colaborado durante la tesis, gracias a ti me inicié en el fascinante mundo de las galaxias durante el proyecto de máster y pude conocer el grupo TRACES del IAC, al cual también agradezco todas las interesantes reuniones de los viernes.

Esta tesis no sería posible sin el apoyo constante y el amor de mi familia. Primer de tot tu, mama, gràcies per haver estat acompanyant-me diàriament a través del telèfon, on has trobat les paraules adequades per treure'm els somriures quan més ho he necessitat. Gràcies per estimar-me com ho fas. Infinites gràcies al meu pare, al que li dec gran part de qui sóc avui dia, i que m'ha posat els peus a terra quan jo estava més aviat pels aires. Gràcies a la meva germana Marta, que ens estimem passi el que passi i que estic molt contenta que, junt amb el Pedro, m'hagin escollit per ser la madrina del Pau. Pau, moltes gràcies a tu també. Segurament llegiràs això d'aquí molts anys per poder entendre-ho, però no et pots arribar a imaginar la força i la vida que m'has donat en aquest últim any. Ets l'amor més honest que conec. També m'agradaria expressar amb molta emoció la gratitut inmensa que sento cap als meus avis Mercè i Pere, perquè vaig aprendre molt al seu costat i, tot i que no entenien per què havia de marxar a Tenerife (no pots fer aquí a Barcelona això que fas, Núria?), sempre em van motivar a fer-ho tot amb il·lusió. Això va per vosaltres també, avis Joan i Encarna. Al avi Joan, a qui li vaig treure un somriure quan li vaig dir que volia fer Astrofísica i em va donar dues carpetes de retalls de diaris amb notícies de l'espai dels anys 70 i 80. Són un tresor. Sé que hauríem tingut converses molt interessants sobre l'Univers, perquè tu sabies de tot. A la resta de familia, que sempre us extranyeu de perquè coi no estic més morena si visc a Tenerife, gràcies per confiar en mi.

En mi día a día aquí en Tenerife, han estado ellas dos, la Núria y la Paula. Ya os estoy echando de menos. Sí, sé que soy un poquito dramas, ya me conocéis. Habéis sido mi principal soporte aquí cuando he pasado por momentos difíciles y estoy muy agradecida de haber compartido esta estapa con vosotras dos. I would like to thank Elham, she is my little sister in science, from who I learned a lot. She inspired me to find motivation in the last few months. I wish this friendship never ends wherever we go. Al Jaume, Federica y Virginia por todas las cenas, comidas y juegos divertidos. A Lucía que, como dice, me presta mucho estar con ella. Aun no nos hemos hecho la foto a estas alturas, así que espero que cuando defienda la tesis ya hayamos cumplido el objetivo. Y como no gracias a Juancar, con el que he compartido 10 años de espacio-tiempo. A Mónica, compañera de mesa, por nuestras charlas y los tés que han hecho más ameno el trabajo. Thanks to Valeriia, Rafa, James, Laura, Javier de Miguel and the rest of the officemates.

No pueden faltar mis amigas y amigos de siempre. A Nacho, mi amigo incondicional, de aquellos que están ahí siempre. No olvidaré aquellos momentos en nuestra cabaña del árbol durante la carrera, o lo bien que nos lo montamos siempre allá donde vayamos. A la meva Olga, no podem estar més conectades. Ja hem comprovat que no hi ha res que ens separi, per molt grans que siguin els oceans. Tu ets la meva meitat. A la Sílvia, l'Adriana i l'Èlia, que m'han acompanyat amb ganes des del primer dia i m'han enviat forces durant 10 anys. I a totes les nenes de Granollers i rodalies, gràcies per compartir tants anys de vida.

Estoy muy agradecida a la vida por haberme cruzado a Sergi, que ha hecho renacer en mi la pasión por la vida. Gracias por escucharme y querer entenderme, fluir conmigo. Gracias a Jonay, por tu apoyo honesto y desinteresado durante años.

Agradecer el apoyo financiero de la beca de doctorado FPI-SO del Ministerio de Ciencia e Innovación (SEV-2015-0548-16-4). Los costes de los viajes han sido también financiados por el proyecto RAVET (AYA2016-77237-C3-1-P y PID2019-107427GB-C32) y por el IAC, en el que me siento como en casa.

Finalment, m'agraeixo a mi, a la Núria que ha pres decisions importants, que s'ha equivocat i ha après, que ha somiat i ha lluitat. Tot el que he viscut fins a dia d'avui em fa ser qui sóc, ni millor ni pitjor, però cada dia més propera al que vull ser i al que em fa feliç.

Núria

x

Resumen

Las galaxias más masivas del Universo local son las galaxias de tipo temprano (del inglés, ETGs) que comprenden las galaxias elípticas y lenticulares. El grueso de sus poblaciones de estrellas son viejas y prácticamente no están formando nuevas estrellas, sino que han seguido una evolución pasiva desde un alto desplazamiento al rojo ($z > 2$) hasta el presente. Su actividad de formación estelar no es lo que llegó a ser en las etapas tempranas del Universo, donde grandes cantidades de gas se transformaron en estrellas. La formación de estrellas se detuvo rápidamente y las ETGs evolucionaron como sistemas rojos y viejos. Cuáles fueron los mecanismos físicos resposables de detener la creación de nuevas estrellas sigue siendo un misterio, aunque se cree que las contribuciones de los núcleos activos de galaxias (del inglés, AGNs) puediron transformar estos sistemas estelares en objetos evolucionando pasivamente con escasa formación estelar.

Tanto las evidencias teóricas como las observacionales apuntan hacia un escenario de dos fases de formación de las ETGs. Durante la primera fase se forman los núcleos a un alto desplazamiento al rojo ($z > 2$), mientras que las regiones externas son el resultado de la acreción de galaxias más pequeñas. Este modelo es respaldado por un gran número de estudios que muestran que las galaxias masivas a $z > 2$ son más compactas que sus equivalentes en el Universo local y que han experimentado un crecimiento tanto en tamaño como, en menor grado, en masa. Esto implica que estas galaxias compactas masivas de alto desplazamiento al rojo son los núcleos de las ETGs locales, mientras que en las regiones externas se deposita el material debido a las fusiones con otras galaxias sin disipación, es decir, pobres en gas. Ésto significa que estas fusiones no desencadenan la formación de nuevas estrellas, o por lo menos de una manera eficiente.

Las estrellas viejas de las ETGs emiten la mayor parte de su luz en el rango espectral óptico. El óptico, sin embargo, es relativamente insensible a pequeñas

fracciones de poblaciones estelares jóvenes, cuya luz domina en el rango ultravioleta (UV). Por lo tanto, los estudios en el óptico están sesgados principalmente por las poblaciones viejas. Afortunadamente, el UV es un trazador óptimo de las poblaciones estelares más calientes como las estrellas jóvenes. Estudios fotométricos en el UV han puesto de manifiesto que las ETGs pueden tener formación de estrellas a un ritmo muy bajo. Sin embargo, el rango UV en los espectros de las ETGs no ha sido explorado para determinar sus poblaciones jóvenes.

El objetivo de esta tesis es cuantificar estas poblaciones estelares jóvenes de las ETGs masivas usando las líneas de absorción de sus espectros. Hemos usado nuevos modelos de poblaciones estelares basados en librerías estelares empíricas para analizar, por primera vez, índices espectrales ópticos y del UV cercano simultáneamente. Comparamos las observaciones con las predicciones de los modelos de dos parametrizaciones de las historias de formación estelar (del inglés, SFH) de las galaxias masivas. Primero hemos investigado si la formación de estrellas residual es una característica común entre la población de ETGs, mediante la suma de miles de espectros de galaxias masivas a un desplazamiento al rojo medio de $z \sim 0.4$. De estos espectros sumados hemos podido obtener las fracciones de población jóven en función de la masa de la galaxia. Hemos encontrado que las ETGs masivas tienen en promedio una fracción de estrellas jóvenes formadas en los últimos 2 mil millones de años por debajo del 1%, y que ésta fracción es mayor para las galaxias menos masivas. Esta tendencia con la masa es consistente con el hecho que las galaxias menos masivas tienen SFH más extendidas en el tiempo que las más masivas. Además, puede estar relacionado con la eficiencia de los efectos de los AGNs para frenar la formación de estrellas, que es mayor para galaxias más masivas. También hemos visto que las galaxias masivas sintéticas de las simulaciones cosmológicas producen demasiadas estrellas de edades intermedias. Ésto implica que los procesos para suprimir la formación de estrellas en galaxias masivas y mantenerla suprimida en el tiempo, aun necesitan ser comprendidos. Nuestros resultados ponen rigurosos límites que necesitan ser satisfechos por las simulaciones.

Para intentar entender el origen de estas poblaciones jóvenes, hemos analizado espectros resueltos espacialmente para obtener información de dónde están situadas en las galaxias. Para ello, hemos analizado un tipo especial de ETGs: las galaxias más brillantes de los cúmulos de galaxias (del inglés, BCGs). Estas galaxias se encuentran en el centro de los potenciales gravitatorios de los cúmulos de galaxias. Nuestro estudio de 6 BCGs cercanas ha demostrado que sus estrellas jóvenes están en el interior de < 2 kpc del centro de las galaxias, es decir, en los núcleos. Las pequeñas fracciones de estrellas jóvenes que encontramos son consistentes con un origen *in-situ*, es decir, la formación de estrellas residual puede producirse gracias al material reciclado de la muerte de estrellas de generaciones anteriores o del gas inicial residual. Sin embargo, debido a la ubicación de estos objetos, un origen *ex-situ* a través los efectos y procesos del entorno del no puede ser descartado.

Estudiar las componentes estelares jóvenes en galaxias reliquias nos ayuda a entender los orígenes de la formación estelar reciente que detectamos en las galaxias ETGs normales. Estas galaxias reliquias, masivas y compactas, han sobrevivido intactas desde su formación a alto desplazamiento al rojo hasta el Universo local, es decir, sin haber experimentado la segunda fase en la que crecen tanto en tamaño como en masa a traves de fusiones e interacciones con otras galaxias. Por ello, hemos estudiado la contribución de las poblaciones jóvenes en la región central de 1 kpc de la galaxia NGC 1277, la galaxia reliquia por excelencia del Universo cercano. Encontramos una población joven que contribuye menos del 1%, similar a los resultados previos, lo que apunta a que la formación estelar reciente encontrada en galaxias masivas ETGs puede estar relacionada con los procesos intrínsecos de las galaxias.

Abstract

Early-type galaxies (ETGs), consisting of ellipticals and lenticulars, are the most massive galaxies in the local Universe. The bulk of their stellar populations are characterised as being old with negligible recent star formation activity, having followed a passive evolution from the high-redshift Universe to the present day. Their star formation activity is not what used to be at the early Universe ($z > 2$), where large amounts of gas were transformed into stars. Star formation was virtually extinguished in rather short time and ETGs evolved as red and dead objects. The exact physical mechanisms responsible for quenching the star formation in these massive systems at high-redshift is not completely resolved. Although, it is widely considered that AGN feedback could turn these stellar systems into passively evolving objects without significant formation of new stars.

There is growing observational and theoretical evidences for a two-phase formation scenario for ETGs. According to this picture, during the first phase the cores of present-day ETGs are formed at $z > 2$ dissipatively, while in the second phase the outer regions are a result of mergers and accretion. This is supported by a large number of studies that have shown that massive galaxies at $z > 2$ are more compact than their local counterparts, and have experienced significant growth both in size and, to a lesser degree, in mass. This suggests that these high-z massive compacts are the cores of local ETGs formed at high redshift, while the outer regions are where the accreted material due to dissipationless mergers (i.e. gas-poor) is deposited. This second phase is mostly "dry", i.e. does not trigger star formation, at least not in any efficient way.

The bulk of the stars in ETGs are ancient and emit much of their light in the optical spectral range. However, the optical is relatively insensitive to small fractions of young stellar populations, whose light dominate the ultraviolet (UV). Studies of the optical range are therefore, biased to the old stellar populations. Fortunately, the UV is an optimal tracer of the hottest stellar pop-

ulations such as young stars. Photometric studies in the UV have previously suggested that ETGs might have recent low-level star formation. However, the UV window of ETG's spectra has not been explored for determining the youngest stellar populations.

This thesis aims to quantify these young stellar populations by using spectral absorption features of massive ETGs. We exploit state-of-the-art stellar population models based on empirical stellar libraries to analyse, for the first time, observed optical and near-UV line-strength indices simultaneously. We compare observations with model predictions from two assumed simple parameterisations of the star formation history (SFH) of massive galaxies. We first explore if the residual star formation is ubiquitous among the massive ETG population by stacking thousands of galaxy spectra at redshift of $z \sim 0.4$. We derive mass fractions of the young stellar component as a function of mass. We find that massive galaxies show, on average, a sub-one percent fraction of young stars formed within the last 2 Gyr, and that this fraction is larger for less massive galaxies. This trend with mass is consistent with the fact that less massive galaxies have more extended SFHs than their more massive counterparts and also may be related to the fact that AGN feedback stops the formation of new stars more efficiently for more massive galaxies. We also find that synthetic massive galaxies from cosmological numerical simulations significantly overproduce both intermediate and young stellar populations. This means that the recipe to quench the star formation in these galaxies, and perhaps to maintain them quenched, still needs to be fully understood. However, the results obtained here put stringent constrains that must be satisfied by these simulations.

In order to understand the origin of these young stars, we turned to spatially resolved spectroscopy to tell us precisely where they are located. For this purpose, we analyse a special type of ETGs: the brightest cluster galaxies (BCGs). These galaxies are located in the centres of the gravitational potential wells of galaxy clusters. Our study of 6 nearby BCGs indicate that their young stars are located within < 2 kpc of the galaxy centres, i.e. in their cores. Our findings of small young mass fractions are consistent with being formed *in-situ*, likely residual star formation from recycled material of dying stars from previous generations. However, due to the particular location of these massive systems, an *ex-situ* origin through environmental processes can not be ruled out.

The study of young stellar components in so-called "relic galaxies" offers us unique clues to understand the possible origins of the recent star formation that we detect in normal ETGs. These massive compact relic galaxies are thought to have survived untouched since their formation at high-z until the present-day, i.e. without having gone through a second phase that is characterised by a growth in size and mass by accretion. For this purpose, we studied the young stellar contribution in the 1 kpc central region of NGC 1277, a well studied galaxy that is regarded as the prototypical relic galaxy in the nearby Universe. We find a sub-one percent level of young mass fractions, similar to our samples of massive ETGs, which points to intrinsic, in-situ, processes that trigger the formation of these young stars.

Contents

1

Introduction

I am following nature without being able to grasp her,
I perhaps owe having become a painter to flowers.

Claude Monet

1.1 General overview

Galaxies are major stellar systems in the Universe in which stars are born, evolve and die. Modern observations through large telescopes have shown that galaxies have a wide range of physical features, shapes and stellar population properties. The epoch of formation of the first galaxies took place at high redshift ($z \sim 10$), when the first stars started to consume their fuel. Galaxies at high redshift looked significantly different from those in the present-day Universe, as a result of their evolution through cosmic time. When we look at the properties of nearby galaxies, we see that their colours and sizes are different from those at higher redshift. It is still a strong challenge finding correlations between properties of galaxies at different epochs to trace how they formed and evolved to become the galaxies we observe today. The commonly assumed Λ-cold dark matter understanding of the Universe (Geller & Huchra 1989, Hernquist et al. 1996, Dave et al. 1999, Colless et al. 2001, Cole et al. 2005, Springel et al. 2005) postulates that large structures grow via gravitational interactions and evolve within dark matter gravitational potential wells. This model assumes that the Universe contains dark energy, dark matter and baryonic matter. Under this paradigm, bigger baryonic structures such as galaxies form through successive mergers of pre-existing smaller structures.

The classification of galaxies started when Edwin Hubble (1929) divided the galaxies he observed in the local Universe in terms of their visual appearence into two broad main classes: early-type galaxies (ETGs) and late-type galaxies (LTGs). ETGs have an spheroidal shape with no clear features and red colours that indicate the dominance of old stars and small amounts of gas. ETGs are arranged in subclasses from completely spheroidal (E0) to extremely elliptical (E7), followed by the more disky-shape lenticular class (S0). LTGs are typically blue and have a spiral structure with a disk and spiral arms and large amount of gas that is constantly contributing to the formation of new stars. Hubble thought that this scheme was an evolutionary sequence. The terms "early" and "late" were initially used to indicate that ETGs were the first galaxies formed in the Universe and they evolve to have a late-type morphology. However, galaxy formation and evolution are much more complex processes than Hubble's picture, involving interactions and mergers with other galaxies, initial formation conditions and the internal stellar feedback due to the star formation. Despite all these complexities, nowadays we still use this nomenclature for referring to galaxies with an "early" or "late"-type morphology. Galaxies with a dominant spheroidal component with red colours are referred to ETGs and spiral and irregular galaxies as LTGs.

Historically, nearby galaxies have been classified in terms of their morphology. However, over the last two decades we have been able to observe high redshift galaxies and have found that this morphological classification of low-redshift galaxies has no direct correspondence. The visual appearence of galaxies evolve from early epochs to the present-day Universe. By $z \sim 2$, the number density of passively-evolving galaxies is 1/6 of the value we observe today according to Kriek et al. (2008). At that redshift, these galaxies look smaller and denser than local galaxies with the same mass (Trujillo et al., 2006). How high-redshift galaxies evolve to the present-day systems remains as one of the major challenges in modern astronomy.

In addition to classifying galaxies according to their morphologies, they are often separated in terms of their star formation activity. Star-forming galaxies such as LTGs are actively forming new stars whereas quiescent galaxies such as ETGs appear as dead stellar systems lacking obvious star formation. Star formation rates (SFRs) have been studied according to the morphological types and across cosmic time. More massive galaxies look redder with lower SFRs than their less massive counterparts (Kauffmann et al. 2004; Baldry et al. 2006; Twite et al. 2012). Local ETGs are quiescent stellar systems compared to LTGs. However, at earlier epochs ($z > 2$), massive galaxies had much higher SFRs (Cowie et al., 1996), when the amount of cold gas available was significant. At some point their SFRs needed to be suppressed as currently no new stars are formed in large amounts in massive ETGs at $z < 2$ when compared to higher redshifts, where highly efficient SFRs lead to a rapid stellar build up in these galaxies. The physical mechanisms for suppressing the star formation activity in massive ETGs at high-redshift still needs to be properly constrained although feedback from their central massive black holes is one of the main candidates.

Optical studies of stellar populations in ETGs supported evidence for being predominantly populated by old stars (Renzini, 2006). However, optical bands relative to bluer wavelengths are less sensitive to small fractions of recent star formation. Fortunately, the ultraviolet (UV) range can be exploited to detect these very small star formation fractions in predominantly old stellar systems (Yi et al. 2005; Vazdekis et al. 2016). Without the UV perspective, one might assume that low-redshift ETGs are purely formed by old stars and have not actively formed new stars since earlier epochs. It is therefore crucial for characterising the young stellar populations in these galaxies to analyse their UV light.

1.2 The early-type galaxy population

1.2.1 General properties of ETGs

The ETG population comprises galaxies with an elliptical and lenticular morphology. These galaxies contain most of the total stellar mass ($\sim$70%) in the Universe, although they constitute only a small fraction of the total galaxy population ($\sim$20%) in the local Universe (Fukugita et al., 1998). The ETG population includes the most massive galaxies in the Universe, so they constitute fundamental pieces to trace the stellar mass assembly and galaxy formation and evolution over cosmic time. They are thought to be end-products of the galaxy assembly process (Ferreras & Silk, 2000). Figure 1.1 shows an optical image of the massive elliptical galaxy M87 obtained with HST, characterised by a smooth and homogeneous distribution of red stars that are more numerous towards the galaxy centre.

The early-type population of galaxies is commonly identified by a large number of uniform properties. Our understanding of the formation and evolution of the ETGs needs to be able to reproduce their main characteristics, which are summarised here:

- **Stellar masses.** Although some dwarfs ellipticals have low stellar masses, the most massive stellar systems in the Universe are ETGs. Throughout this thesis we refer to massive ETGs at those with stellar masses $> 10^{11}\ M_{\odot}$. The assembly of their mass content across cosmic time is still

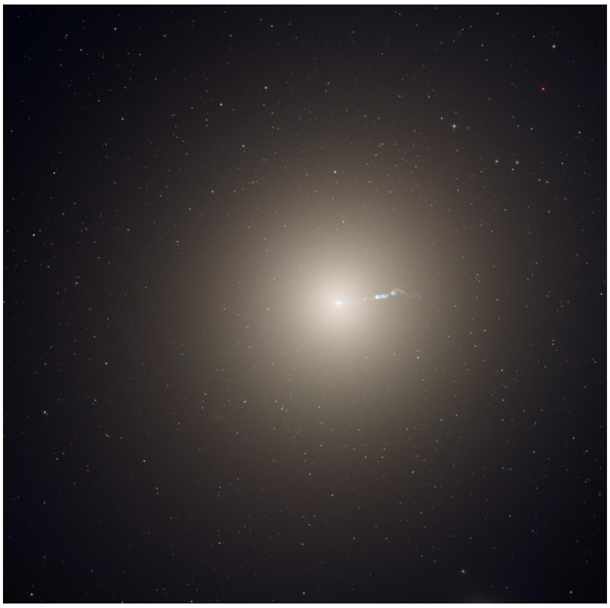

FIGURE 1.1— **Elliptical galaxy image.** Optical image of the giant elliptical galaxy M87 observed with the HST telescope. The galaxy is located at the centre of the Virgo cluster of galaxies. Credit: NASA, ESA, and the Hubble Heritage Team (STScI/AURA).

not completely resolved. Due their old stellar populations, most of their stars and therefore, their stellar masses, were already in place at redshift $z \sim 1-2$. However, whether these first stars were formed in smaller galaxies and then merged (i.e. the hierarchical picture) or if they were formed in very short time *in-situ* (monolithic-like scenario) still remains an open question.

- **Stellar populations.** Extensive observational evidences indicate that massive ETGs formed the bulk of their stars over short time-scales at early epochs of the Universe (redshift $z > 2$). ETGs host predominately old stars distributed homogeneously out to their external regions and contain negligible amounts of gas and no significant star formation activity. ETGs also harbour metal-rich stellar populations. Their colours and integrated spectra are dominated by old, red stars, which mainly contribute to the optical and infrared rather than to the UV spectral window. As it can be seen in the galaxy of Figure 1.1, its yellow-red colours indicate an overwhelming presence of old stars. Interestingly, more massive galaxies tend to be older and more metal-rich (Citro et al. 2016; Jackson et al. 2020).

- **Stellar velocity dispersion.** ETGs are the galaxies with the highest stellar velocity dispersion (σ), which essentially measures the statistical deviation of the motion of the stars with respect to the mean value. This indicates that, unlike spirals, they are dominated by pressure support rather than by rotation, i.e. supported by random motions of their stars. The stellar velocity dispersion correlates strongly with many population properties of ETGs (Bernardi et al. 2005; La Barbera et al. 2013) and relates directly to their dynamical stellar masses (Faber & Jackson 1976; Zahid et al. 2016). Thus, more massive galaxies have higher stellar velocity dispersions and we expect that galaxies with $\sigma > 200\,\mathrm{km\,s^{-1}}$ have predominantely an early-type morphology.

- **Fundamental Plane.** The homogeneity in their properties includes a strong connection between elemental galaxy properties, the so-called Fundamental Plane (FP). ETGs follow a remarkably tight correlation between these three global parameters: central velocity dispersion (i.e. mass), effective radius (i.e. size) and mean effective surface brightness (i.e. luminosity or mass surface density) (Dressler et al. 1987; Djorgovski & Davis 1987). This strong correlation luminosity-size/mass-size has been studied deeply in local Universe ETGs (Cappellari et al. 2006; La Barbera et al. 2010b) and in higher redshifts (van de Sande et al., 2014). The FP is used to estimate important galaxy parameters of their dynamical and structural properties (van der Wel et al., 2005).

- **Environment.** ETGs can be found both isolated in the field, i.e. in low-density environments, or in denser and richer environments such as galaxy groups or large and massive galaxy clusters. A larger fraction of ETGs are found in high-density environments rather than in low-density environments, suggesting that environment plays a role in the morphological evolution (Dressler, 1980). At a given luminosity, ETGs are found to be younger and more metal-rich in lower-density regions (Kuntschner et al., 2002). Galaxy clusters are ensembles of a large number of galaxies bound by gravity that favour the galaxy – galaxy encounters, especially in the cluster centre. Figure 1.2 is an HST image of the galaxy cluster Abell

1689 located at z ∼ 0.184, in which hundreds of galaxies of various morphological types, as their colours and shapes suggest, are gravitationally connected. In the centre of the gravitational potential well of galaxy clusters are located the largest and most massive ETGs found in the Universe, the so-called brightest cluster galaxies (BCGs), which will be explained in detail in Section 1.5. They are usually surrounded by satellite galaxies, with those satellites at the smallest galactocentric distance from the BCG mostly likely having an early-type morphology.

FIGURE 1.2— **Image of a galaxy cluster.** The image shows the galaxy cluster Abell 1689 at z ∼ 0.184. The image combines visible and infrared HST data. Credit: NASA, ESA, the Hubble Heritage Team (STScI/AURA), J. Blakeslee (NRC Herzberg, DAO) and H. Ford (JHU).

- **Alpha-element abundances.** It has been widely shown that massive ETGs are enhanced in some elements (Thomas et al., 1999), and particularly in magnesium (Mg). Mg is an α-element, as are O, Mg, Ca, Ne, S, Si and Ti. They are mainly created by the supernovae Type II, which occurs when the core of massive stars ($M_\star > 8\,M_\odot$) collapses and explodes delivering such chemical elements. The lifetime of these massive stars is relatively short (time-scales of ~ 10 Myr) compared to low-mass stars. Therefore, α-elements are delivered during the first stages of a star formation burst. The non α-element Fe, on the other hand, is ejected on time-scales of ~ 1 Gyr mostly in supernovae Type I. A greater amount of Fe is produced in a longer star formation burst. Thus, the study of the abundance of an α-element relative to Fe abundance [α/Fe] is related to the time-scale of the star formation period in galaxies. One of the most commonly used abundance ratios to study the chemical abundances in ETGs is [Mg/Fe]. ETGs are known for being overabundant in [Mg/Fe] (Vazdekis et al. 2004; Martín-Navarro et al. 2018b), suggesting that these galaxies were formed in a rapid and intense star formation episode. Interestingly, alpha-element abundances appear to be similar whether they are located in clusters or in low-density regions (Kuntschner et al. 2002; Thomas et al. 2005), suggesting that the star formation time-scales in ETGs are independent of the environment.

- **Initial mass function (IMF).** The IMF is the distribution of stellar masses at birth. Traditionally, the IMF has been considered as universal across galaxy morphologies and cosmic time (Salpeter 1955; Miller & Scalo 1979; Kroupa 2001) with its value derived from resolved stellar populations in the Milky Way. In recent years, the use of spectral features that are sensitive to the IMF slope (representative of the ratio between dwarf and giant stars) revealed an excess of low-mass stars in high-mass quiescent systems with respect to the expectations from a standard (Milky Way-like) IMF. There is a growing consensus that the IMF varies systematically with velocity dispersion or stellar mass of galaxies, with more massive galaxies having bottom-heavier IMFs (Cenarro et al. 2003; van Dokkum & Conroy 2010; Cappellari et al. 2012; La Barbera et al. 2013; Ferreras et al. 2013; Spiniello et al. 2014). A bottom-heavy IMF means a higher ratio of low-mass stars to high-mass stars than the Milky Way IMF. Low-mass stars in galaxies with a bottom-heavy IMF have a relevant contribution to the total stellar mass of the galaxy but not substantially to its luminosity. Moreover, the IMF also varies radially within massive galaxies, becoming progressively bottom-heavier toward the centre (Martín-Navarro et al. 2015a; La Barbera et al. 2016, 2017, 2019; van Dokkum et al. 2017; Sarzi et al. 2018; Domínguez Sánchez et al. 2019).

Interestingly, the majority of the general properties of the early-type galaxy population are well correlated with galaxy mass. In general, more massive

ETGs tend to be older, more metal-rich, with larger stellar velocity dispersion, more enhanced in alpha-elements and have a bottom-heavier IMF. This clearly indicates that the galaxy mass plays an important role in driving the evolution of these massive galaxies. However, although the simplicity of their visual appearence, the physical processes involved to their stellar mass buildup remains unknown.

1.2.2 Galaxy formation and evolution scenarios

To explain what causes the different morphologies we see on present-day galaxies, we also need to investigate higher redshift systems in order to find connections between properties of galaxies at different epochs. As we started to study galaxies in more detail, several galaxy formation and evolution scenarios have been suggested and developed to reproduce the observed properties of galaxies at all epochs.

How ETGs have formed and evolved is still a subject of an intense debate, which was led mainly by two models. Historically, ETGs were typically believed to be formed through a "monolithic collapse" (Eggen et al. 1962; Larson 1974, 1975), in which an initial collapse of intergalactic material produced a rapid and highly efficient star formation burst at high redshift. This model predicts that massive ETGs should have formed all their stars already at $z \sim 2-3$, evolving since then purely passively to the present. The optical stellar population properties and the simple scaling relations are compatible with this simple galaxy formation scenario. An alternative model within a cosmological context is the hierarchical scenario in which massive ETGs are assembled through successive mergers (Toomre & Toomre 1972; Toomre 1977; White & Frenk 1991; Barnes 1992; Somerville & Primack 1999; Cole et al. 2000; De Lucia & Blaizot 2007), whereas spirals form first from the collapse of gas clouds. In this model, ETGs buildup is through mergers and interactions of galaxies already existing and, as a consequence, their star formation histories are much more complex than in the monolithic galaxy formation model. The hierarchical galaxy formation model is consistent with the generally assumed Λ-cold dark matter framework. These models postulate that ETGs form through the mergers of lower mass galaxies, which may include equal-mass mergers of LTGs.

Important constraints come from investigations of the size evolution of ETGs. The evolution of the FP of ETGs observed at $z > 1$ (Blakeslee et al., 2003) is found to be consistent with the monolithic scenario, so that the stellar populations of high-redshift massive galaxies are old, supporting a passive evolution (Trujillo & Aguerri 2004; McIntosh et al. 2005; Choi et al. 2014). However, observations have shown that elliptical galaxies at $z \sim 2$ look smaller in size and, to a less extent, in mass than their local descendants (Trujillo et al. 2004, 2006; Papovich et al. 2005; van der Wel et al. 2008; Saracco et al. 2009; Fan et al. 2010; Stockmann et al. 2020). Massive ellipticals have increased by a factor of 4 their sizes and a factor of 2 their masses since $z \sim 2$ to the present (Trujillo et al. 2007; Fan et al. 2013). These massive galaxies are already old at those redshifts, suggesting that they have grown through dry mergers in the last Gyr and not by a significant formation of new stars, where the latter would result in dramatically different stellar population properties than we see in nearby massive galaxies.

Numerical simulations of Hilz et al. (2013) show that equal-mass mergers are not able to reproduce the observed properties of present-day massive galaxies. The remnant galaxy that results from a minor merger of mass ratio 1:5 assembles the accreted mass in the outskirts of the host galaxy. If this is the case, this suggests that stellar population properties in the cores of present-day massive galaxies should be the same of those of compact high-z galaxies, as the accreted material is placed in the outskirts.

To explain these observables, the emerging picture of the formation and evolution of ETGs is a two-phase scenario. In this model, massive galaxies first form stars *in-situ* in a very intense and short star formation burst at $z > 2$ (monolithic-like phase), creating the core of local massive galaxies and the observed red nuggets at $z \sim 2$. This is followed by a inside-out growth both in size and mass through mergers with smaller galaxies (Bezanson et al. 2009; Naab et al. 2009; Hopkins et al. 2009; van Dokkum & Conroy 2010; Oser et al. 2010, 2012; Hilz et al. 2012; Pérez et al. 2013; Hilz et al. 2013; Bédorf & Portegies Zwart 2013; Fan et al. 2013; Dubois et al. 2013; Patel et al. 2013; Wellons et al. 2016; Zibetti et al. 2020; Gao & Fan 2020). During this phase, the accreted stars are deposited gradually in the outskirts via minor mergers, growing in size and mass in the outer regions and leaving the core unaltered out to the present. Thus, compact high-redshift galaxies become the cores of nearby ETGs.

Compact massive galaxies are more numerous at high redshifts. Due to their significant size evolution, the local ETG population is dominated by large ellipticals, so that compacts galaxies may be extremely rare in the nearby Universe. However, some of these high-redshift compacts may not have experienced the second stage in the two-phase model, so they grow neither in mass nor size. These rare untouched galaxies have been observed in the local Universe and are called "relic" galaxies. They are massive and compact nearby galaxies with very old stellar populations, bottom heavy IMFs, fast rotators and high surface mass density.

1.3 Star formation histories of ETGs

Based on the old ages and high [Mg/Fe] abundances observed, massive ETGs formed the majority their stars in the early Universe in a very fast and intense star-forming episode, which would be consistent with the monolithic scenario if evolving completely passively until present. These galaxies transformed large amounts of gas in stars very efficiently at $z > 2$ so that they are overwhelmingly dominated by old stars. The star formation activity that took place in these galaxies is much stronger at earlier epochs than is found in present-day ETGs (Cowie et al. 1996; McDermid et al. 2015). Their star formation needs to be rapidly suppressed (quenched) at high redshift ($z > 2$). It used to be thought that ETGS are no longer forming new stars.

The primary ingredient for the formation of new stars is a gas reservoir, which is required to be sufficiently cold and in high density regions. The removal of these gas reservoirs in ETGs could be due to different processes: ram pressure stripping by the intracluster medium, tidal disruption with the intra-cluster light, mergers and interactions with other galaxies, type Ia supernovae heating and feedback from active galactic nucleus (AGN) from supermassive black holes (Binney & Tabor 1995; Springel et al. 2005). Even though all these mechanisms might contribute to some extent to physically remove the gas reservoirs, there is a general agreement for AGN feedback to be a key agent for suppressing the star formation in massive galaxies (Schawinski et al. 2007; Weinberger et al. 2017; Scholtz et al. 2018). The efficiency of AGN feedback peaks at high-redshift when the stars in massive galaxies were formed with high SFRs. Feedback from the galaxy central supermassive black hole may supress the star formation by preventing gas cooling. This feedback is known to have a more important role for higher black-hole mass galaxies (Martín-Navarro et al., 2018a). Since this parameter is directly correlated to the stellar mass of a galaxy, the star formation needs to be quenched more efficiently for more massive galaxies.

The dependence of star formation history (SFH) on galaxy dynamical mass has been investigated empirically (de La Rosa et al. 2011; McDermid et al. 2015) but also from numerical simulations (Thomas et al., 2005). Figure 1.3 shows the well-known downsizing scenario (Cimatti et al. 2006; Thomas et al. 2019), in which more massive galaxies are estimated to show narrower SFHs than their less massive counterparts. In addition, the peak of the star formation activity, i.e. the highest star formation rate, is placed at higher redshifts for more massive galaxies, producing, on average, older and more metal-rich stellar populations than for lower-mass galaxies (Gallazzi et al. 2006; Jackson et al. 2020). Therefore, the star formation in less massive galaxies extends over longer time-scales, so that, on average, younger stars are expected to be found than in the high-mass end population. The metal-rich stellar populations in massive ETGs are associated with a rapid chemical enrichment at the initial epochs of the SFH (Vazdekis et al. 1996, 1997) due to the intense star formation burst at high-redshift revealed by their enhancement in alpha-elements. As a consequence, the short lifetime of massive stars ($\sim 10\,$Myr), which are the first stars to die, deliver chemical elements that will feed the next generations of stars.

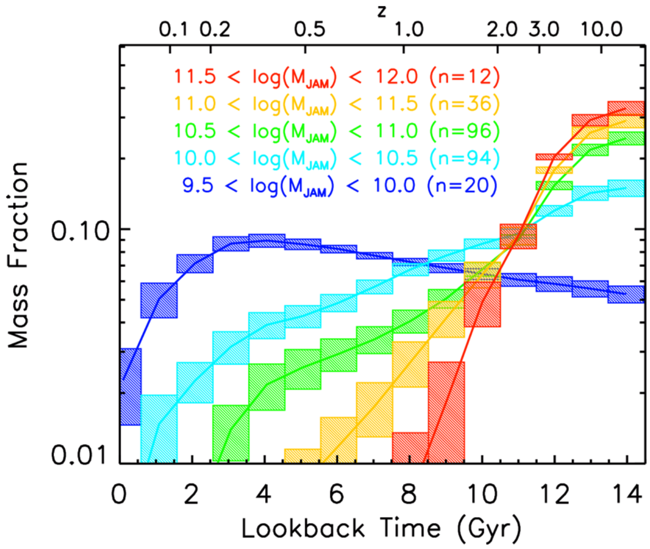

FIGURE 1.3— **Star formation histories as a function of galaxy mass.** The plot shows the relative fraction of stellar mass formed at each epoch in logarithmic scale according to the dynamical mass of galaxies. More massive galaxies peak their star formation at earlier epochs with also narrower star formation bursts than less massive systems. Figure from McDermid et al. (2015).

1.4 Constraints to the SFH from the UV

A galaxy spectrum is the result of the integrated light emitted by all the stars that populate a galaxy and each type of star emits distinctly in each spectral range. The observed flux depends on the stellar components and is strictly correlated with the morphological type of galaxies. The overwhelming bulk of old stellar populations in ETGs contribute mainly to the optical spectral range (> 4000 Å). In addition, due to a relative lack of blue-sensitive instruments the majority of the spectroscopic studies of ETGs have focused on the optical spectral window. Less dominant components in ETGs can be better characterised in other parts of the spectrum, where the bulk of the stars decreases its contribution and permits to the light of minor stellar components be relatively more noticeable. This is the case of young stars in the UV spectral range. Massive young stars classified as O-type and B-type, are hot enough to emit intense light in the UV so that even a very small fraction of them can easily be detected in this wavelength range. Therefore, the UV light from galaxies might be intimately associated with the presence of young stars and is an effective tracer for the youngest stellar populations in old galaxies such as ETGs. However, UV is a good tracer for the hottest stars of a stellar population and these hot stars may also be evolved stars.

The impact of small fractions of young stellar populations in ETGs is relatively low in optical photometric bands since their relative contributions are negligible compared to that from the bulk of old stars. Although U-band photometry comprises bluer wavelengths ($3000-4000$ Å) than the optical, it is less sensitive to young stars relatively to bluer ranges. Bower et al. (1992) associated the small scatter in the U-band light to the absence of recently formed stars in ETGs. Constraining the most recent tail of the SFH of massive galaxies from photometry is required to be done at even bluer (than U) wavelengths.

Before the Galaxy Evolution NASA Explorer (GALEX) started to release its first images in 2003 (Martin et al., 2005), it was often assumed that ETGs were formed exclusively by old stars and that they are completely quiescent stellar systems, i.e. without any star formation activity. GALEX observed the Universe through near-UV (NUV) and far-UV (FUV) photometry, looking for star-forming regions in galaxies. As a result, our knowledge of the star formation histories of massive ETGs has changed. A large number of studies found evidence of recent star formation in ETGs with UV observations from broad-band photometry (Yi et al. 2005; Donas et al. 2007; Jeong et al. 2007; Kaviraj et al. 2007; Jeong et al. 2009; Kaviraj et al. 2009; Salim & Rich 2010; Sheen et al. 2016; George 2017; Werle et al. 2020).

From studies based on photometric colours, 30% of massive ETGs show hints of recent star formation (Kaviraj et al., 2007). Their UV colours and fluxes are compatible with residual star formation in the local Universe (Kaviraj et al. 2006b) and high redshift galaxies ($0.5 < z < 1$) (Kaviraj et al., 2007), but at a reduced star formation rate, contributing a few percent of the stellar mass. These results imply that a low-level of star formation was a common signature in ETGs during the last Gyr. The detected NUV-fluxes are too strong from that expected from old, passively-evolving UV-bright stars such as the Post-Asymptotic Giant Branch (PAGB) evolutionary stage. In this phase, the hot cores of stars are exposed and shine bright in the UV. In addition, the NUV light, relative to the FUV, is less affected by these evolved UV-bright stars, making it a better tracer for recent star formation.

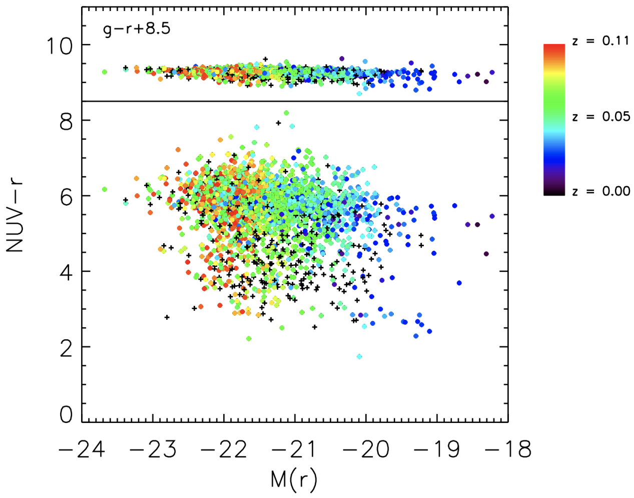

FIGURE 1.4— **Optical and NUV colour-magnitude relations of ETGs.** The upper panel shows an optical CMR whereases the lower panel shows the NUV-optical CMR of ∼ 1000 ETGs. Unlike the optical, the NUV-r colour shows a wide spread in the blue bands, indicative of differences in their SFHs regarding their recent star formation. Data is coloured according to the galaxy redshift. Figure adapted from Yi et al. (2007).

Whereas optical colour-magnitude relations (CMRs) show a tight relation that is compatible with a single star formation burst at high-redshift with a small scatter of 0.05 mag (Bernardi et al. 2003b), supporting the commonly assumed scenario, a wide spread in the UV-optical CMRs have been found, not only for ETGs at low redshifts (Yi et al. 2005; Kaviraj et al. 2007) but also for the ETGs in a cluster at z ∼ 0.41 (Ferreras & Silk, 2000). The NUV-optical CMRs show a spread with a larger scatter of 1 mag in their NUV colours, which are consistent with a more recent star formation burst. Yi et al. (2005) found that 15% of their sample of optically old ETGs show very strong UV fluxes that are better fitted with a recent burst of 200 Myr that require, on average, 1.2% of the total mass. Such small star formation fractions do not affect optical colours.

Some ETGs (∼10% of nearby ETGs) show a flux rise at wavelengths bluer than ∼ 2000 Å. This phenomenon is commonly known as the UV-upturn. Different stellar candidates have been proposed as being responsible for this increase in flux, such as extreme Horizontal-Branch stars, PAGB stars or binary systems (Dorman et al. 1995; Yi et al. 1997; Buzzoni et al. 2012; Hernández-Pérez & Bruzual 2014; Le Cras et al. 2016). However, for the purposes of this thesis, the impact of the UV upturn is not an important concern since our analysis is restricted to wavelengths ≥ 2500, redder than the regime where this phenomenon becomes significant.

1.5 The brightest cluster galaxies

Most galaxy clusters are dominated by a remarkable class of elliptical galaxies commonly located at the cluster core (Ostriker & Tremaine 1975; Hausman & Ostriker 1978; Postman & Lauer 1995). They are usually the brightest and the largest galaxy in a cluster and are commonly referred as brightest cluster galaxies (BCGs). BCGs are the most massive and luminous galaxies in the present-day Universe, differing from normal ellipticals for their extended brightness distributions. The BCG in Figure 1.2 is the largest elliptical located at the centre of the image and surrounded by hundreds of smaller galaxies.

Like normal elliptical galaxies, the analysis of the stellar populations in the inner regions of BCGs indicates that the bulk of their stars was formed rapidly in a very intense star burst at redshift $z > 2$ (Renzini, 2006). However, despite sharing similar morphologies with normal massive ellipticals, in addition to red colours, old and metal-rich stellar populations and alpha-enhancements (Brough et al. 2008; Loubser et al. 2009; Donahue et al. 2010; Loubser & Sánchez-Blázquez 2012; Barbosa et al. 2016; Edwards et al. 2020), BCGs constitute a special category of objects with peculiar SFHs seen from both observations (Tran et al. 2008; Barbosa et al. 2016) and models (Dubinski 1998; De Lucia & Blaizot 2007). The evolution of BCGs is significantly affected by their surrounding environments. Due to their central positions in the gravitational potential well of their host clusters, central cluster galaxies accrete stars and gas from satellite galaxies that orbit around them and fall in, developing extended light profiles. The more representative SFHs of their dominant stellar population include components from *in-situ* star formation, and from the interaction with other galaxies and with the intracluster medium, where the outer regions in BCGs are continually assembling mass (Cooke et al., 2019).

The stellar populations of a large sample of observed BCGs have been recently studied in Edwards et al. (2020), from the galaxy core into the intracluster light (ICL) out to 4 effective radii. They found old stellar populations of $\sim$ 13 Gyr and high metallicities [Fe/H] $\sim$ 0.3 in the galaxy cores, whereas the average age in the ICL (at 40 kpc) is estimated to be slightly younger, $\sim$ 9.2 Gyr with lower metallicities -0.4 < [Fe/H] < 0.2. This broadly supports the idea of two-phase galaxy formation, with the BCG cores and inner regions formed faster and earlier than the outer regions that have formed more recently or have accreted mass afterwards through galaxy mergers and thereby, also increasing in size (Oser et al. 2010; Kubo et al. 2017; Cooke et al. 2019).

The star formation rate in BCGs in the local Universe is much lower than what it used to be at higher redshifts ($z > 2$) where the bulk of the stars was formed. Several studies provide important insights of recent star formation in some low redshift BCGs (Crawford & Fabian 1993; Cardiel et al. 1998; Crawford et al. 1999; Edge 2001; O'Dea et al. 2008; Bildfell et al. 2008; Pipino et al. 2009; O'Dea et al. 2010; Hicks et al. 2010; Hoffer et al. 2012; Liu et al. 2012; Fraser-McKelvie et al. 2014; Cooke et al. 2016; Loubser et al. 2016; Runge & Yan 2018; Cerulo et al. 2019). In particular, using GALEX UV data, Pipino et al. (2009) found the existence of blue cores in a sample of 7 BCGs as evidence of recent star formation. Specifically, their young component is younger than 200 Myr and contribute less than one percent to the total stellar mass. Liu et al. (2012) also find similar ongoing star formation in BCGs, whose level of star formation is higher for more massive BCGs located in richer galaxy clusters.

The mechanisms that trigger star formation in BCGs have been a matter of study in the last two decades. In central cluster galaxies with high velocity dispersions, the origin of the cold gas necessary to form new stars is unlikely to originate from wet mergers (i.e. gas-rich) in the present Universe. Such mergers are rare between galaxies with high relative velocity dispersion, such as BCGs and their surrounding galaxies, and both observations and semi-analytical approaches seem to indicate that they were common at high redshift, whereas at low redshift dry mergers (i.e. gas-poor) dominate (Lidman et al. 2012; Edwards & Patton 2012; Hilz et al. 2013; Lavoie et al. 2016; Stockmann et al. 2020). Several studies have shown that BCGs that experience recent star formation are commonly located in clusters with the presence of cooling flows from the intracluster medium (ICM) (Bildfell et al. 2008; Rafferty et al. 2008; Donahue et al. 2010; Liu et al. 2012; Loubser et al. 2016; Cerulo et al. 2019). Bildfell et al. (2008) investigated BCG colours in a wide variety of clusters X-ray morphologies, including cool-core and non-cool core clusters. They show that 25% of their BCG sample exhibit colour profiles that become bluer towards the galaxy core and they associate this with ongoing star formation. They suggest that this recent star formation is linked to environmental processes within the cluster, as they find that these blue-core BCGs are all located within ∼ 10 kpc distance to the cluster X-ray peak, where the cooling flow is preferentially going to and the cold gas of the ICM is preferentially deposited. More recently, in agreement with Bildfell et al. (2008), Cerulo et al. (2019) show that this cool-core process that fuel the star formation in BCGs is not related to the halo mass of the clusters.

Intimately connected to their environment, BCGs are very special objects to study how their young stars are spatially distributed. Due to their deep gravitational potential wells, they are expected to have a larger concentration of gas towards the galaxy central regions that can trigger the formation of new stars. Thus, their cores are expected to have greater star formation activity than in their outer regions.

1.6 Relic galaxies

The population of massive compact galaxies was more numerous 10 Gyr ago, i.e. at $z \sim 2$. Massive quiescent galaxies at high redshift are tipically smaller than present-day galaxies of similar stellar mass, i.e. have higher stellar mass densities (Daddi et al. 2005; Longhetti et al. 2007; Toft et al. 2007; Trujillo et al. 2007; Cimatti et al. 2008; van Dokkum et al. 2008; Buitrago et al. 2008; Damjanov et al. 2009, 2011; van de Sande et al. 2013; Belli et al. 2014). Although most of those galaxies became more extended resulting in larger effective radii due mainly to accreted material, in a few cases they have evolved until present-day Universe preserving their structural properties and remained untouched as compacts since their initial formation. This means that these galaxies evolved without significant merging events until the present. These extremely rare and unique nearby objects are known as ”relic” galaxies. Properties of relic galaxies at $z \sim 0$ are similar to those of massive galaxies at $z \sim 2$, which make them an important tool for studying properties of high-redshift massive compact galaxies in a more accessible way. Massive compact galaxies are more common at higher redshifts, clearly indicating that massive galaxies have become less dense with cosmic time.

Numerical simulations of Stringer et al. (2015) show that massive compact galaxies are preferentially found in denser regions, suggesting that the environment plays a significant role in galaxy mass assembly for high-z massive compact quiescent galaxies. The recent observational work of Baldry et al. (2021) confirms these predictons by studying the compactness and the environment of SDSS massive galaxies suggesting that these compact nearby galaxies are more likely to be located in high-density environments.

Relic galaxies can be very massive, with typical stellar masses of 10^{11-12} $M_{\odot}$, but really small compared to large ellipticals, with an effective radii $R_e < 4$ kpc (Yıldırım et al., 2017). There is one particular relic galaxy NGC 1277 that has been studied in extensive detail. It is a very massive galaxy located in the Perseus cluster with a stellar mass of 1.2×10^{11} $M_\odot$ and extremely compact, with an effective radius of $R_e = 1.2$ kpc (Trujillo et al., 2014). The bulk of its stellar populations is old and significantly enhanced in Mg (Trujillo et al. 2014; Martín-Navarro et al. 2015b; Yıldırım et al. 2017), indicating that most of its stars were formed in a extremely short and intense star formation burst at $z > 2$, followed by passive evolution. Beasley et al. (2018) showed that it has had an unusually uneventful merger history, with at most 10% of its mass coming from in situ accretion. By comparison, normal ETGs of the same stellar mass typically comprise $50 - 90\%$ accreted material.

The exploration of the young stellar components in relic galaxies would provide important clues of the possible origins for the formation of new stars in massive galaxies. If nearby massive ETGs are still forming new stars, whether these new stars have an *in-situ* or *ex-situ* origin will be difficult to constrain. However, if relic galaxies have recently formed stars, it would suggest that the main source of gas for the formation of these new stars is mainly associated with intrinsic galaxy processes, since these galaxies have not experienced important mergers with other galaxies. In such a case, the sources that may fuel the star formation activity in relic galaxies would be not only the gas ejected from stars due to stellar evolution but also some pristine gas that has survived since the galaxy was formed at earlier epochs. If, on the contrary, relics do not host any star formation activity, it would directly indicate that any finding of young stars in massive ETGs would be mostly related to external processes, since local ETGs are expected to be the surviving population of massive compact high-z galaxies that have grown in size through mergers and not surviving as "relics" to the present.

1.7 Outline of this thesis

In this thesis, we attempt to constrain the most recent epochs of the SFHs of massive ETGs using the unexplored NUV spectral range. We aim to quantify the amount of young stellar populations in ETGs by means of detailed stellar population analysis with high quality spectra. The project was initially motivated by the latest version of the MILES stellar population models developed by Vazdekis et al. (2016), which are extended to bluer wavelengths (E-MILES) and fully based on empirical stellar libraries. These models allow us to study the stellar population properties of massive galaxies in great detail not only from the more frequently used optical but also from the UV range. The novelty of the present thesis is that we measure and fit for the first time spectral indices from both ranges simultaneously, obtaining robust solutions for both spectral windows. Within the described framework, we are tackling to the following goals:

- **Exploration of the NUV spectral indices using the E-MILES stellar population models.** The majority of the stellar population studies up to date making use of galaxy spectra have been focused on the optical range, where the bulk of stars of ETGs largely contributes. Thus, NUV indices of massive ETGs are almost unexplored by the literature, so we aim to investigate the behaviour of these indices with respect to stellar population parameters by measuring them in massive ETG spectra.

- **Characterisation of the amount of young stellar populations of the early-type population of galaxies.** To understand galaxy formation and evolution it is crucial to explore star formation signatures in the most massive galaxies of the Universe. From UV photometry it has been extensively shown that a large fraction of ETGs present signs of recent star formation but their NUV line-strength indices are largely unexplored. We aim to estimate to what extent the population of ETGs are actively forming new stars by comparing their NUV and optical features of their spectra with predictions from models.

- **Correlation between the amount of young stars with galaxy mass.** As galaxy mass is a fundamental parameter for the majority of the ETG's properties, it is important to determine whether the amount of young stars has any correlation with this parameter. Thanks to the large data-set available from SDSS, we are able to analyse ETG spectra of different intervals of stellar mass. If the quantified young stars have a larger contribution for less massive galaxies, it may suggest that such a result is expected from a purely passive evolution of massive galaxies, where lower mass galaxies have more extended SFHs and their star formation is less efficiently suppressed due to the AGN at high redshift.

- **Comparison with numerical simulations within a cosmological framework.** These simulations have proven to be an extremely useful tool to answer important questions in galaxy formation. To understand the physical processes that regulate the formation and evolution of massive galaxies, we need to be able to reproduce the observed stellar population properties across cosmic time in cosmological simulations. Our observational constraints are compared to the properties of simulated massive galaxies to provide new stringent constraints to improve these models.

- **Analysis of young stellar population gradients in nearby BCGs.** Massive ETGs located at the centres of galaxy clusters have been actively interacting with their environment by accreting surrounding galaxies, i.e. amounts of stars and gas. By constraining the young mass fractions in the cores of nearby BCGs and investigate their distribution according to the distance to the galaxy centre, we will be able to understand more accurately their origins and discuss different ETG evolution scenarios.

- **Exploration of the amount of young stars in a nearby relic galaxy.** A few massive compact galaxies have survived from high redshift and have not experienced any external perturbations (mergers) and have preserved their structure with a purely passive evolution of their stars until the local Universe. On the contrary, nearby massive galaxies have interacted with other galaxies and accreted material in their outskirts, becoming less dense and more massive than the massive compact galaxies at higher redshift. The study of the young stellar components in a relic galaxy will help us to investigate the origin of the star formation in the cores of nearby massive galaxies, i.e internal vs. external.

We compare NUV and optical line-strength indices from observed galaxy spectra with model predictions that result from simple parametrizations of the SFH of massive galaxies to find the fraction of young stars that match the observations. We use two modeling approaches. The first considers two single stellar population (SSP) models, representative of the old and the young components, are linearly combined in order to find the relative fraction that better match the observations. The second model consists of a parametrization where the old component is combined with a constant SFR for the most recent tail of the SFH of massive galaxies. The latter attemps to quantify the amount of stars formed in the last 1 or 2 Gyr. The red optical colours, relatively short star formation time-scales and other stellar population properties mentioned above of massive ETGs point to the fact that young stellar populations are expected to have in general a low contribution to the total stellar mass of massive ETGs.

The young components will be studied in different samples of ETGs. First, we constrain the young component of stacked spectra from the BOSS survey, representative of the general ETG population at $z \sim 0.4$. Thousands of individual galaxy spectra are stacked as a function of their central velocity dispersion, which is widely known to correlate with the galaxy stellar mass. We study the amount of young stars as a function of galaxy mass for massive ETGs at that redshift. Then, we focus on two special cases. One is the BCGs, i.e. the bulge-dominated stellar systems located in the central regions of galaxy clusters. We estimate the fraction of young stars as a function of the galactocentric distance from stacked spectra of a sample of six BCGs, from the galaxy cores out to 4 kpc. The other one comprises the analysis of a relic galaxy that, compared to BCGs, has experienced few interactions or mergers with other galaxies. Quantifying the young properties of these two special categories of massive galaxies and comparing the results with those found for the general population of ETGs will provide us constraints for the understanding the origin of the recent star formation and the most plausible scenario for ETGs evolution.

The thesis is organised as follows. In Chapter 2, we describe the methodology employed during this thesis to derive the young stellar components of ETGs by means of fitting a given set of absorption line-strength indices with predictions from modelling approaches. This section also describes the set of single stellar population models exploited throughout this thesis. The young stellar populations as a function of velocity dispersion of stacked spectra of thousands of massive galaxies at $z \sim 0.4$ are investigated in Chapter 3. We derive the young stellar population gradients from stacked spectra of a sample of 6 nearby BCGs in Chapter 4. The young stellar contribution of a relic galaxy is analysed in Chapter 5. Finally, our discussion and conclusions are included in Chapter 6 while future work is presented in Chapter 7. Throughout this thesis, we assume a Λ-cold dark matter Universe with values of the Hubble constant $H_0 = 70\ \mathrm{km\,s^{-1}\,Mpc^{-1}}$, matter density parameter $\Omega_m = 0.30$ and a cosmological constant $\Omega_\Lambda = 0.70$.

2

Methodology

If we take care of nature, nature will take care of us.
It's now time for our species to stop simply growing,
to establish a life on our planet in balance with nature.

David Attenborough in *A life on our planet* (2020)

In this chapter we describe the methodology used throughout this thesis to estimate the young stellar components present in massive ETGs. Basically, the method consists of fitting the observed spectral lines in both NUV and optical spectral ranges with stellar population synthesis model predictions that are derived from simple parametrizations of the SFH of massive galaxies.

Most of the content of this chapter is based on the paper *Sub one per cent mass fractions of young stars in red massive galaxies.* Salvador-Rusiñol, N.; Vazdekis, A.; La Barbera, F.; Beasley, M. A.; Ferreras, I.; Negri, A.; Dalla Vecchia, C. 2019, Nat. Astron., 4, 252-259; and on the paper *Young stellar population gradients in central cluster galaxies from NUV and optical spectroscopy.* Salvador-Rusiñol, N.; Beasley, M. A.; Vazdekis, A.; La Barbera, F. 2020, MNRAS, 500, 3368-3381.

2.1 Determining the stellar content of galaxies

Most of the information we learn from galaxies comes from spectroscopic observations. Currently, we are able to resolve single stars only from the Milky Way and galaxies in the Local Group. At larger distances, we can study only their integrated light to which all stars present in a galaxy or in a given region of it, contribute, to study their stellar populations. A galaxy spectrum encondes valuable information about the properties of its stellar and gas content. The study of stellar populations of galaxies requires confronting observational galaxy spectra with stellar population models. Measurements on the observed spectra of galaxies are compared to the model predictions to determine stellar population parameters, which provide clues to understand their formation and evolution. Relevant parameters characterising galaxy stellar populations include the mean metallicity and the age.

Many studies have derived the stellar population parameters in massive ETGs by approximating their SFHs with simplistic modelling approaches (Ferreras & Silk 2000; Pipino et al. 2009; Groenewald & Loubser 2014; Loubser et al. 2016). Even a single burst at high redshift (i.e. an old SSP) provides a good approximation of their SFHs (Trager et al., 2000), at least judging from their optical spectra, for galaxies whose stellar mass is larger than $10^{11}\,M_{\odot}$ (Vazdekis et al. 1997; Renzini 2006), such as those studied here. Since the integrated light of galaxies comes from different type of stars, they can be studied as a combination of SSPs of different ages and metallicities. Their SEDs give us the opportunity to disentangle these components and, in doing so, we can constrain the star formation and chemical histories of galaxies.

2.1.1 Stellar population models

To study physical properties from unresolved stellar populations in galaxies, we need to rely on SSP models. A SSP represents a population of stars born at the same time with the same metallicity and in the same region of space. The SSPs represent the building blocks of galaxies. The stellar population models are described by different SSPs that help to estimate phyisical parameters such as age, metallicity and star formation rates from observed SEDs. These models are generally constructed with three main ingredients: a set of evolutionary theoretical isochrones, stellar spectral libraries and an assumption of an IMF. Stellar libraries are sets of theoretical or empirical (i.e. observed) spectra of stars. They are integrated along an isochrone assuming an IMF to predict a spectrum representative of a single population of stars, i.e. a SSP. The more complete the stellar library, the better represented then the isochrone, and therefore the more reliable the SSP model. Ideally, all the stellar evolutionary stages along the isochrones should be represented, which increases the reliability of the computed SSP.

The SSPs employed in this thesis are the E-MILES models described in Vazdekis et al. (2016). E-MILES is currently the only set of models publicly available covering the UV range that are based entirely on empirical, rather than theoretical libraries. The wavelength range of these models extends from

1680.2 Å to 49999.4 Å. The empirical stellar libraries of these models cover from the UV (NGSL, Gregg et al. 2006), optical (MILES, Sánchez-Blázquez et al. 2006b) to the near-infrared (Indo-US, Valdes et al. 2004, CAT, Cenarro et al. 2001, IRTF, Cushing et al. 2005, Rayner et al. 2009) spectral ranges.

The E-MILES SSP spectra allow us to study in great detail a wide range of galaxy stellar poplation properties at moderately high spectral resolution. The age grid ranges from 63 Myr to 14 Gyr and the metallicity grid spans from [M/H] = −2.27 to 0.22 dex. These models allow also to vary the IMF shapes and slopes. In particular, throughout this thesis we adopt a low-mass tapered "bimodal" IMF Γ_b (Vazdekis et al., 1996), characterised by a logarithmic slope Γ_b for stars above 0.6 $M_{\odot}$. For reference, $\Gamma_b = 1.3$ is close to the standard Kroupa IMF for the Milky Way (Kroupa, 2001). For younger ages, we used the version of E-MILES models extended to 6.3 Myr descibed in Asa'd et al. (2017). We use the version constructed with Padova isochrones (Girardi et al., 2000) to be consistent in the whole wavelength range, since the youngest models are only available for this set of isochrones. In summary, a given SSP model is characterised by an age, metallicity and IMF slope.

The models are computed for the total metallicity [M/H], which represents the elements heavier than helium relative to the hydrogen and is related to the abundance of Fe with respect to H [Fe/H] and the alpha-abundance ratio [α/Fe] by:

$$[M/H] = [Fe/H] + b[\alpha/Fe] \tag{2.1}$$

The parameter [α/Fe] indicates the abundance of the so-called alpha-elements relative to the Fe-peak elements, so that if [α/Fe] = 0, [Fe/H] = [M/H]. The parameter b depends on the chemical abundance assumed, so that $b = 0.75$ when [α/Fe] = 0.4 (Vazdekis et al., 2015). As explained in Chapter 1, massive ETGs are known to have very old and metal-rich ([M/H] > 0) stellar populations and are enhanced in alpha-elements ([α/Fe] > 0), at least in their central regions.

2.1.2 Line strength indices

In the integrated spectra of galaxies a large number of absorption lines can be identified, which correspond to transitions of certain chemical elements. By analysing the strength of these lines and molecular absorption features it is possible to derive relevant stellar populations parameters. A line-strength index quantifies the strength of a given absorption line with respect to its continuum. For this purpose, an index is defined by a central bandpass between λ_1 and λ_2 and two local pseudo-continuum bandpasses, in the blue and red sides of the absorption line. A line-strength index is typically calculated as the equivalent width that measures the flux enclosed within a given absorption line divided by the average flux of the two pseudo-continua. Here we use the definitions of atomic and molecular indices I_a and I_m, based on those expressed in González (1993), where they are calculated in Å and in magnitudes units, respectively, as:

$$I_a = \int_{\lambda_1}^{\lambda_2} \left(1 - \frac{S_\lambda}{C_\lambda}\right) \, d\lambda \tag{2.2}$$

$$I_m = -2.5 \; log10 \; \frac{\int_{\lambda_1}^{\lambda_2} (1 - S_\lambda/C_\lambda) \; d\lambda}{\lambda_2 - \lambda_1} \tag{2.3}$$

where S_λ is the observed spectrum and C_λ is the pseudo-continuum obtained through a linear interpolation of the flux between the two local spectral bandpasses.

Line-strength indices are commonly exploited as stellar population indicators of galaxies. It can be found in the literature a large number of indices available for different wavelength ranges. The most often used indices when analysing the stellar populations of ETGs are the Lick index system (Faber et al. 1985; Worthey et al. 1994; Worthey & Ottaviani 1997), which defines indices in the optical range. Index fitting has been used by a large number of spectroscopic studies based on optical data to obtain stellar population properties of massive galaxies (Gorgas et al. 1997; Sánchez-Blázquez et al. 2006a; Peletier et al. 2007; Brough et al. 2007; Loubser et al. 2009; Zhu et al. 2010; Harrison et al. 2010; Choi et al. 2014; Ferré-Mateu et al. 2014; François et al. 2019; Domínguez Sánchez et al. 2019), but the young stellar populations were missed due to their low contribution to the optical spectra of massive ETGs.

The indices used throughout this thesis are presented in Table 2.1. NUV indices are used here to disentangle very small fractions of young stellar components in old stellar populations. The bluer the index, the larger the relative contribution of young stars, as will be described in more detail below. For our purposes, we refer to NUV as the spectral range between 2500 – 3700 Å. The set of indices includes also age-sensitive indicators in the optical range such as the HγF and Hβ_o absorption lines. We use the Hβ_o instead of Hβ, since it is found to be more sensitive to the age (Cervantes & Vazdekis, 2009) and minimises the metallicity dependence unlike Hβ, which retains some metallicity sensitivity. The Hβ Balmer line is an excellent stellar clock of a galaxy spectrum by tracing the temperature of main sequence turn-off stars of a stellar population. The optical Mgb5177, Fe5270 and Fe5335 indices are sensitive to the [α/Fe] abundance, so that we combine them to use the optical index [MgFe]$'$ defined by Thomas et al. (2003), which is found to be insensitive to the alpha-element abundances. This index is well known to correlate with metallicity [M/H] and is obtained via:

$$[MgFe]' = \sqrt{\mathrm{Mgb5177}(0.72\mathrm{Fe5270} + 0.28\mathrm{Fe5335})} \qquad (2.4)$$

Index (1)	Blue passband (Å) (2)	Index passband (Å) (3)	Red passband (Å) (4)	Reference (5)
Fe2609	2562.000 – 2588.000	2596.000 – 2622.000	2647.000 – 2673.000	1,2,3
BL2720	2647.000 – 2673.000	2713.000 – 2733.000	2762.000 – 2782.000	1,3
BL2740	2647.000 – 2673.000	2736.000 – 2762.000	2762.000 – 2782.000	1,3
Mg2852	2818.000 – 2838.000	2839.000 – 2865.000	2906.000 – 2936.000	1,2,3
Fe3000	2906.000 – 2936.000	2965.000 – 3025.000	3031.000 – 3051.000	1,2,3
Mg3334	3310.000 – 3320.000	3328.000 – 3340.000	3342.000 – 3355.000	4
NH3375	3342.000 – 3352.000	3350.000 – 3400.000	3415.000 – 3435.000	4
Ni3520	3499.000 – 3508.000	3511.000 – 3530.000	3532.000 – 3548.000	5
Fe3581	3532.000 – 3548.000	3548.000 – 3594.000	3594.000 – 3602.000	5
Fe3631	3625.500 – 3628.500	3628.500 – 3637.500	3659.000 – 3674.000	5
Fe3646	3625.500 – 3628.500	3642.500 – 3659.000	3659.000 – 3674.000	5
HγF	4283.500 – 4319.750	4331.250 – 4352.250	4354.750 – 4384.750	6
Hβ_o	4821.175 – 4838.404	4839.275 – 4877.097	4897.445 – 4915.845	7
Mgb5177	5142.625 – 5161.375	5160.125 – 5192.625	5191.375 – 5206.375	8
Fe5270	5233.150 – 5248.150	5245.650 – 5285.650	5285.650 – 5318.150	8
Fe5335	5304.625 – 5315.875	5312.125 – 5352.125	5353.375 – 5363.375	8
TiO1	5816.625 – 5849.125	5936.625 – 5994.125	6038.625 – 6103.625	8
$\mathrm{TiO2_{SDSS}}$	6066.625 – 6141.625	6189.625 – 6272.125	6422.000 – 6455.000	9

TABLE 2.1— **Definitions of the spectral indices used in this thesis.** Each index listed in the Col. 1 is defined by a central passband (Col. 3) and a blue and a red pseudo-continuum (Col. 2 and 4, respectively). The references numbered in the last column are 1: Fanelli et al. (1990); 2: Maraston et al. (2009); 3: Chavez et al. (2007); 4: Serven et al. (2011); 5: Gregg (1994); 6: Worthey & Ottaviani (1997); 7: Cervantes & Vazdekis (2009); 8: Worthey et al. (1994); 9: La Barbera et al. (2013).

The set of indices from Table 2.1 used in each science case of this thesis mainly depends on the wavelength range of the galaxy spectra analysed. Each set always combines NUV and optical indices, as we require our stellar population estimates to be compatible with a wide spectral range, since most of the studies based on spectral indices to date focused on a given spectral window, i.e. the NUV or the optical, but not both at the same time. The use of Hβ_o and [MgFe]$'$ simultaneously allows one to break the age-metallicity degeneracy and derive the mean age and metallicity of a population of stars. In addition, for the specific science case in Chapter 4, where we study the variation of the amount of young stars with respect to the distance to the galaxy centre for six massive central galaxies, we include the highly IMF-sensitive indices TiO1 and $TiO2_{SDSS}$. Those galaxies are known for hosting a strong IMF gradient (La Barbera et al. 2019), from a bottom-heavy IMF in their galaxy centres to a Kroupa-like IMF in their outskirts.

The UV window is more affected by the internal dust of galaxies than optical wavelengths, so the shape of the continuum in our spectra may be affected by reddening, especially at bluer wavelengths. One of the main advantages of using spectral indices for the analysis over approaches based on broad-band colours is that the effect of internal dust reddening of galaxies is expected to be much lower, as the indices are rather narrow to be sensitive to longer wavelength scales affected by the dust. The wavelength-dependent dust attenuation law is modelled by a smooth function along with a few broad resonant features. Therefore, the presence of dust in galaxies will mostly affect measurements covering large wavelength intervals, e.g., broad-band photometry. All our indices are defined with two local pseudo-continua, making them less sensitive to the possible impact of dust (MacArthur, 2005). Thus, narrow spectral features will be, at most, weakly affected, especially in massive ETGs, where the dust content is minimal. We have performed some tests and found that most of the NUV spectral indices are insensitive to dust attenuation. Therefore, the effect of dust in the analysis of the spectral indices studied throughout this thesis is negligible so that we did not correct the galaxy spectra for internal dust extinction.

Line-strength indices are sensitive to the spectral resolution of the data and velocity dispersion of the galaxy. When comparing with theoretical predictions or between different galaxies, the spectra need to be at the same spectral resolution $R = \lambda/FWHM$. FWHM is the full width half maximum and is correlated with the velocity dispersion σ by:

$$\sigma = \frac{FWHM\ c}{2.355\ \lambda} \tag{2.5}$$

An observed spectrum has two intrinsic "velocity dispersions" that we need to take into account: the intrinsic resolution associated with the instrumental configuration of the observations σ_{instr} and the stellar velocity dispersion of the target σ_{galaxy}. In the case of massive galaxies such as ETGs: $\sigma_{galaxy} >> \sigma_{instr}$. The total velocity dispersion of an observed spectrum is:

$$\sigma_{obs}^2 = \sigma_{instr}^2 + \sigma_{galaxy}^2 \tag{2.6}$$

Thus, in order to compare line-strength indices, we need to smooth the spectra in order for them all to be at the same resolution σ_f, which would be tipically the lowest resolution (i.e. the highest σ) of the spectra. For smoothing, we apply a normalised Gaussian function G at each wavelength λ with a standard deviation equal to σ_{diff} and taking a given range of the spectrum x centered at each λ:

$$G = exp\left(\frac{-x^2}{2\ \sigma_{diff}^2}\right) \tag{2.7}$$

where σ_{diff} may change with wavelength and is calculated at each λ by:

$$\sigma_{diff}^2 = \sigma_f^2 - \sigma_{obs}^2 \tag{2.8}$$

2.2 Young stars from the UV and optical spectra

In order to easily detect the youngest stellar components of old stellar systems such as ETGs, we need to investigate UV wavelengths, where the young stars maximise their relative contribution to the total light. The bluer the wavelength, the easier to detect those small contributions from newly formed massive stars. Figure 2.1 shows the impact on a spectrum of an old SSP model if a tiny mass fraction ($\sim$0.1%) of a young SSP is added. The combined stellar population plotted in black shows that the luminosity below 3500 Å comes mainly from this small amount of young stars rather than from the old dominating stellar population in the visible. I.e. in the optical range, the contribution from this small fraction of young stars has virtually a negligible impact. Also, the relative contribution of this young stellar population is larger toward bluer wavelengths.

Figure 2.2 shows the expected variation from the E-MILES SSP models of the NUV indices due to the presence of the fraction of the young SSP relative to an old SSP shown in Figure 2.1. The bluer the index, the higher its sensitivity. Indices below 3000 Å are 5 times more sensitive to the presence of small fractions of young stars than redder ones. Therefore, the UV data provide essential information to constrain the details of the young ($<$1Gyr) stellar population components, especially for very old systems such as massive ETGs.

2.3 Parametrization of the SFH of massive ETGs

There is a well-established relationship between galaxy mass and its SFH. More massive galaxies exhibit narrower SFHs that peak at older ages (i.e. higher redshifts) than their less massive counterparts. For galaxies with $\sim 10^{11}\,M_\odot$ a purely old SSP is a good first approximation. However, as shown in the following sections, while the optical indices measured in the observed spectra are

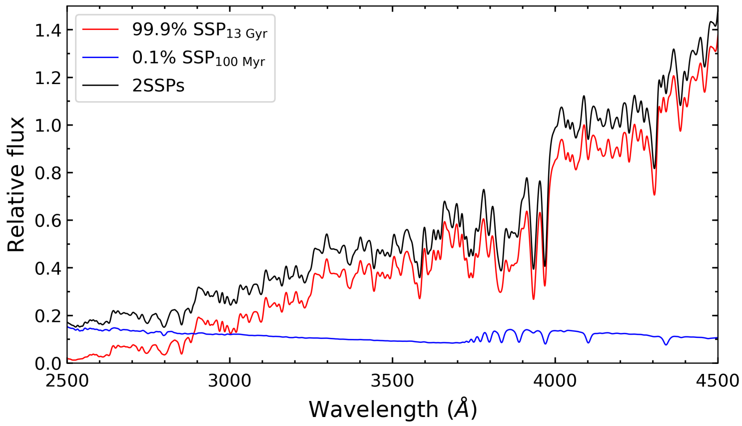

FIGURE 2.1— **Spectral sensitivity to small fractions of young stars.** The plot shows the impact of a small fraction of a young stellar population on top of an old stellar population spectrum. Red line represents 99.9% in mass of an old (13 Gyr) SSP model whereas the blue line represents a 0.1% of a young (0.1 Gyr) SSP model. The combination of these two spectra is shown in black. Although the optical is almost unaltered, wavelengths bluer than 3500 Å are relatively sensitive to an small fraction of a young stars.

in excellent agreement with the old SSP model predictions, there is an increasing difference between model predictions and observed data towards bluer indices. This behaviour provides clear evidence of the inability of a pure old SSP to fully describe the SFH of massive ETGs, indicating the presence of young stellar populations (Vazdekis et al., 2016).

For this purpose, the SFH has been approached by parameterising it in two different simple ways, both considering two stellar components: an old and a young stellar population, explained in more detail below. The deviation of NUV features from the old SSP model predictions cannot be caused by intermediate-age stellar populations because they barely contribute in the NUV. If such contributions were significant they would alter the optical indices leading to younger mean luminosity-weighted ages, as measured with the Hβ_o vs. [MgFe]$'$ diagnostic. Thus, intermediate stellar populations are not parameterised in our different SFH choices, as the aim of this thesis is to constrain the relative fraction of the youngest stellar contributions. For each galaxy spectrum, we compare the observed indices to index predictions from these two modelling

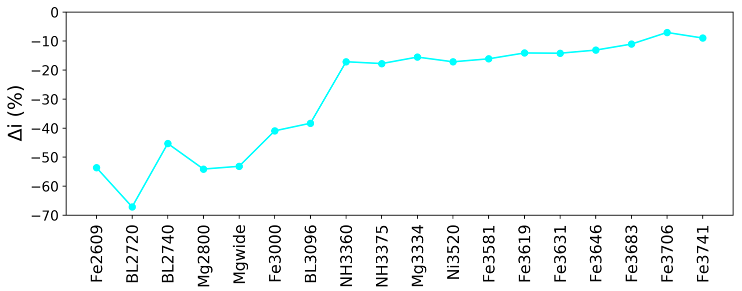

FIGURE 2.2— **Sensitivity of the NUV indices to young stars.** The values show the effect on the NUV indices labelled on the horizontal axis due to the presence of a small fraction of a young stellar population, based on the E-MILES model predictions. The plot shows how 0.1% mass fraction of a young stellar component combined with a 13 Gyr SSP changes the line strength of each index with respect to the predictions of a purely old SSP.

approaches to derive the relative contribution from young stars

2.3.1 2SSPs modelling approach

The first modelling approach (hereafter, called *2SSPs* model) consists of a superposition of two individual SSPs. The old stellar component is described by a SSP, which corresponds to a single burst at high redshift that represents the bulk of the stars in the galaxy. This is a valid approximation, as the expected age spread in the old component is comparatively narrower than the lookback time. A single SSP is used to describe the contributions from all the young stellar components. The parameters control the age of the old component between 1 and 13.5 Gyr (or, alternatively, the age of the Universe at the redshift of the galaxies), the age of the young component between 6.3 Myr and 1 Gyr or 2 Gyr (the former is the minimum age of the E-MILES SSP models), the metallicity of the old component typically in the range between −0.2 and +0.22, and the relative contribution of the young component, measured by mass. The metallicity of the young component is fixed at solar ([M/H] = 0.0) since a small change in metallicity can be compensated by a much smaller change in the age of the young stellar population. In addition, the hottest stars, particularly those around the turn-off with effective temperature Teff > 10000 K, which have little dependence on the metallicity, are the major contributors to the NUV. In this model, the age and metallicity of the old component, the mass fraction and the age of young component are left as free parameters in the fitting process.

This model can be visually represented by the left panel of Figure 2.3. We note that this modelling approach is affected by the burst-age – burst-strength degeneracy of the young component. This model is defined by:

$$2SSPs = SSP_{young} \times f_{young} + SSP_{old} \times (1 - f_{young}) \tag{2.9}$$

2.3.2 Constant recent star formation modelling approach

In this second model (hereafter, called *1SSP+cSFR*), the young component is not parameterised as an instant starburst, but as an extended contribution by assuming a constant SFR in a given period of time to estimate the relative fraction of stars formed during that period. The old component is described by a SSP, as in the *2SSPs* approach, i.e. using 2 parameters that cover the same range of age and metallicity, as represented by the right panel of Figure 2.3. The spectrum of the young component is obtained by integrating the individual SSPs with ages between 6.3 Myr and 1 (or 2) Gyr, spaced logarithmically over time. This spectrum is added to an old stellar population, leaving the relative mass contribution as an additional free parameter (giving a model described by three parameters). The age and metallicity of the old component and the mass fraction of young stars are left as free parameters in the fitting process. This approach is therefore free from the burst-age – burst-strength degeneracy affecting the young population (Leonardi & Rose, 1996), as the age of the young component is not a free parameter in the fitting process, as it is in the *2SSPs* model. This model is defined by:

$$1SSP + cSFR = SSP_{old} \times (1 - f_{period}) + cSFR_{period} \times f_{period} \tag{2.10}$$

The two modelling approaches are motivated by the fact that massive ETGs formed the vast majority of their stars at early times, over a relatively short time-scale ($\lesssim$1–2 Gyr, consistent with their high [Mg/Fe] and old ages). Consequently, the stellar populations originated after the main episode of formation do not contribute significantly to the flux in the optical range, as their relative mass fraction is small and their corresponding mass-to-light ratios do not differ notably from those characteristic of the oldest stellar populations that dominate this spectral range.

The *2SSPs* approach serves to understand better the origin of the departure of the UV absorption index strengths in relation to the 1SSP that describes well the line indices in the optical. This model is a simplistic assumption, as it assumes the young component forming instantaneously at a given specific time, while we actually expect any residual star-formation happening over an

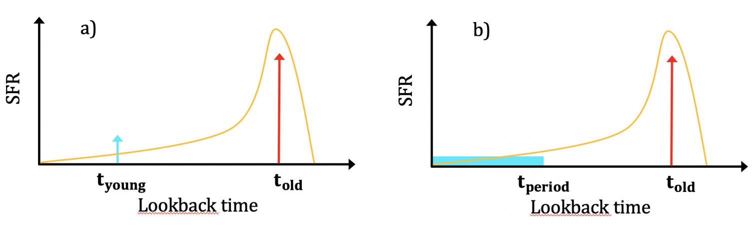

FIGURE 2.3— **Representations of the adopted modelling approaches of the SFH of massive ETGs.** The star formation rate in the y-axis is plotted as a function of the lookback time in the x-axis. Red arrows represent the old stellar component burst in both panels, while blue arrow in panel a) represents the young stellar burst of the *2SSPs* approach and blue rectangle in panel b) indicates a constant SFR in a given period of time, described in the *1SSP+cSFR* model.

extended time interval. For this reason, we believe that the *1SSP+cSFR* assumption for the young component is a more realistic approximation.

2.4 Index fitting methodology

For each galaxy spectrum, we employ a Markov Chain Monte Carlo (MCMC) algorithm to fit a set of optical and NUV line indices simultaneously with those predicted by the modelling approaches described above. The best-fitting solution is obtained by maximising the log-likelihood function $\ln \mathcal{L}$ given the observed set of indices ($\mathcal{I}$), which is equal to the probability $\mathcal{P}$ for the model parameters (Θ) of getting the observed indices ($\mathcal{I}$):

$$\mathcal{P}(\mathcal{I}|\Theta) = \ln \mathcal{L}(\Theta|\mathcal{I}), \tag{2.11}$$

where the likelihood is defined by $\ln \mathcal{L}(\Theta|\mathcal{I}) \propto -\frac{\chi^2}{2}$, where the χ^2 statistic is:

$$\chi^2 = \sum_{i}^{N} \left(\frac{I_{\mathrm{model_i}} - I_{\mathrm{stack_i}}}{\sigma_{\mathrm{stack_i}}} \right)^2, \tag{2.12}$$

where the subscript i refers to the i-th line index, I_{model} and I_{stack} are the model and observed indices, respectively, and σ_{stack} represents the index error.

The model that maximises the likelihood is the best-fitting model. Each set of indices measured in a given spectrum is fitted with the index predictions from the SFH parametrizations described above. We compute the sampling with the *emcee* package (Foreman-Mackey et al., 2013), a Python implementation of an ensemble sampler (Goodman & Weare, 2010). This process performs a linear interpolation of the SSP models predictions to generate continuous coverage of the parameter space given by the fitted parameters. The algorithms used are based on the generation of Markov chains defined by a given number of walkers and iterations. First, the walkers start in a chosen initial point of the parameter space and then explore the rest of the parameter space, taking into account its current position and the positions of all the other walkers. Each walker takes a new position that has a probability distribution that depends on the previous value, i.e. the walkers have their own "memory" that contains the previous likelihood value. In that point, the likelihood between the observed data and the interpolated models is calculated. The walkers continue exploring the parameter space during a given number of iterations searching for the region that maximises the likelihood. All the iterations create a Markov chain for each fitted parameter that converges to a stationary state that is independent of the initial point we set.

A large number of model realizations through a given number of walkers – that depend on each science case – explore the parameter space to obtain the best-fitting values. 1000 burn-in steps are used in all scientific cases of the present thesis. We take into account all the probabilities that we get for a given parameter through the other parameters to create the probability distribution function (PDF). We use these marginalised PDFs for the estimation of the best-fitting parameters and assume the median as the best-fitting value and the 16^{th} and 84^{th} percentiles as the uncertainties. By this way, the error bars we obtain from the fits are marginalised over each fitting parameter.

We give equal relative weight to the optical and NUV indices, separating the χ^2 statistic at 3700 Å, and slightly rescaling the error bars on both ranges so that each set of indices has the same weight on the final χ^2 of the best-fitting model. As a result, the best-fitting solution will be equally representative of both spectral windows. We also performed some tests for each scientific case by excluding some subsets of indices or by varying the relative weight of the UV and optical spectral indices in the fitting. Varying these weights give a wider range of solutions, and we regard this as a conservative approach. This allows for the exploration of extreme cases when one has more information from one spectral range or the other.

Recently, Martín-Navarro et al. (2018b) detected residual star formation in massive galaxies from full-spectral fitting of their optical spectra, finding larger amount of young stars for galaxies with relatively lower mass black holes for their stellar mass. Interestingly, throughout the development of this thesis it turned out that with sufficient S/N is possible to disentangle small fractions of young stars only from optical spectral indices, i.e. without NUV indices. From the theoretical point of view, this can be understood since the optical is affected by several types of populations contributing in the galaxy spectrum. Thus, some of the optical indices still have sensitivity to small young mass fractions if the spectra analysed have sufficient signal. The UV, in contrast, is mainly sensitive to the hottest populations and requires a combination with the optical range in order to distinguish between young and old populations. However, the main disadvantage from studies only based in optical indices is that they require very high S/N in optical wavelengths.

3

Young stars in massive ETGs at z∼0.4

To see we must forget
the name of the thing we are looking at.

Claude Monet

In this chapter we obtain precision measurements of the mass fraction of the young component in the ETG population at $z \sim 0.4$, and characterise these fractions as a function of galaxy stellar mass. This is particularly important since mass is the primary parameter that governs galaxy evolution, so it is crucial to know if there exist any correlation of the amount of young component with the galaxy stellar mass. Our analysis explores not only NUV features but also optical indices simultaneously, making the results consistent with both ranges of galaxy spectra. We find a measurable, but very small fraction in young stars that decreases with increasing galaxy mass. We discuss these results in the context of state-of-the-art cosmological numerical simulations.

The content of this chapter is based on the paper *Sub one per cent mass fractions of young stars in red massive galaxies.* Salvador-Rusiñol, N.; Vazdekis, A.; La Barbera, F.; Beasley, M. A.; Ferreras, I.; Negri, A.; Dalla Vecchia, C. 2019, Nat. Astron., 4, 252-259.

3.1 BOSS galaxy data

3.2 Data selection

We used galaxy spectra from the SDSS-III/DR12 Baryon Oscillation Spectroscopic Survey (BOSS) survey (Dawson et al., 2013). The main aim of this survey was to determine cosmological parameters via the baryon acoustic oscillations by mapping the spatial distribution of luminous red galaxies and quasars in the early universe until the present. Those luminous red galaxies were selected by their colours in order to target the reddest, most massive and brightest galaxies as a function of redshift to $z \sim 0.7$. Their red colours are indicative of primarily old stellar component comprising the bulk of their stars, which is the main property of ETGs. In Chen et al. (2012) and Tojeiro et al. (2012) BOSS galaxies are characterised to be dust free. Masters et al. (2011) cross-matched the BOSS sample with HST images from the COSMOS survey (Capak et al., 2007) and found from colours that the observed BOSS morphologies are predominantly (∼73%) massive quiescent galaxies with an early-type morphology. Maraston et al. (2013) showed that the mass distribution of the survey peaks at $10^{11.3}$ solar masses. Thus, targets observed by BOSS are mostly massive ETGs.

Since this is an SDSS survey that employs an optical spectograph, we select high redshift galaxies for which their UV luminosity is shifted into the optical range. We selected galaxies in the redshift range $0.35 \leq z \leq 0.6$, so that the spectra map rest-frame wavelengths between 2500 and 6500 Å, providing both NUV and optical data. We restricted the sample with $S/N > 7\,Å^{-1}$ in the SDSS-r band, in order to avoid excessively noisy spectra, because at this redshift massive ETGs are quiescent and therefore faint in the NUV. Further, since the stellar velocity dispersion is directly related with the galaxy stellar mass, we chose massive galaxies with stellar velocity dispersions between 220 and $340\,\mathrm{km\,s^{-1}}$, to select massive galaxies. The stellar velocity dispersion of the individual galaxies was obtained by Thomas et al. (2013) through the `pPXF` technique (Cappellari & Emsellem, 2004) in the wavelength range 4500 – 6500 Å, covering a sufficient number of absorption features suitable to measure the kinematics. Note that the early type population of galaxies becomes more dominant with increasing mass. Thus, at such velocity dispersions the sample should be practically free from LTGs (La Barbera et al., 2010a). However, we additionally adopt the colour cut $(g\text{-}i) > 2.35$ to remove remaining late-type galaxy contamination (Masters et al., 2011). Since massive galaxies become redder with increasing mass, the number of galaxies out of this colour cut of our initial galaxy sample is larger for the lowest mass bin (∼18%) than for the highest mass bin (∼8%), indicating a wider variety of stellar populations at lower masses. Distribution of our selected BOSS galaxy sample as a function

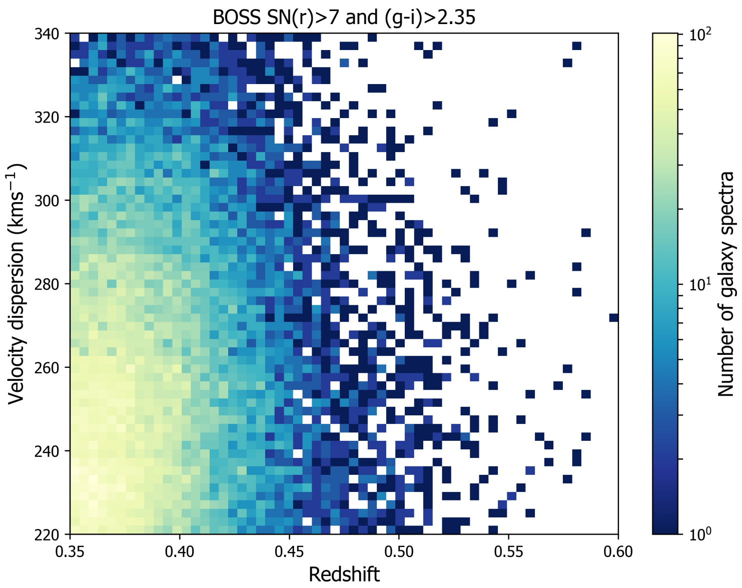

FIGURE 3.1— **BOSS galaxy sample as a function of velocity dispersion and redshift.** The plot illustrates the number density in logarithmic scale of available BOSS spectra with S/N > 7 Å^{-1} in the SDSS-r band and (g-i) > 2.35. We select BOSS galaxies with redshift $0.35 \leq z \leq 0.6$, and velocity dispersion between 220 and 340 km s^{-1}. Lowest density regions show individual galaxies in dark blue.

of redshift and velocity dispersion is illustrated in Figure 3.1. Note that the galaxy distribution is biased towards lower redshifts, as expected from our S/N criterion, which is more difficult to reach at higher redshifts.

The BOSS sample that satisfies all these criteria comprises 28663 galaxies and primarily consists of ETGs. No environmental criteria have been taken into account in the selection process, therefore our sample includes not only field galaxies but also galaxies potentially in galaxy clusters. The diameter of the BOSS fibers maps into 2 arcsec on the sky, covering ∼10 kpc aperture at the median redshift distance of the sample (z ∼ 0.38), so we are basically looking at the central regions of the galaxies.

The BOSS spectra are given in vacuum wavelengths. We convert them to the air system using the IAU standard equation (Morton, 1991). We also applied a Milky Way dust extinction correction following the standard Cardelli law (Cardelli et al., 1989) with $R_V = 3.1$ and the official SDSS foreground dust extinction values (g-band), A_g, transformed into a colour excess via (Stoughton et al., 2002) E(B-V) = $A_g/3.793$. Note that the effect of internal dust is virtually negligible in this study since we analysed a set of spectral features which encompasses a narrow spectral region with respect to the variations in the extinction law (see next section).

3.2.1 Stacking the spectra

The individual BOSS galaxy spectra have too low S/N to derive reliable information from some of the absorption line strengths, especially in the NUV (S/N$\sim 2\,Å^{-1}$). Our detailed stellar population analysis requires at least a S/N of $13\,Å^{-1}$ for measuring some NUV indices to disentangle small young stellar mass fraction contributions. Given the large index uncertainties in the individual spectra the tiny young stellar contributions cannot be properly estimated. The maximum S/N of an individual galaxy spectrum reaches $9\,Å^{-1}$ in the NUV range, which is lower than the S/N needed to perform this analysis. Therefore, stacking is the best approach to increase S/N of the spectra, given that our sample comprises a large number of spectra and allows us to average over individual variations. Most importantly, the stacking procedure allows us to obtain results that apply to the general ETG population, by washing out galaxy-to-galaxy variations at fixed velocity dispersion.

σ (km s^{-1})	N	z	log(mass)
(1)	(2)	(3)	(4)
220-230	4180	0.376±0.030	11.32±0.16
230-240	4517	0.376±0.030	11.33±0.16
240-250	4136	0.378±0.031	11.35±0.16
250-260	4077	0.378±0.030	11.36±0.17
260-280	5623	0.381±0.030	11.39±0.18
280-300	3516	0.383±0.031	11.43±0.19
300-340	2614	0.388±0.032	11.47±0.20

Table 3.1— **General properties of the BOSS stacked spectra**. They are shown with respect to the velocity dispersion range of the stacks (Col. 1). Col. 2 shows the number of individual galaxy spectra added in each bin. Col. 3 and Col. 4 show the average redshift and stellar mass (Maraston et al., 2013).

The BOSS data are grouped into seven stacks, binned in velocity dispersion σ from 220 to 340 $\mathrm{km\,s^{-1}}$ in steps $\Delta\sigma = 10\,\mathrm{km\,s^{-1}}$ for the first 4 stacks, and slightly wider for the stacks corresponding to the three highest velocity dispersion bins, with $\Delta\sigma$=20 $\mathrm{km\,s^{-1}}$ and $\Delta\sigma = 40\,\mathrm{km\,s^{-1}}$, to achieve a roughly constant number of individual spectra per bin and sufficient S/N to perform the analysis.

We create the stacks by bringing the data to rest-frame wavelengths and co-adding all the spectra that correspond to the same group using a grid with fixed sampling in log-wavelength, $\Delta\log(\lambda/\text{Å}) = 10^{-4}$. The flux per pixel is shared between neighbouring reference pixels, proportional to their level of overlap with the original, de-redshifted pixel. Given the redshift range of the sample, the shifted data spans the wavelength range 2500 – 6500 Å. The error on the flux is coadded (in quadrature) in the same way as the flux, from the individual values at each wavelength. The final stacked spectra and their corresponding S/N are shown in Figure 3.2. The seven stacks achieve very high S/N, above 30 in the NUV and several hundreds in the optical. General properties of each σ bin are listed in Table 3.1. The stacked spectra are smoothed at $\sigma = 340\,\mathrm{km\,s^{-1}}$.

The spectral continuum in the NUV region can be significantly affected by dust intrinsic to the galaxies. Note that the foreground attenuation from the Milky Way is already corrected for in the individual spectra. We check the effect of dust on our measurements by artificially reddening the stacked spectrum corresponding to the lowest velocity dispersion range. The effect is expected to be more important in lower mass galaxies since expected to have the higher dust content. We adopt an extinction curve with $\mathrm{R}_V = 3.0$, typical of ETGs (Patil et al., 2007), and extinction $\mathrm{A}_V = 0.5$. Note that this is a large extinction for ETGs, but we explore an extreme case. The indices obtained in this dusty stack do not differ significantly from the original ones. The largest variations are found in the BL2720 and BL2740 features, which increase by ∼12% and 3%, respectively, but the other NUV indices change less than 1% with respect to the dust-free spectrum. The optical indices are completely unaffected by dust. Therefore, the role of internal dust reddening in the analysis of the narrow NUV spectral indices studied here is negligible and does not affect our estimates.

3.3 Constraints on the age and metallicity

As a first approximation, we constrain the global properties of the stellar populations of each stacked spectrum by fitting two widely used optical indicators, $\mathrm{H}\beta_o$ and [MgFe]′ with E-MILES SSP models. These serve as proxies for the mean luminosity-weighted ages (MLWA) and metallicities of a stellar population, respectively. Note that we take a single SSP as an approximation for the whole stellar population of the ETGs, representing the global contribution

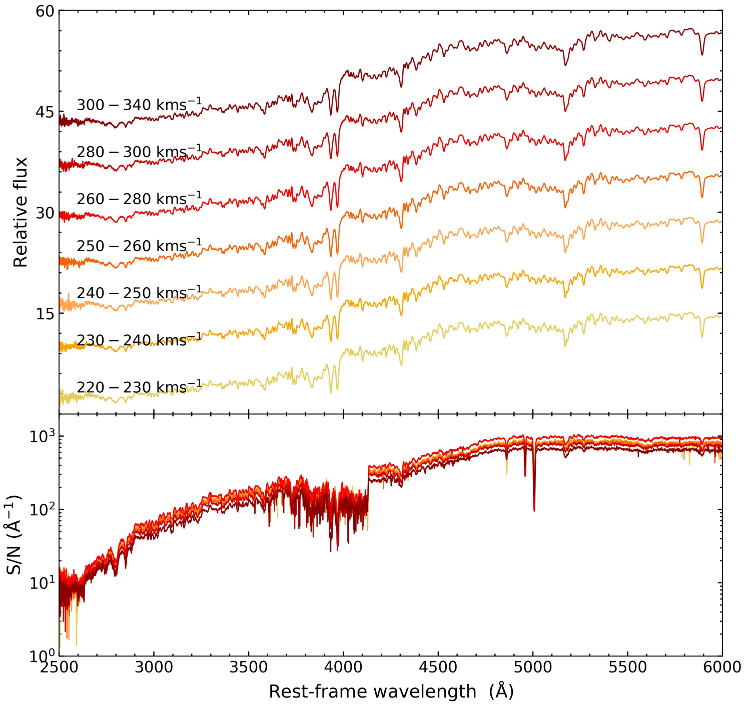

FIGURE 3.2— **BOSS stacked spectra and S/N.** Upper panel shows our stacked spectra from the BOSS survey, colour coded with respect to the stellar velocity dispersion range labelled on the top-left of each spectrum. The spectra have been shifted vertically for ease of visualization. Lower panel represents the signal-to-noise ratio, following the same colour scheme.

to the spectra. As a visual guide, left panel of Figure 3.3 shows the grid of stellar population model predictions for these two indices for a range of ages and metallicities. The observed strengths indicate an overall old and metal-rich ([M/H] > 0) population for all the observed values, suggesting that the stellar component of massive galaxies were formed at early epochs as expected (Renzini, 2006). We fit the observed $H\beta_o$ and [MgFe]′ with the SSP model predictions to determine the MLWA and metallicity of each stack, by minimising the χ^2. The inferred stellar population parameters are shown in the right panel. The age of the stellar populations of ETGs correlate with the stellar velocity dispersion whereby more massive (i.e. higher velocity dispersion) galaxies are older. Moreover, we note that the age obtained for the most massive stack (the oldest) is 8.6±0.5 Gyr, compatible with the age of the Universe at the median redshift of the sample (z ∼ 0.4), namely 9.4 Gyr. For more massive galaxies with shorter star formation time-scales, the MLWA is well representative of the oldest stellar populations. For lower mass galaxies, the MLWA shifts to younger ages primarily because they have more extended SFHs, not because their old stellar populations are thought to be younger.

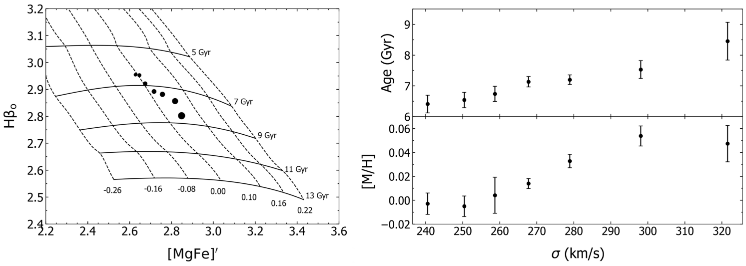

FIGURE 3.3— **Estimates of the mean ages and metallicities of the BOSS stacks.** Left panel: measurements of the age-sensitive spectral index Hβ_o are plotted as a function of the total metallicity proxy [MgFe]′. The grid shows the model predictions over a range of SSP ages (solid lines) and metallicities (dashed lines), as labelled. The black dots are the observed BOSS index measurements, with dot size increasing with galaxy mass and uncertainties smaller than the point size. The model grid and observational spectra are smoothed to a common velocity dispersion of 340 km s^{-1}. Right panel: Mean luminosity-weighted ages and metallicities as a function of the velocity dispersion of each bin derived from Hβ_o and [MgFe]′ indices.

ETG spectra may include some nebular emission, revealing the presence of ionised gas due to a modest level of star formation activity. Although weaker than in LTGs, we are required to correct for this component, especially those features based on the hydrogen recombination lines – in particular Hβ_o – as even a weak emission may partly fill the absorption feature, affecting the estimated MLWA. To correct the Hβ_o line-strength for nebular emission, we subtract a best-fitting SSP model spectrum in the region of Hβ_o from each stack and measure the residual of the index. We typically find a small but detectable nebular emission (ΔH$\beta_o \sim 0.07$ Å, on average), lower in the most massive bins, but significant enough to change the estimated ages of their stellar populations

– at most by +0.8 Gyr at the lowest velocity dispersion range. This residual is added to the observed index value to derive the age. We do not correct the higher order Balmer line strengths in our analysis (H_γ and H_δ) as the contribution from nebular emission – directly measured from the residuals – is negligible.

3.4 NUV and optical line-strength indices

We measure 14 absorption line indices covering the NUV and optical ranges. Figure 3.4 show the variation of the indices used for the fitting process as a function of the MLWA of a single SSP for two different metallicities: solar metallicity [M/H] = 0 (solid line), and super-solar metallicity [M/H] = +0.22 (dashed line). This illustrates the behaviour of each index with the population parameters. The observed indices are shown as black dots with 1 σ level uncertainties. Note that while the observed optical indices are in excellent agreement with the old SSP model predictions, there is an increasing difference between model predictions and observed data towards bluer indices. This behaviour of the NUV data provides clear evidence of the inability of a pure old SSP to fully describe SFH of our massive ETGs and calls for an additional component to be fitted, as suggested by Vazdekis et al. (2016). This component needs to be a very hot stellar population responsible for the decrease of NUV absorption features possibly due to young stars. The decrease of the NUV indices cannot be due to intermediate-age stellar populations, because they barely contribute in the bluest wavelengths of the NUV range. Here we aim to quantify the upper limit mass fraction of very young stellar populations in massive ETGs at z ∼ 0.4 as a function of mass.

To understand this additional component, we adopt the two parametrizations of the expected SFH of a massive and old ETG described in Section 2.3 as a superposition of an old and a young component. Briefly, the old component is described by a SSP. The young component – tracing the recent star formation episodes – is given either by an additional SSP (*2SSPs* model), or by a composite population following a constant SFR within the last 2 Gyr of galaxy evolution (*1SSP+cSFR* model), which is more representative of the real SFH of a massive ETG than the *2SSPs* model.

At the high S/N of the stacked spectra, the index uncertainties are extremely small and may influence and bias the final fits with the model predictions. We explored the statistical uncertainty derived from the construction of the stacks. We approached this by generating Monte Carlo simulations for each velocity dispersion bin, which give us a better estimate of the dispersion in the indices given the true variation of galaxy properties in each bin. We bootstrap resample

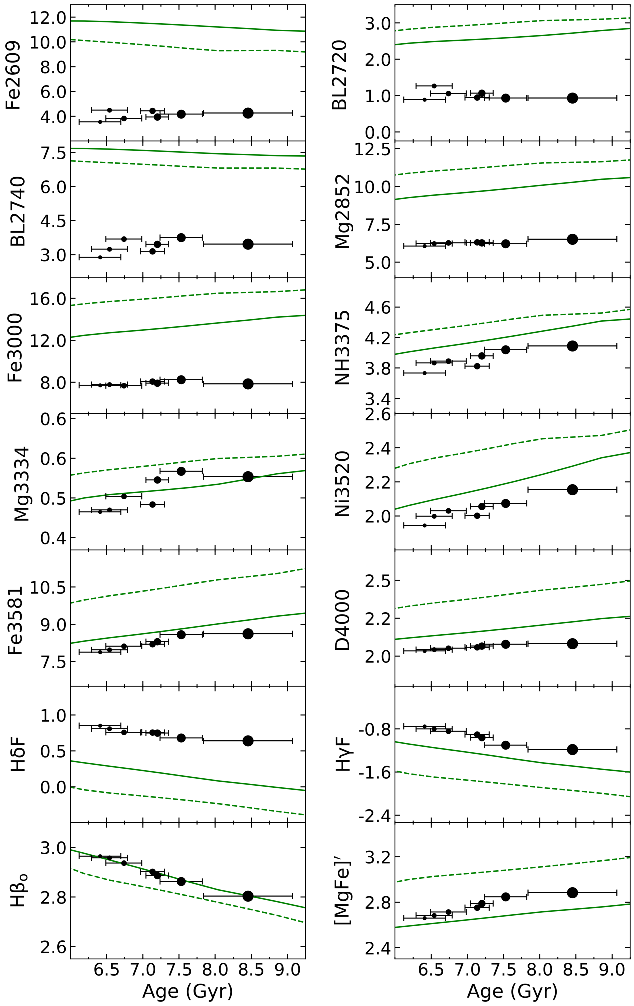

FIGURE 3.4— **BOSS NUV and optical line-strength indices.** The panels show in green lines the behaviour of selected NUV and optical SSP model indices as a function of age, for two different metallicities ([M/H] = 0.0 (solar), solid lines; [M/H] = +0.22 (super-solar), dashed lines). The black solid dots correspond to the observed measurements of BOSS stacked spectra of massive ETGs. Both SSP models and data are convolved to a common velocity dispersion of $\sigma = 340\,\mathrm{km\,s^{-1}}$.

for a large number of realizations (N = 1000) to detect possible variations within sample selection for each bin. Different subsamples of the individual galaxy spectra in each bin are randomly selected, where a given galaxy can be selected more than once, and then stacked. The measured values in each realization create the index distributions shown in Figure 3.5. We approximated these distributions by a Gaussian function finding that the intrinsic variation within the index values is relatively small. We obtain a standard deviation of typically ~ 0.07 with respect to the median value of the index distribution. We have been very conservative by using the average of the 5th and 95th percentiles of the distribution in the index uncertainties instead of the standard deviation, in order to include a significantly wider range of possible index values. This value is added in quadrature to the intrinsic error of the indices measured on the stacked spectra.

3.5 Results

The *2SSPs* and *1SSP+cSFR* modelling approaches are compared with the stacked spectra by fitting 14 absorption line indices via the MCMC technique explained in Chapter 2 to estimate the young stellar contribution in massive ETGs. For this scientific case, we performed 10000 model realizations, for both model approaches, sampling the probability distribution for each parameter through 100 walkers that explore the parameter space. We also tried a larger number of realizations (50000) but it is computationally much more expensive and the results are exactly the same.

3.5.1 2SSPs approach

As explained in Section 2.3, the *2SSPs* model assumes that the spectrum of a massive ETG comprises two individual SSPs, with appropriate weights. For the present case, we do not permit ages larger than the age of the Universe at the mean redshift (i.e. 9.4 Gyr at $z \sim 0.4$) for the old stellar component. By applying the MCMC we realised that the metallicity of the young component for the *2SSPs* approach cannot be properly constrained, as explained in Section 2.3. Therefore, we fixed the metallicity of the young component at solar ([M/H] = 0.0), so that this is a 4-parameter instead of a 5-parameter model. By adopting this value, the best-fitting parameters do not show any difference due to their insensitivity to the metallicity of the young component.

These best-fits require a combination of a small but detectable mass fraction in young stars (< 1 Gyr) on top of an old component, which increases towards lower velocity dispersion. Panels of Figure 3.6 show the derived young mass fractions and their MLWA as a function of σ, suggesting that massive ETGs

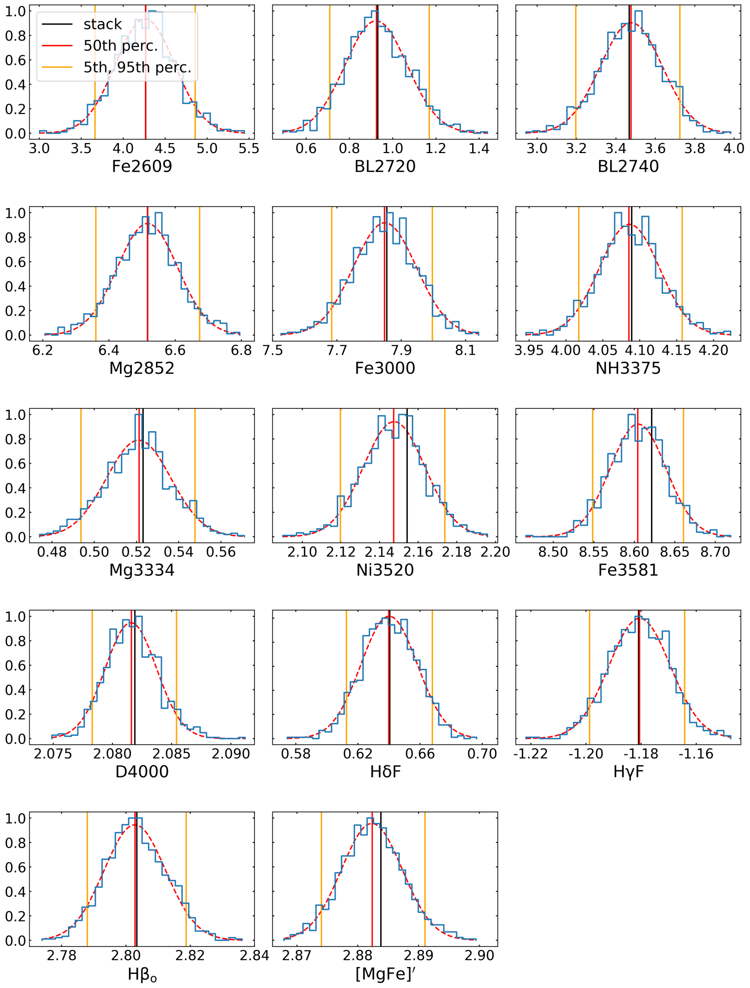

FIGURE 3.5— **Bootstrap index distributions.** Each panel shows the index distribution for 1000 resampling realizations normalised to 1. Red dashed line shows the Gaussian fit of each index distribution. Black and red solid lines indicate the index values from the stack and the median of the distribution, respectively, and orange lines represent the 5th and 95th percentiles of the distribution, which have been included as uncertainties in each index.

at z ∼ 0.4 have small mass fractions of young components, between 0.09% and 0.15%, decreasing with increasing stellar mass. The average young age also shows a trend with velocity dispersion, from 109 Myr at the lowest σ stack to 65 Myr in the most massive galaxies. Results and summarised in Table 3.2. The best-fitting indices, shown as red stars in Figure 3.7, show very good agreement with the observations.

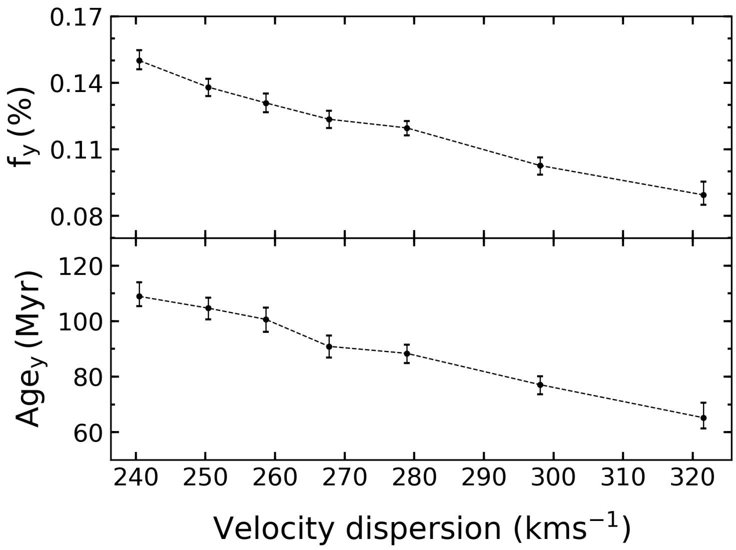

FIGURE 3.6— **Young stellar population results of *2SSPs* model.** Best-fitting results from the *2SSPs* modelling approach as a function of the velocity dispersion of each stacked bin. Top panel shows the estimated mass fractions of young stars of ages showed in the lower panel.

In Figure 3.8 we show the sampled probability distribution functions (PDFs) as histograms and the two-dimensional contours between each pair of fitted parameters of an intermediate velocity dispersion bin that result from the MCMC fitting process (they show 50000 model realizations in order to better populate the contours and simplify their visualization), which represent the joint PDFs between a given pair of parameters. Note that the PDF of the age of the old stellar component is truncated at the maximum age we allowed 9.4 Gyr, which

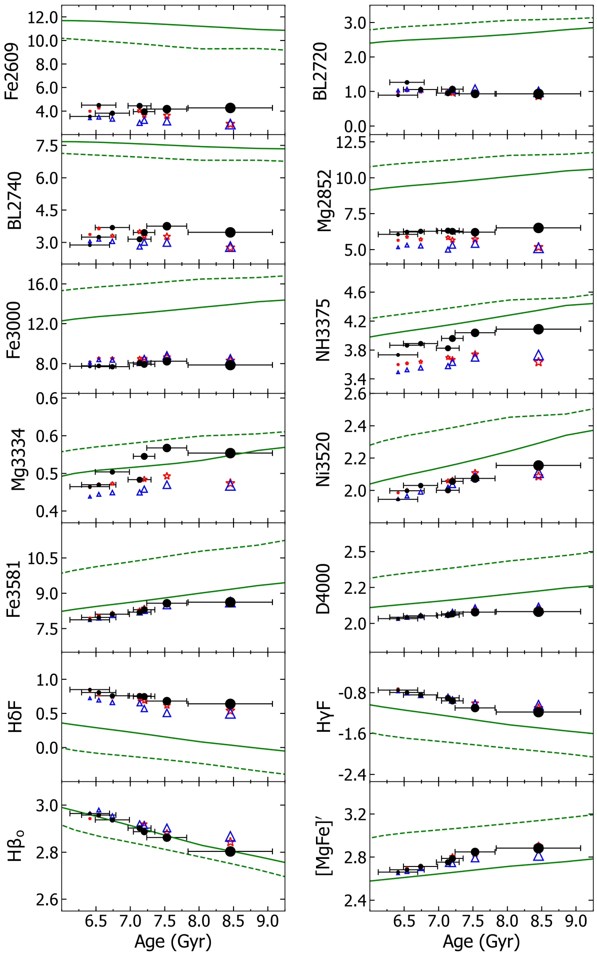

FIGURE 3.7— **Best-fitting NUV and optical line-strength indices.** The panels show the behaviour of selected NUV and optical spectral SSP model indices as a function of age, for two different metallicities following the same colour code. Red stars indicate the best-fitting *2SSPs* model predictions, that assume a superposition of an old and a young component, and blue triangles show the best-fitting *1SSP+cSFR* model predictions, that models the young component as a composite population with constant SFR between 6.3 Myr and 2 Gyr. Error bars on the black dots indicate the 1σ uncertainty on the index measurements. The impact of very small fractions of young stars on the NUV indices, with respect to a single SSP model, is significant. In contrast, the optical indices are mainly unaffected by these residual populations. The SSP models and data are convolved to a common velocity dispersion of $\sigma = 340\,\mathrm{km\,s^{-1}}$.

is the age of the Universe at the average redshift of our BOSS galaxy sample (z ∼ 0.4). We do not expect an age of the old stellar population older than the age of the Universe at that redshift. Contours between the age and the young mass fraction reveals the degeneracy between these two parameters, as expected from the well-known burst-age – burst-strength degeneracy.

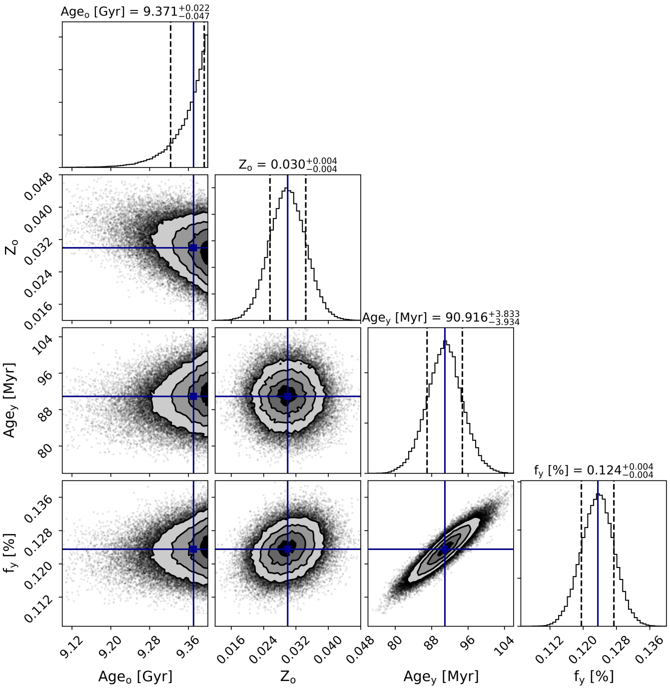

FIGURE 3.8— **MCMC probability distribution functions.** Each panel shows the PDF of an intermediate velocity dispersion stack (250 − 260 km s^{-1}) of the 4 model parameters of the *2SSPs* approach. From the top to the bottom: age and metallicity for the old component, and age and mass fraction of the young component. Upper panels show the PDF for each parameter marginalised over the other parameters. Contours show the two-dimensional projections between all parameters. The solid lines indicate the medians of each distribution. We assume as uncertainties the 16 and 84 percentiles shown with dashed lines.

The *2SSPs* best-fitting model spectrum for the highest velocity dispersion stack is illustrated in the top panel of Figure 3.9. The solution only requires 0.09% in mass of a young (∼65 Myr) component, in addition to an old population, to match the stacked spectrum reasonable well. This is indicated by the ratio in the bottom panel of the figure. Note that this ratio does not represent residuals from a full spectral fitting of the whole spectrum, rather it comes from fitting the 14 line strengths simultaneously.

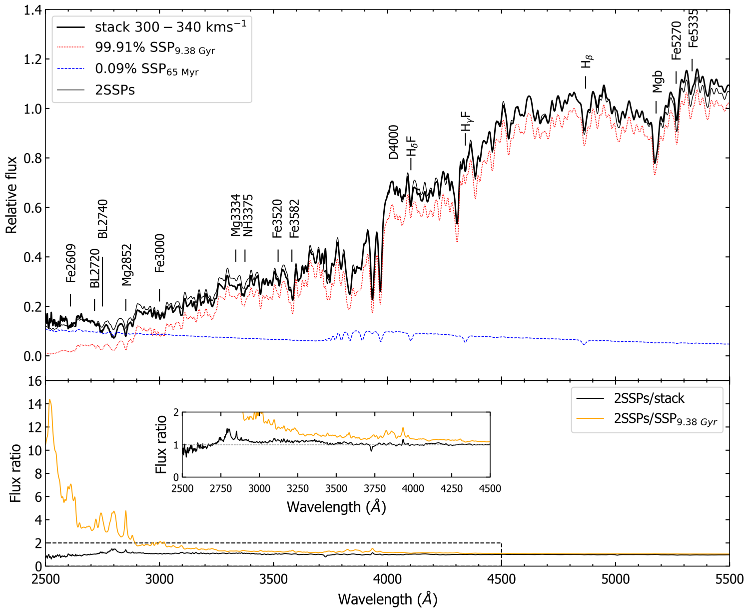

FIGURE 3.9— **2SSPs best index fit spectrum.** Top panel shows the stacked spectrum with the highest velocity dispersion range (thick black line). Overplotted is the *2SSPs* model (thin black) that best fits the 14 indices (Figure 3.7). The main purpose of this figure is to illustrate the relative effect of the young component as a function of wavelength but note it does not represent a full-spectrum fit. The *2SSPs* model can be split into the young (65 Myr) component (blue dashed) which contributes a 0.09% mass fraction, and the old (9.38 Gyr) dominant population (red dotted). Bottom panel shows the ratio between the *2SSPs* best-fitting model with the stacked spectrum (black) and with a pure old SSP model of 9.38 Gyr (orange). The inset subplot shows the flux ratio of the dashed box in more detail.

For comparison, we also show the ratio between the *2SSPs* and a pure old

SSP model spectrum in the lower panel, to clearly illustrate how this ratio is much higher in the NUV range than the ratio between the *2SSPs* best-fit and the stack. This suggests that the observed spectrum it is not well-resembled, especially to the bluer spectral regions, by a pure old SSP and requires an additional young component. Note the significant impact of such a small fraction of the young component in the composite *2SSPs* spectrum at NUV wavelengths, which dominates the total flux budget at $\lambda \lesssim 3000$ Å. In the optical range, this young contribution has an insignificant effect and the main contribution comes from the dominant old stellar population.

The *2SSPs* model is a simple representation of the real SFH of ETGs, which is valid for parametrising the young component from the NUV range. As a consequence, some differences are expected between the real spectrum and the best-fit. It is important to emphasize that we do not use all the information present in the spectrum, and therefore some residuals are to be expected. This is particularly true at those wavelengths that are strongly affected by, for example, abundance issues as reflected in the regions of the Mg2800 and Mg2852 features since the models used are scaled-solar so the alpha-enhancement of ETGs is not taken into account. Note that Mg2800 index is not included in the fitting process because it is also affected by chromospheric emission. Also, some emission appears in [OII] 3727 Å line. Note also that the S/N decreases towards the bluest end of the spectrum, which is reflected in the increasing wiggles (residuals) in this spectral region.

3.5.2 Constant recent star formation approach

Next, we confront the observed index-strengths with the predictions of the *1SSP+cSFR* approach. We tested different age intervals and found that limiting the duration of constant SFR between 6.3 Myr and 2 Gyr gives the best fit to the data. However, the results do not change significantly when varying the upper limit down to 1 Gyr (although the χ^2 becomes slightly worse). The best-fitting results for the young mass fractions are shown in Figure 3.10 and summarised in Table 3.2. We find that the contribution from the young stellar populations formed between 6.3 Myr and 2 Gyr is 0.48% at the highest velocity dispersion, weakly increasing towards the lower mass stacks, up to 0.58% for the lowest velocity dispersion stack. Note that although small, the increasing trend is significant in terms of light contribution to the NUV spectrum. From this we determine a specific SFR (sSFR) of $\sim 2.6 \times 10^{-12}$ yr^{-1} averaged across all bins. The *1SSP+cSFR* best-fitting indices are shown as blue triangles in Figure 3.7.

We are dealing with very old galaxy spectra that have very old mean stellar ages (from 6 to 8.5 Gyr towards the most massive bin) and therefore the

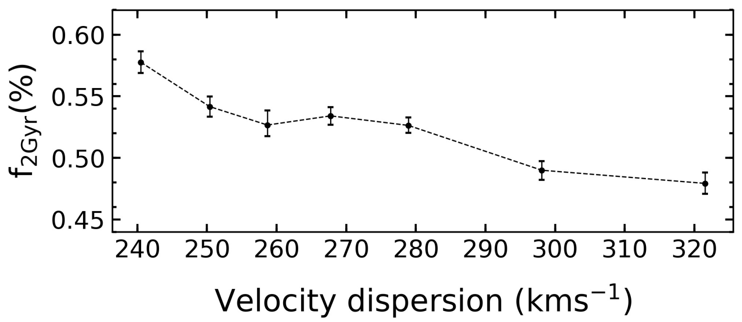

FIGURE 3.10— **Young stellar population results of *1SSP+cSFR* model.** Best-fitting results from the *1SSP+cSFR* modelling approach as a function of the velocity dispersion of each stacked bin. The panel shows the estimated mass fractions of young stars formed in the last 2 Gyr.

intermediate populations have very little contributions to the total light. Note that all but the tiniest mass fractions of intermediate-aged stellar populations resulting from varying star formation histories would be obvious in the optical range, affecting age-sensitive indices like Hβ_o (as happens to the simulated galaxies as we will show in Section 3.7.3).

3.5.3 Effect of the alpha-abundances on the indices

The observed indices are perfectly fitted with the predicted values from the *2SSPs* model, except three indices: Mg2852, Mg3334 and NH3375. These indices are slightly affected by the overabundance of alpha-elements in ETGs. NH3375 is affected by the Nitrogen abundance (Serven et al., 2011). The other two indices are influenced by Mg (alpha). Both elements are found to be enhanced with respect to the solar-scaled abundance pattern in massive ETGs as previously shown in the literature. The deviation shown between the best-fitting solutions and the observed values increases with velocity dispersion. Such a result is expected from the well-studied correlation between Mg and σ in that Mg strongly increases with σ (Vazdekis et al., 2004). However, the models used here are scaled-solar and there are no empirical stellar population models available in the literature with non scaled-solar alpha-abundances covering the UV range. When excluding these indices, the best-fitting results do not change significantly, but the χ^2 slightly decreases, as expected, because now the dif-

σ (km s^{-1}) (1)	Age (Gyr) (2)	[M/H] (3)	Age$_o$ (Gyr) (4)	[M/H]$_o$ (5)	Age$_y$ (Myr) (6)	f$_y$ (%) (7)	f$_{2Gyr}$ (%) (8)
220-230	6.6±0.2	-0.008±0.009	$9.35^{+0.04}_{-0.08}$	$-0.013^{+0.004}_{-0.004}$	109^{+5}_{-4}	$0.150^{+0.005}_{-0.004}$	$0.58^{+0.01}_{-0.01}$
230-240	6.8±0.2	-0.003±0.008	$9.37^{+0.02}_{-0.05}$	$-0.010^{+0.004}_{-0.004}$	105^{+4}_{-4}	$0.138^{+0.004}_{-0.004}$	$0.54^{+0.01}_{-0.01}$
240-250	7.2±0.4	-0.005±0.015	$9.38^{+0.02}_{-0.03}$	$-0.004^{+0.004}_{-0.004}$	101^{+4}_{-4}	$0.131^{+0.004}_{-0.004}$	$0.53^{+0.01}_{-0.01}$
250-260	7.3±0.1	0.014±0.004	$9.37^{+0.02}_{-0.05}$	$0.030^{+0.004}_{-0.004}$	91^{+4}_{-4}	$0.124^{+0.004}_{-0.004}$	$0.53^{+0.01}_{-0.01}$
260-280	7.2±0.2	0.03±0.01	$9.38^{+0.01}_{-0.02}$	$0.052^{+0.004}_{-0.004}$	88^{+3}_{-4}	$0.119^{+0.004}_{-0.004}$	$0.53^{+0.01}_{-0.01}$
280-300	7.8±0.3	0.05±0.01	$9.38^{+0.02}_{-0.03}$	$0.082^{+0.005}_{-0.005}$	77^{+3}_{-3}	$0.103^{+0.004}_{-0.004}$	$0.49^{+0.01}_{-0.01}$
300-340	8.6±0.5	0.05±0.02	$9.38^{+0.02}_{-0.04}$	$0.095^{+0.006}_{-0.006}$	65^{+5}_{-4}	$0.089^{+0.006}_{-0.005}$	$0.48^{+0.01}_{-0.01}$

TABLE 3.2— **General properties and best-fitting parameter results of the BOSS stacked spectra**. They are shown with respect to the velocity dispersion range of the stacks (Col. 1). Col. 2 and 3 is the MLWA and metallicity derived from the Hβ_o and [MgFe]' indicators. Col. 4 and 5 show the SSP age and metallicity of the old component. Col. 6 and 7 show the stellar mass fraction and age of the young component of the *2SSPs* model. Col. 8 is the young mass fraction following the *1SSP+cSFR* approach, with a constant SFR to describe the young component.

ferences between data and models are lower, improving the quality of the best fit.

Although we cannot quantify properly the effect of varying the abundances, as no such models are currently available in the UV, it is worth showing these indices despite they are not perfectly fitted, not only because they also show a deviation with respect to a pure old SSP model, but also the best fits show the expected mismatch. For example, Mg3334 would get stronger when increasing the [Mg/Fe] abundance ratio. It is worth pointing out that the UV continuum flux of a stellar population increases with increasing alpha abundance. If alpha-enhanced models are used for massive ETGs with alpha-enhanced stellar populations, the young mass fractions would represent a lower contribution than those found here, since the models used here are scaled solar. Therefore, alpha enhancement would affect the results by slightly decreasing the derived young stellar mass fractions. However, there are no empirical stellar population models in the literature with alpha-abundances covering the NUV spectral range that can be used to explore how these indices are affected. Producing reliable alpha-enhanced models in the UV is extremely challenging, even though this possibility is currently being explored by the stellar population modelling researchers.

3.5.4 Uncertainties on the estimated young mass fractions

We have tested that the measured young mass fractions we find are not biased by a small fraction of ETGs that may have recently experienced some star formation event. For this purpose, we defined two criteria to select those galaxies with strong emission in Hβ_o and [OII] lines, coming from newly formed massive stars: Hβ_o <0 and [OII]5007/[OII]4959 $\sim$ 3. We found that a very small fraction of galaxies (only $\sim$ 0.5% on average for all the stacks) has significant emission in those lines. To guarantee that these galaxies are not biasing the results, we repeated the fitting process by excluding these targets from the stacking procedure. The young mass fractions turned out to be the same as those obtained for the whole sample. Therefore, we conclude that our estimates for the young stellar component mass fractions are typical for the whole population of massive ETGs at z $\sim$ 0.4, confirming the robustness of our results.

As a check, we performed the fits when changing the upper prior of the age of the old stellar component to the age of the Universe, 13.5 Gyr for the *2SSPs* approach. We find that the mass fraction and age of the young component for the most massive bin fit has changed from 0.10% to 0.11% and from 70 to 77 Myr, respectively. For the least massive bin the young mass fraction has changed from 0.15% to 0.19%. These variations are small although the old component is ∼4 Gyr older than before, when the upper limit for the age was left free up to 9.4 Gyr. This can be understood as a stellar population older than 7 Gyr affects fundamentally the optical region of the spectra and not the NUV where the young population (<1 Gyr) is the major contribution. In other words, the small fractions of young components we find are more strongly reflected in the NUV spectral features.

We have also explored how the results vary when adopting a more restrictive prior, which now corresponds to the MLWA inferred from the Hβ_o – [MgFe]$'$ line-strengths in Section 3.3. We note that it would be inconsistent and unphysical for the prior for the old component to be younger than the MLWA. This corresponds to 8.6±0.5 Gyr and to 6.6±0.2 Gyr for the most and least massive stack, respectively. These results are shown in orange in Figure 3.11. Estimates from the *2SSPs* model show differences when varying the prior. Although the trend is preserved, it is less prominent, with young mass fractions lower than 0.1% in all mass bins, since the less massive stacks have younger stellar ages than the most massive stacks. In addition, the quality of the best-fits has decreased considerably. In particular, for the less massive bins where the reduced χ^2 is 2.5 times higher than the one from the best-fits with a 9.4 Gyr prior. We also obtain lower young component ages, an effect of the burst age – burst strength degeneracy, which does not affect the *1SSP+cSFR* model.

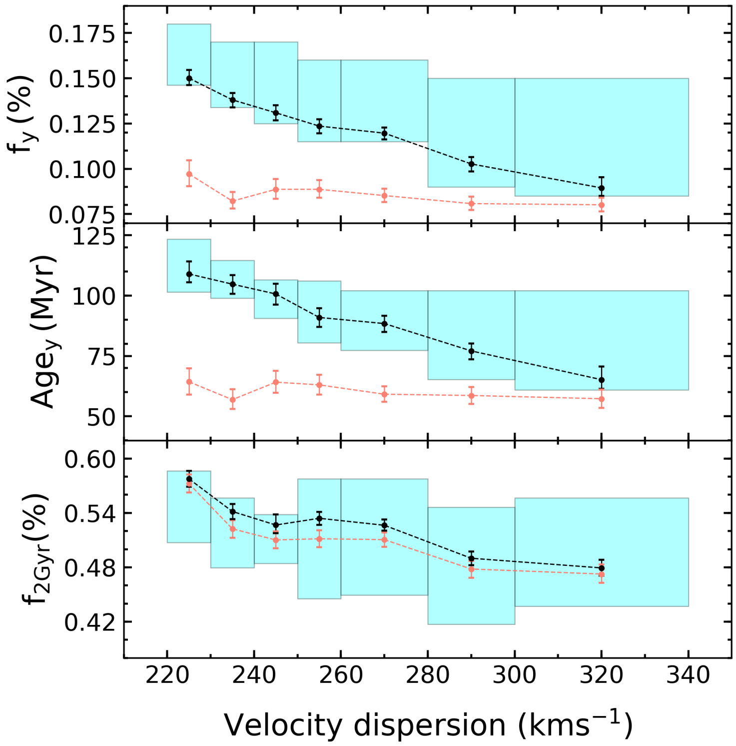

FIGURE 3.11— **Variation on the best-fitting results according to different fitting tests.** Results from the *2SSPs* (top and medium panels) and *1SSP+cSFR* (bottom panel) modelling approaches as a function of the velocity dispersion of each stacked bin. Results from the *2SSPs* approach (top and medium panels) and 1SSP+cSFR (bottom panel) modelling approaches for different upper priors of the age of old stellar component: age of the Universe at z$\sim$0.4 (black), mean luminosity-weighted age of each sigma bin (orange). The figure shows that the *1SSP+cSFR* is robust against our choice of prior for the old component. Blue areas show the range of solutions when varying the weights of the optical and NUV set of indices from 100% to 0% in the χ^2 minimization with the index uncertainties at the 1$\,\sigma$ level.

Interestingly, we find that the results from the *1SSP+cSFR* model do not experience significant variations when the upper prior of the age of the old component is shifted to ages younger than 9.4 Gyr (i.e. setting the prior on the old component to the youngest possible age which is the MLWA). This is because it is only stellar populations with ages < 2 Gyr that fundamentally contribute to decrease the NUV line-strengths. Therefore, the mass fractions of stars formed in the last 2 Gyr are mostly independent of intermediate and old age stellar populations, which make these results very robust.

Additionally, another source we took into consideration when presenting the results comes from varying the relative weights of the NUV and optical spectral indices in the fitting process. Note that this is not regarded as an uncertainty, but we want to show the change in the results when one lacks indices from one or another spectral range, since they allow us to explore a much wider range of possibilities. Thus, we explore how the best-fitting results change by separating the χ^2 statistic at 3400 Å, slightly rescaling the error bars so that each set of indices above and below that wavelength has a given weight on χ^2. We varied the weights from 100% to 0% in the χ^2 minimization within the index uncertainties at the 1σ level. This allows us to be extremely conservative. The variation is shown by the blue shaded areas in the Figure 3.11. In most cases, the largest differences with respect to the reference solution in the derived values is obtained when giving more weight to the NUV indices, due to their age degeneracy. We find that by giving 100% weight to the NUV indices our solutions become more degenerate and the trend with velocity dispersion is less clear, something that does not occur when giving 100% to the optical range. The latter is expected as described in Chapter 2. The optical galaxy spectrum is contributed by several types of stars and therefore some of the optical indices, such as the Balmer lines, may be used to trace small amounts of young stars, given the high S/N of our stacked spectra.

3.5.5 Exponentially declining SFH (a ”tau” model)

We investigated the results from another parametrization of the SFH for the most massive spectra adopting an exponentially declining SFH by varying the declining time τ ranging from 0.1 and 2 Gyr, in which the SFR at each evolutionary epoch has this form:

$$SFR(t) = exp(-t/\tau) \tag{3.1}$$

This SFH is characterised by one single burst of star formation in the past. It represents the formation of the bulk of the stellar populations of ETGs at high redshift. The SFH model templates are generated with the E-MILES models where a Kroupa IMF and solar metallicity are assumed. The stacked spectral indices are compared to the SFH model predictions. We use the best-fitting template to obtain one estimate of the stellar mass formed in the last 2 Gyr. The best-model shown in the Figure 3.12 is defined by $\tau = 1.2$ and leads to 0.57% of stars formed in the last 2 Gyr, which means that the specific star formation rate is $2.9 \times 10^{-12}\,\mathrm{yr}^{-1}$, matching that derived from the *1SSP+cSFR* modeling that is, on average for all the stacks, $2.6 \times 10^{-12}\,\mathrm{yr}^{-1}$. Hence, our results regarding the mass fraction contribution of youngest populations are very robust with respect to the assumed parametrization of the SFH. According to these findings, we conclude that our two modelling approaches assumed *2SSPs* and *1SSP+cSFR*, where the old component is a unique SSP in both cases, are a reasonable representation of the SFH of a massive ETG, for the purpose of determining the fraction of very young stellar populations.

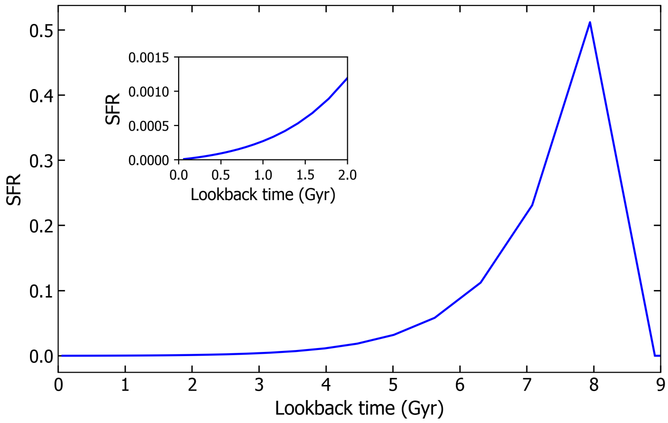

FIGURE 3.12— **Exponentially declining SFH.** Best-fitting star formation history template with the shape of an exponentially declining SFH, SFR(t) = exp(-t/τ), with $\tau = 1.2$. The inset shows the SFR in the last 2 Gyr. The cumulative mass fraction of the stellar populations formed in the last 2 Gyr is 0.57%.

Note that such a modelling approach does not account for any recycled material from stellar evolution and these fractions would change if the recycled material was included, since the best-fitting declining time τ would be lower than 1.2. The *2SSPs* and *1SSP+cSFR* approaches only parameterise the mass fractions of some periods of time of the SFH of a galaxy, and whether these stars come from pristine or recycled material cannot be derived from this work.

3.6 Testing other SSP models

The E-MILES models used throughout this thesis are the only ones in the literature based on fully-empirical stellar libraries that cover the UV spectral range for a wide range of stellar population parameters. The best-fitting models not only match reasonably well with the observed absorption features (Figure 3.7) but also with the stacked spectra (as shown in Figure 3.9). However, we also have investigated how the results change when using different SSP models. Despite the fact that they are not publicly available, we appreciate very much that Gustavo Bruzual kindly provided us a new version of Bruzual & Charlot SSP models (hereafter, BC2019) extended to the UV range. Vidal-García et al. (2017) employed these models to study the relation between star-forming galaxies and ISM through UV-indices.

We employed the Kroupa IMF SSP models based on PARSEC isochrones to be as consistent as possible with the set of E-MILES models used here. We performed various tests applying the same methodology to obtain results and analyse the differences with respect to E-MILES. For reference, a comparison between model predictions for the two bluest and reddest indices is shown in the Figure 3.13. BC2019 models lead to mean luminosity-weighted ages for the stacks 1.5 – 2 Gyr younger than the ages obtained with the E-MILES models from the optical indicator Hβ_o. The NUV indices remain weaker with respect to the BC2019 1SSP model predictions.

As a check, we use the BC2019 models and apply precisely the same methodology as for E-MILES set of models (i.e. fitting the 14 line-strength indices with the *1SSP+cSFR* model approach). We obtain slightly larger mass fractions of stars formed in the last 2 Gyr than with EMILES models. However, we note that the fractions remain below 1% and we still find a trend with velocity dispersion (that ranges from 0.78% to 0.95% at lower mass stacks.) These differences are a consequence of the fact that we derive younger ages for the old component using BC2019 models. However, the BC2019 models provide much poorer fits to the data, the reduced χ^2 increases considerably ($\chi^2 \sim 50$) in comparison to the $\chi^2 \sim 4$ we obtain with the E-MILES models.

We also have explored how much the young mass fraction changes with the *2SSPs* and *1SSP+cSFR* modeling approach, when fixing the parameters at the best-fitting solutions obtained with E-MILES models and only having the young mass fraction as a free parameter in the fit. These young mass fractions are 0.10% and 0.05% higher for the least and most massive bins, respectively, for the *2SSPs* approach, but decrease the quality of the fit by a factor of 10 – 100 in terms of the reduced χ^2. For the 1SSP+cSFR approach, with an age of 9.4 Gyr for the old component, the fractions of stars in the last 2 Gyr vary from 0.73%

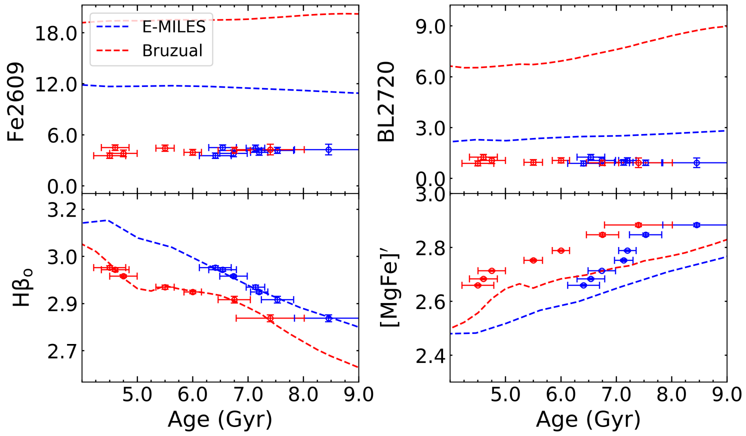

FIGURE 3.13— **Index comparision between E-MILES and BC2019 SSP models.** Comparison between E-MILES (blue) and BC2019 (red) model predictions for two NUV (Fe2609 and BL2720) and two optical ($H\beta_o$ and [MgFe]′) indices. Dashed lines show the 1SSP indices as a function of the age for solar metallicity. Open symbols correspond to the observed measurements of BOSS stacked spectra as a function of the derived mean luminosity-weighted age derived from each set of models.

to 0.88% to lower masses.

3.7 Discussion

3.7.1 Star formation not completely suppressed in massive ETGs

At present, the physical processes involved in the residual star formation activity found in massive ETGs are not well understood. It is known that feedback mechanisms must be invoked to prevent protracted star formation in massive galaxies. Such extended SFHs are expected from a naive connection between dark matter growth and stellar mass growth in a hierarchical context. Feedback will alter this connection, by preventing the infalling gas from cooling and forming stars. Physical mechanisms such as AGN activity and type Ia supernovae are known to influence the SFR in massive galaxies (Gabor et al., 2010). Supernova feedback is not thought capable of driving this phenomenon by itself to produce quiescent galaxies (Springel et al., 2005). AGN feedback provides a plausible solution, as proposed by numerical simulations that suggest it is the most likely process by which the available cold gas is heated and expelled by their energetic jets in massive ETGs (Schawinski et al. 2006; Dubois et al. 2013), preventing the star formation in the galaxy. These processes are more effective in the most massive systems, agreeing well with our results, where the fraction in young stars is anti-correlated with the stellar mass of the galaxy. However, our findings also show that quenching mechanisms are not able to completely stop star formation in the central regions of ETGs, even in the most massive galaxies, at the observed stringent levels. Therefore, additional processes must be present to control the cold gas supply that results in the formation of new stars at late times in massive ETGs. Cold gas has been found in atomic and molecular form in various samples of ETG (Welch et al., 2010), a result that has been connected to the SFH over the last few Gyr (Young et al., 2014).

From photometric studies has been shown that the residual star formation in ellipticals correlates strongly with velocity dispersion, where lower velocity dispersion galaxies contain higher recent star formation (Schawinski et al., 2006), in perfect agreement with our findings. We find that there is a strong anti-correlation between the derived mass fractions and ages of the young stars with velocity dispersion, with an Spearman's correlation coefficient of -0.98 and -0.96, respectively, which reflects that the derived young stellar population parameters are highly connected with the velocity dispersion (i.e. mass) of ETGs. Negative values indicate that when velocity dispersion increases, both young mass fractions and ages decrease, as seen in Figures 3.6 and 3.10.

3.7.2 Robustness of our SFH parametrizations

We would like to emphasize the appropriateness and the robustness of the *1SSP+cSFR* approach, since the mass fractions of stars formed in the last 2 Gyr that we estimate are mostly independent of intermediate and old age stellar populations. This approach represents better the most recent tail of the SFH of a massive ETG than the *2SSPs* model. Moreover, this approach is insensitive to the effects of the burst age – burst strength degeneracy characteristic of stellar populations younger than 1 Gyr, which on the other hand has a large impact when the young component is represented by a single burst model. For a younger old stellar component, a lower mass fraction of the young component is required and, as a consequence, a younger young stellar population. However, this does not come out from the *1SSP+cSFR* approach.

We note that our results only constrain the fraction of stellar populations below 2 Gyr, which is the main goal in this work. We do not attempt to constrain the shape of the SFH of intermediate-ages (i.e. between 2 and 6 Gyr). However, for SFHs such as those inferred from detailed optical studies, which are reproduced to some extent by the τ-model shown, the contribution from the stellar populations in this intermediate-age regime is sufficiently small such that they do not alter the line-strength indices in the optical range. Therefore, they do not contribute to a major dilution of the NUV indices. The results of such extended SFHs would not match the Hβ_o vs. [MgFe]$'$ diagram. The existence of such populations would contribute to lower the fraction of younger populations inferred.

3.7.3 Contrasting with EAGLE numerical simulations

Numerical simulations of galaxy formation help to understand the role of the complex physics at play. Our observational results are compared with numerical, cosmological simulations to explore our findings. We employ the publicly available database from the high-resolution cosmological hydrodynamic modelling from the EAGLE simulation project (Schaye et al. 2015; McAlpine et al. 2016), that consists of catalogues of galaxies extracted from cosmological, hydrodynamic simulations.

The EAGLE simulation

The EAGLE model of galaxy formation, includes a pressure law for star formation (Schaye & Dalla Vecchia, 2008), line cooling in photoionisation equilibrium(Wiersma et al., 2009a), stellar evolution (Wiersma et al., 2009b), thermal supernova feedback (Dalla Vecchia & Schaye, 2012) and massive black hole growth and feedback (Rosas-Guevara et al., 2015). An extensive description of the model, its calibration and the hydrodynamic solver are given in several works (Schaye et al. 2015; Crain et al. 2015; Schaller et al. 2015).

The EAGLE simulation used here reproduces several global relations of observed galaxies at the current epoch and earlier redshifts. It consists of a cosmological cubic volume with 100 comoving Mpc on a side, and contains 2×1504^3 dark matter and baryon particles. The initial conditions have been evolved from z = 127 to z = 0. The standard database provides most of the global properties of simulated galaxies, whereas we use the full particle data to compute the rest frame integrated spectra, line-of-sight velocity dispersions and SFHs of the synthetic galaxies.

Simulated ETG spectra at z∼0.4

We use the snapshot at redshift z = 0.365, which is the closest in time to the observed median redshift of the BOSS galaxies. The luminosities are computed following a method similar to that used by the EAGLE team (Trayford et al., 2015), but employing the same E-MILES spectral library of the observational analysis. Fluxes from single SSPs are associated with each stellar particle in the simulation, which are characterised by their initial mass, metallicity and age. We avoid any extrapolation outside of the metallicity and age range of the population synthesis model by limiting the metallicities and ages of the simulation data. We include the effect of intrinsic dust attenuation following the standard modelling (Trayford et al., 2015), but normalising the extinction law with the surface density inside the stellar half-mass radius, of heavy elements in the gas with hydrogen number density above $\sim$0.1 cm^{-3}, instead of the gas total mass. This prescription produces reasonable attenuation values over a wide range of stellar masses and is compatible with the observational constraints of attenuation in massive ETGs. Following the EAGLE team methodology, recent (<100 Myr) star formation is resampled with finer time intervals, alleviating the effects of stochasticity of the star formation model.

All spectra are computed within a three-dimensional aperture of 10 kpc for a better comparison with the observed stacks. We compute the mass-weighted stellar velocity dispersion along the line of sight within a cylindrical aperture of 10 kpc. Finally, we extract the SFHs of each galaxy in the sample by binning the initial stellar mass of the SSPs as a function of their formation time in bins of 50 Myr and retrieve from the database the mass-weighted age of the galaxies.

The EAGLE simulation targets average density environments, typical of those inhabited by BOSS galaxies. To create a simulated sample whose properties should be compatible with those of our stacked spectra, we applied the BOSS colour criteria and selected EAGLE galaxies within our σ range. From the set of 3186 EAGLE galaxies with stellar mass above 10^{10}M$_\odot$, only 26 galaxies satisfy those criteria, suggesting that the simulated galaxies are generally bluer than the BOSS galaxies for a given mass. Their optical Hβ_o and [MgFe]$'$ indices indicating substantially younger MLWAs than those derived from the stacks (Figure 3.14). For this reason, with the exception of the two objects that match the data – which also happen to be the oldest –, simulated galaxies are excluded when applying the colour cut (g-i) >2.35 due to their young ages. Figure 3.14 also illustrates the SFHs of a young and an old simulated galaxies in panels a) and b), respectively. Clearly, the younger galaxy has a more extended stellar age distribution and contains more intermediate stellar populations than the older galaxy and, as a consequence, Hβ_o is stronger in the younger galaxy. Observations indicate that massive ETGs formed the bulk of their stellar populations at earlier epochs without a significant component of intermediate and young age stars, in sharp contrast with the simulations, which overproduce recent star formation. Hence, the SFHs of our stacked spectra should broadly resemble the one shown for the old simulated galaxy. The mass fraction in young stars formed over the last 2 Gyr from the SFHs of the two EAGLE galaxies that best compare with the observations are 9.23% and 0.07%, from left to right in the grid plot.

We also have mass-weighted ages directly from the EAGLE simulations, but here we want to be consistent and obtain the MLWAs using the same methodology that we apply to the BOSS stacks, i.e. using the Hβ_o and [MgFe]$'$ absorption features from their integrated spectra. A strong aspect of this analysis is that we are doing the same as we do in the observational plane, as we want to do it consistently and, in this particular case, it is not sufficient to take an age from the simulation and compare with the observations, if they are not obtained in the same way.

An important source of uncertainty in the present work is the lack of simulated galaxies with SFHs resembling the observations. Only one simulated galaxy appears to approach the behaviour of the BOSS galaxies, in terms of young mass fractions. This result urgently needs to be better understood with a larger sample of simulated massive galaxies. Therefore, our results suggest a revision of how numerical models control feedback and the baryonic processes of galaxy formation in massive BOSS-type galaxies. The observations presented here provide the most stringent limits on recent star formation in ETGs to date and represent a key benchmark that theoretical models must satisfy in order to provide a more realistic description of galaxy formation and evolution.

Simulated massive ETGs are too blue

We have chosen to analyse the EAGLE simulations as they can reproduce basic properties of galaxy evolution (Furlong et al. 2015, 2017, Trayford et al. 2015, Crain et al. 2017), such as luminosity functions. However, Hill et al. (2017) show a correlation between luminosity-weighted age with mass for a much more significant sample of galaxies than in this work. Given our small sample size of simulated galaxies (26 galaxies), it is not fair to conclude any anti-downsizing for the EAGLE galaxies. However, we have looked at their stellar populations in a more detailed analysis by measuring their ages from two optical indices, Hβ_o and [MgFe]$'$. Our fundamental point is that, overall, the simulated galaxies are far younger than the observed data, except for only two candidates. Clearly, the youngest galaxy has a more extended stellar age distribution with more intermediate stellar populations than the oldest galaxy. We do not claim that massive EAGLE galaxies do not have old populations, but rather they have too extended SFHs, which yield much higher Hβ_o values than in the BOSS stacked spectra. The SFHs of our lowest mass stacked spectra should broadly resemble the one shown for the old simulated galaxy in Figure 3.14. The bulk of the stars of the most massive galaxy stack should, therefore, form at even higher

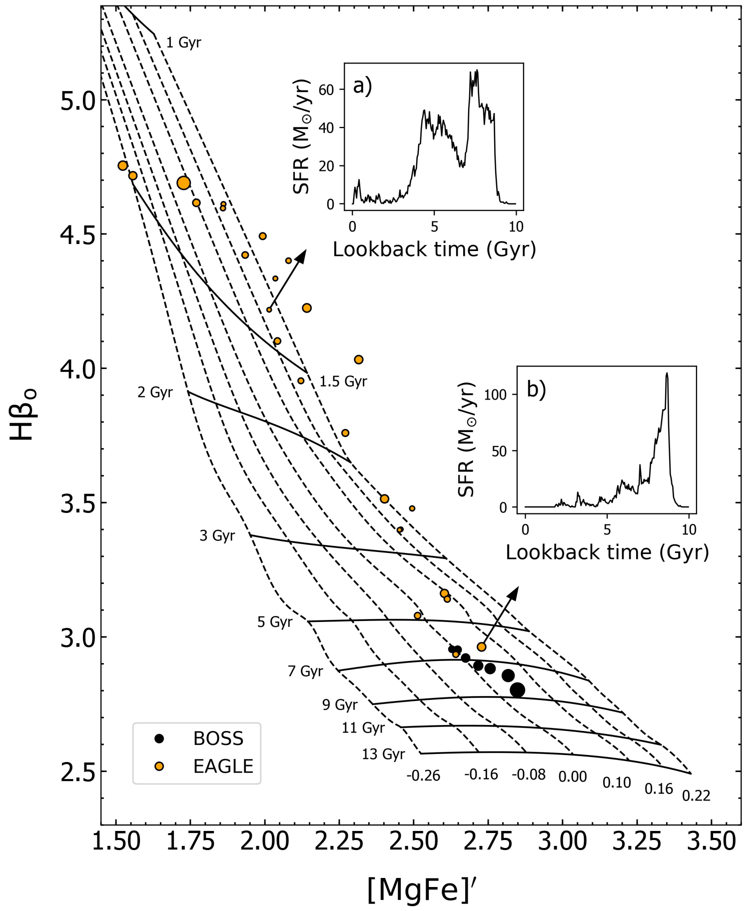

FIGURE 3.14— **Comparison with numerical simulations of galaxy formation.** Measurements of the age-sensitive spectral index $H\beta_o$ are plotted as a function of the total metallicity proxy [MgFe]′. The grid shows the model predictions over a range of SSP ages (solid lines) and metallicities (dashed lines), as labelled. The black dots are the observed BOSS index measurements, with dot size increasing with galaxy mass and uncertainties smaller than the point size. The orange dots represent synthetic galaxies from the EAGLE simulation, chosen to match the same selection criteria as in our BOSS data, except for the colour cut (g-i) > 2.35, that only is satisfied by the two simulated galaxies closest to the BOSS data indices. Their symbol size increases with galaxy mass. The figure also shows the SFHs of a young and old simulated galaxies, in panels a) and b) respectively, illustrating why most of the simulated galaxies have younger ages than expected from the BOSS data. The model grid and both simulated and observational spectra are smoothed to a common velocity dispersion of $340\,\mathrm{km\,s^{-1}}$.

redshift.

3.7.4 Other potential contributions

Contribution from hot-evolved stars

The NUV is not only sensitive to young stars but also to hot-evolved stellar components such as stars from the PAGB evolutionary stage (Le Cras et al., 2016), where the cores of stars are exposed and emit light in the UV. These stars may contribute to the NUV spectra of massive ETGs. We cannot exclude the possible contribution of PAGB stars due to our inability to distinguish between the two scenarios with our method.

As a test, we fit the data with models that combine an old SSP with the spectrum of a high temperature (Teff $\sim$ 10000 – 25000 K) star, which resembles a PAGB star. This yields a 4-parameter model, which are the age and metallicity of the old stellar population plus the temperature and the relative V-band light contribution of the hot-old stellar component. Note that in this case we derive light fractions in a given band instead of mass fractions. On average, a $\sim$3.8$\pm$0.07% light contribution in the V-band from a star with Teff $\sim$ 13600 K is required to fit the line-strengths, on top of an old component. This light fraction is substantially higher than the values predicted by the stellar evolution theory, in the framework of stellar population synthesis (Buzzoni 1989; Charlot & Bruzual A 1991; Conroy 2013) that predict significantly less than 1% of the flux in the optical V-band from the PAGB, i.e. much less than the requirements in our index fits.

Furthermore, the χ^2 values increase notably at lower masses for the PAGB model approach, with significantly higher values (by a factor of more than two at the lowest mass bin) with respect to the *2SSPs* models. We explore the Bayesian Information Criterion (Schwarz, 1978) (BIC) model selection criterion, which penalise models with larger number of free parameters, to choose between both models. Selecting the model with the lowest BIC values, one selects the young component model where the difference between both BIC values $\Delta\mathrm{BIC} = \mathrm{BIC}_{\mathrm{PAGB}} - \mathrm{BIC}_{\mathrm{2SSPs}}$ is $\Delta\mathrm{BIC} > 2$, except for the two most massive bins. Additionally, the obtained best-fitting temperature of Teff $\sim$ 13600 K is low, which corresponds to the first stages after envelope ejection, and a higher temperature is expected for this evolutionary stage of the stars. This is a extremely rapid phase, making it unlikely to contribute significantly. Furthermore, photometric studies that have analysed the NUV range of massive ETGs have found much higher NUV colours than those expected from these hot-evolved stars (Kaviraj et al., 2007).

Despite it cannot be robustly ruled out one model against the other, all these arguments favor that the decrease of the NUV absorption features with respect to those of an old SSP is likely due to a young population contribution rather than a hot-old PAGB stellar component. We conclude that even if these PAGB component was present, it has to be sub-dominant with respect to the very young stellar population we detect. Our inferred young mass fractions, albeit upper limits, are not affected substantially by a PAGB-like stellar population component. Thus, it is fair to state that, given the possible presence of PAGB stars, our results represent an upper limit for the young contribution.

NUV indices affected by the ISM

Vidal-García et al. (2017) study the influence of the nebular emission and interstellar medium (ISM) on the UV spectral indices of star-forming galaxies. They analysed the impact of the ISM in star-forming galaxy models with ages younger than 3 Gyr and with constant SFR of 1 $M_\odot\,yr^{-1}$. The NUV features analysed in common with this work are Fe2609, Mg2852 and Fe3000. They find that Fe3000 is not affected at all by the ISM contamination, while we find that this index shows a discrepancy with respect to a pure old stellar population and is well fitted with an additional small young component. Fe2609 and Mg2852 feature strengths are strengthened due to the interstellar absorption in young star-forming galaxies. We find, however, a much lower SFR of $\sim 10^{12}\,M_\odot\,yr^{-1}$ in the old and massive ETG stack in this work. Additionally, star-forming galaxies have significant amounts of dust, while massive ETGs have little dust content. Then, the rate of ionising photons striking the intercloud medium in the centre of the galaxies that are represented by our stacked spectra is very low, so the contribution in the NUV absorption features from the ISM is expected to be negligible.

3.7.5 Environment of BOSS galaxies

Our sample comprises ETGs with mean stellar mass higher than $\sim 10^{11}\,M_\odot$ (Maraston et al., 2013). Such massive galaxies mostly live in groups. Abundance matching (AM) provides a simple way to statistically relate the observed galaxies to their dark matter halo hosts. AM models (Moster et al. 2010; Guo et al. 2010) compare the observed stellar mass function of galaxies with the halo mass distribution from N-body numerical simulations. We used the functional form provided by Behroozi et al. (2010), interpolating between their estimates at $z = 0.1$ and $z = 0.5$ to assess the expected correlation between stellar mass and halo mass at the median redshift of our sample ($z \sim 0.4$). We created, via Monte Carlo sampling, a random set with the same number of galaxies as in our sample and with the observed stellar mass distribution of BOSS galaxies

(Maraston et al., 2013). If we assume galaxy clusters inhabit halos more massive than $\sim 10^{14}\,\mathrm{M}_{\odot}$, we obtain a cluster fraction of $\sim 1/2$.

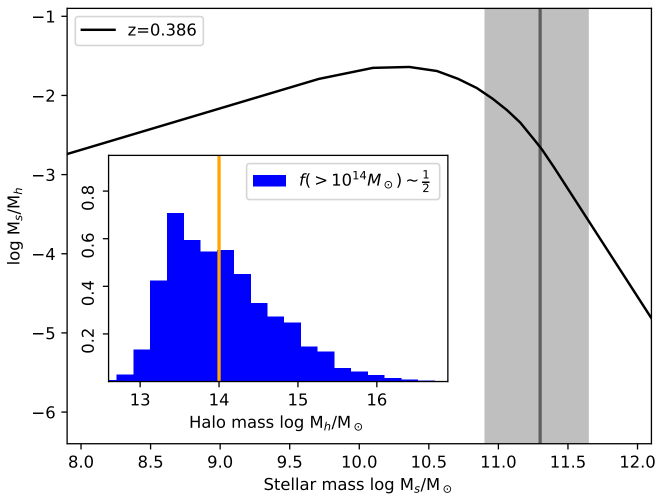

FIGURE 3.15— **Environment of BOSS galaxies from Abundance Matching**. We show the ratio of stellar to halo mass from abundance matching at the median redshift of our BOSS sample (z∼0.386), interpolating the functional form. The shaded area marks the stellar mass range of the BOSS sample. The inset shows the resulting distribution of halo masses, with the orange vertical line roughly marking the low-mass threshold of galaxy clusters.

Half of the BOSS sample used is expected to inhabit galaxy clusters with stellar masses $> 10^{14}\mathrm{M}_{\odot}$, suggesting that both *in-situ* and *ex-situ* mechanisms may trigger the small amount of residual star formation found here. Its origin might be from the pristine gas together with residual gas from the stellar feedback but also might be triggered by gas-rich interactions with their companion cluster galaxies if reached the central 10 kpc galaxy regions. The young mass fractions obtained here must be understood as an average value over the ETG population at z∼0.4. It is feasible also to expect some differences related to different environmental properties of each individual galaxy.

3.7.6 Comparison with other galaxy surveys

The LEGA-C survey (van der Wel et al., 2016) investigated optical galaxy spectra at a larger lookback times ($0.6 < z < 1.0$) than the BOSS survey. We expect that galaxies at these redshifts should have somewhat different (younger) stellar populations than those in our stacked spectra at $z \sim 0.4$. Wu et al. (2018) obtained the light-weighted stellar ages of 1000 galaxies at redshift $z \sim 0.8$ from two age-sensitive spectral indices, D4000 and Hδ. The age of the Universe at that redshift is ∼2.6 Gyr younger than that at the redshift of this work. They defined a spectral age index as a combination between these two indices, which is: $I = 15 \times D4000$ - Hδ - 20.5. From this spectral index is derived that, the SSP equivalent ages for galaxies at $z \sim 0.8$ with a stellar mass of $10^{11.1-11.5}$ $M_\odot$ are on average ∼3 Gyr old assuming a single SSP as SFH, but the oldest galaxies are ∼5.5 Gyr old. That matches reasonably well the equivalent age derived from the Hβ_o index for the most massive bin at $z \sim 0.4$ of 8.6 Gyr, taking into account the difference between the age of the universe at both epochs.

However, to make a fairer comparison we have estimated the ages of the stacked spectra using the spectral age index I defined above from the D4000 and Hδ indices. We derive ages of 5 Gyr for the lowest mass bin ($10^{11.3}$ $M_\odot$) and 6.5 Gyr for the most massive bin ($10^{11.5}$ $M_\odot$). Like Wu et al. (2018) we also find that, with respect to galaxies at redshift $z \sim 0.1$ from SDSS, the differences between the derived ages at redshifts 0.4 and 0.8 are smaller than the difference in the age of the Universe from both redshifts, at least for the less massive bins, which means that they are younger than they would be if passive evolution is the only driving mechanism. Their findings are also consistent with the correlation between stellar ages and galaxy mass derived in our work, suggestive of galaxy downsizing also at higher redshifts. Thus, we expect that the average age inferred at $z \sim 0.8$ of ∼3 Gyr would be higher when excluding galaxies with masses lower than $10^{11.3}$ $M_\odot$, which is the lowest mass stack, since more massive galaxies have older stellar populations. In addition, Wu et al. do not distinguish between star-forming (younger) and quiescent (older) galaxies when deriving ages for LEGA-C. If they were to have selected only quiescent galaxies, then the age differences would decrease.

Chauke et al. (2018) inferred stellar ages of 892 LEGA-C galaxies at $z \sim 1.0$ from the D4000 and Hδ line indices derived of their reconstructed SFHs and distinguishing between the galaxy stellar velocity dispersion and mass. Galaxies with velocity dispersions larger 220 km s^{-1} and stellar mass larger than $10^{11.3}$ $M_\odot$ are mainly old (~ 4.8 Gyr) and quiescent at $z \sim 1.0$. They derived their SFHs to find a population of old galaxies that formed most of their stars early on and were quiescent for several Gyrs, but they had at some point a period of growth, since they have significant recent star formation, either due to star formation or merging with a younger population.

In the nearby Universe, ATLAS-3D (Cappellari et al., 2011) explored the stellar population properties of nearby ETGs from integrated spectra within different apertures. Figure 9 of McDermid et al. (2015) shows the derived mass-weighted ages and metallicities within the effective radius as a function of velocity dispersion. Galaxies with $\sigma > 220\,\mathrm{km\,s^{-1}}$ are fundamentally old (∼13 Gyr) and metal-rich. In Figure 16 they illustrate the derived average SFHs for different dynamical mass ranges. ETGs of mass between $10^{11.1-11.5}\,\mathrm{M_{\odot}}$ have on average a specific SFR at z ∼ 0.4 of $\sim 10^{-12}\,\mathrm{yr^{-1}}$, which is in full agreement with the results we estimate from BOSS stacks by considering a constant SFR in the last 2 Gyr. In addition, SFHs are less extended for more massive ETGs, supporting also the downsizing scenario in nearby ETGs.

3.8 Conclusions

This work focuses on the luminous red galaxies targeted by BOSS at z ∼ 0.4. This survey selects, by construction, the most massive red galaxies, expected to be dead, quiescent systems. These galaxies pose a severe challenge to models of galaxy formation, as they require fine tuning in their feedback prescriptions to avoid large amounts of recent star formation from the available gas that keeps on flowing to the systems. Therefore, our finding of a measurable, but very small fraction in young stars likely poses the most stringent constraints on the modelling of massive galaxy formation. The use of a large sample allows us, for the first time, to average over individual variations and provides a clear picture of the incidence and mass fractions of very young stellar populations in massive ETGs. Our analysis explores NUV and optical features simultaneously, making the results consistent with both ranges of galaxy spectra. Note that this is not straightforward to achieve, given the varying sensitivities of these spectral ranges to different types of stars. We find that combining NUV + optical indices is crucial in order to anchor the mass-fractions of both the young and old components in ETGs.

With this work, our main goal is to estimate the average young stellar component of massive ETGs at z ∼ 0.4. We apply our criteria to select thousands of SDSS/BOSS spectra of massive galaxies, which have too low S/N in the blue wavelengths so we stacked them by velocity dispersion. Stacking spectra is a good approach for obtaining the average properties of a large number of low S/N galaxy spectra with similar characteristics. A bootstrap resampling indicates that, whatever sub-sample of galaxies we choose from the whole galaxy sample within a given velocity dispersion range, the obtained absorption line-strengths values do not change significantly. Also, the colour cuts applied by the BOSS survey, the velocity dispersion cuts for massive galaxies and the additional colour cut adopted from Masters et al. (2011) to avoid late-type contamination, have allowed us to stack massive ETGs with similar properties in a robust manner. Thus, the stacked spectra computed here are a good representation of typical ETGs.

From the optical Hβ_o and [MgFe]′ line-strength indices, we derive old mean SSP ages and high metallicities (Figure 3.3), in good agreement with previous findings. This suggests that the bulk of the stellar component of massive galaxies were formed at early epochs (Renzini, 2006). We also find that these stellar populations become older and more metal-rich with increasing mass. As far as these optical indices show old ages at that redshift and many other previous works in the literature have shown before (Thomas et al. 2005; de La Rosa et al. 2011; McDermid et al. 2015), there is a relationship between the galaxy mass and its SFH. More massive galaxies are found to exhibit narrower SFHs that peak their star formation activity at older ages than their less massive counterparts, consistent with our estimates of older ages for more massive stacked spectra. In this regime, a pure old SSP fit is a good first approximation for a galaxy with mass larger than 10^{11} solar masses, like the stacked spectra studied here.

As shown in Figure 3.4, the bluer the index, the more it deviates relatively from a single SSP model, which is a result of the additional young component whose contribution is further emphasised at shorter wavelengths. In contrast, the two reddest indices, Hβ_o and [MgFe]′ are quite insensitive to the younger component and measurements are in agreement with the old, single-age like, SSP predictions. The NUV indices are diluted with respect to the values of a purely old SSP and require an additional very young component to be fitted. This is precisely the young mass fractions we are able to constrain here. This has been approached in two different ways: a young SSP and a constant star formation in the last 2 Gyr, both on top of an old SSP, which characterises the population in the visible. Basically, we have employed a MCMC technique to obtain the best-fitting model parameters and their uncertainties from the probability distribution functions for each parameter marginalising over the rest of parameters. It turns out that the two modeling approaches provide a reasonable description as shown in the fitted data in Figure 3.7.

This aim is achieved thanks to the unprecedented sensitivity of our analysis and due to the high S/N spectra and a large sample size, which allows us to cover a wider coverage of masses with respect to previous works. Our results show, for the first time, that the population of massive ETGs at redshift z $\sim$ 0.4 hosts a population of young stars, at the sub-one percent level, whose contribution anti-correlates with galaxy stellar mass. We find the total mass fraction of stars formed over the last 2 Gyr is 0.48% in the most massive galaxy stack (i.e. highest σ), with a weak increase to 0.58% at the lowest σ. This trend can be interpreted within a downsizing scenario (Cimatti et al., 2006), which argues that the formation of stars in less massive systems extends over longer time-scales with respect to more massive galaxies (Thomas et al., 2005). Thus, lower mass ETGs are expected to have a relatively higher level of recent star formation. The fact that in the lower mass stacks we obtain older ages for the young component in the *2SSPs* model might be indicative of a more prominent intermediate-age stellar population, with respect to more massive galaxies, i.e. consistent with a longer formation time-scale.

The NUV is not only sensitive to young stars but also to hot, old stars such as those from the PAGB evolutionary stage. We cannot rule out that both young and PAGB contributions are at work, in which case our young mass fraction estimates should be considered, to some extent, as an upper limit. If these old UV-bright stars have some relative contribution, we find it has to be sub-dominant from arguments based on SSP modelling. Therefore, we quantify the upper limit fractions of very young stellar populations in ETGs at z∼0.4.

We compare the stellar population properties of our stacked spectra to those from simulated massive galaxies from the EAGLE simulation. After applying the same selection criteria of the observations we only find two simulated galaxies that match the stacks. This is mainly because the simulations produce far more extended SFHs than observed for massive galaxies. Our results impose fundamental constraints on the later stages of the evolution of massive ETGs.

The best-fitting model reveals a small but detectable presence of young stars. However, what triggers the star formation is a matter of debate. We still need to understand which are the mechanisms that allow new stars to be formed at such low levels. The most extreme model of the monolithic scenario where all stars in ETGs are formed at high redshift is ruled out. More massive black holes are found in larger velocity dispersion galaxies so that they are more efficient at preventing gas cooling in more massive galaxies than their less massive counterparts and therefore, quenching massive ETGs. Whatever process that causes quenching at high redshift does not seem to prevent these small amounts of recent star formation. Whether this gas comes from internal sources, i.e. recycled or pristine, or from interactions with galaxies and surrounding environment requires further modelling analysis.

4

Young stellar population gradients in nearby Brightest Cluster Galaxies

Nature is our biggest ally
and our greatest inspiration.
We just have to do what nature has always done.

David Attenborough in *A life on our planet* (2020)

In this chapter we present an analysis of young stellar population gradients in massive central cluster galaxies at different galactocentric distances. We study how the young mass fractions presented in Chapter 3 are distributed within galaxies. Such analysis can be made in nearby massive galaxies with extremely high signal-to-noise spectra. BGCs are the largest and most massive galaxies in the Universe. Although they host very old stellar populations, several studies found the existence of blue cores in some BCGs indicating ongoing star formation. Our analysis is based on stacked spectra in the NUV and optical spectral ranges at different distances to the galaxy centre for a sample of six massive BCGs at redshift z$\sim$0.05. We measure the distribution of young stars with radius in this special category of ETGs and find that they are preferently located at the galaxy cores. This provides important constraints on the evolution of massive galaxies.

The content of this chapter is based on the paper *Young stellar population gradients in central cluster galaxies from NUV and optical spectroscopy.* Salvador-Rusiñol, N.; Beasley, M. A.; Vazdekis, A.; La Barbera, F. 2020, MNRAS, Volume 500, Issue 3, pp.3368-3381.

4.1 Data

The data used consist of galaxy spectra from the VLT/X-Shooter spectrograph (Vernet et al., 2011) of six very massive central cluster galaxies at different galactocentric distances, covering from 0 to 4.2 kpc, within redshift $0.048 \leq z \leq 0.056$. We use the same data-set used in La Barbera et al. (2019) (hereafter LB19), except for one target, named XSG2, that has been classified as a satellite galaxy and therefore, it is not included in our sample of BCGs. Notice that the main scientific goal was to explore the radial gradients of the stellar IMF in a set of very massive ETGs.

A detailed description of how the observations and data reduction of these data have been performed is described in LB19. Briefly, the X-Shooter data consist of spectra taken with three independent arms, ultraviolet-blue (UVB), visible (VIS) and and near-infrared (NIR). The data were obtained with 0.9, 0.9, and 1.0 arcsec slit widths in UVB, VIS, and NIR, respectively. The wavelength range of the final joined spectra is $\sim 3000-23500$ Å. In this work, we focus our analysis from the bluest (NUV) to optical wavelengths. Observations were carried out in service mode and have typical exposure times on each target of 1.7, 1.9, and 2.1 hours, in the UVB, VIS, and NIR arms, respectively, with a median seeing of $\sim$0.8 – 0.9 arcsec. The spectra were extracted at different galactocentric distances. The innermost spectra of all galaxies were extracted within an aperture of width 1.3 arcsec around the photometric centre. The aperture size was then increased outwards, in order to ensure a median $S/N > 90$ per Å in the optical range of the individual galaxy spectra. These spectra have been corrected for Galactic reddening and shifted to rest-frame accordingly.

4.2 Galaxy sample properties

Following the same nomenclature as LB19, we refer to the galaxies as XSG1, XSG6, XSG7, XSG8, XSG9 and XSG10. Main galaxy properties are summarised in Table 4.1. Despite we exclude the XSG2 galaxy from our sample, which is the only genuine satellite according to the analysis presented in LB19, we also analyse its young stellar contribution separately. Five galaxies were selected from the lowest redshift limit ($z \sim 0.05$) of the SPIDER sample (La Barbera et al., 2010a), while one target (XSG10) was selected from SDSS-DR7 applying the same criteria as SPIDER ETGs, but at slightly lower redshift ($z \sim 0.048$). This sample was selected to comprise very massive galaxies, so they have very high central velocity dispersions ($> 300\,\mathrm{km s^{-1}}$ for the innermost spectra for all galaxies). With the exception of XSG7, all targets have been classified as the central galaxy of a group or cluster of galaxies, i.e. BCGs. However, relevant for the present work, is that XSG7 has similar stellar mass to those of the brightest galaxy of their parent groups. Also, this galaxy is also located at the central region of a group with another bright companion classified as group central galaxy. Therefore, although not being classified as a central cluster galaxy, it was likely central to the infallen group for most of its evolution (see LB19 for more details). BCGs are generally located at the cluster centroid, but there do exist some cases of BCGs located away from the centre of their host cluster (Lidman et al., 2013).

ID (1)	SDSS ID (2)	RA (deg) (3)	DEC (deg) (4)	z (5)	σ_c (km s^{-1}) (6)
XSG1	J142940.63+002159	217.419	0.366	0.0558	333±3
XSG6	J144120.36+104749.8	220.335	10.797	0.0512	305±13
XSG7	J151451.68+101530.4	228.715	10.258	0.0548	319±17
XSG8	J015418.07-094248.4	28.575	-9.713	0.0524	332±8
XSG9	J005551.88-095908.3	13.966	-9.986	0.0548	349±6
XSG10	J075354.98+130916.5	118.479	13.155	0.0476	338±4

TABLE 4.1— **Main properties of the X-shoother BCG sample**. Col. 1 is the label used for each galaxy in FLB19. Col. 2 is the galaxy ID from SDSS. Col. 3 and Col. 4 are the RA and DEC coordinates, while Col. 5 is the average galaxy redshift derived from the X-Shooter spectra. Col. 6 lists the stellar velocity dispersion of each galaxy measured in the centre.

The main result from LB19 is that these galaxies show negative IMF gradients, with bottom heavy IMFs ($\Gamma_b \sim$2.8 – 3.5) in the innermost galaxy regions which smoothly changes to a standard logarithmic slope $\Gamma_b \sim$1.3 at galactocentric distances of $\sim$4 kpc. Also, they show that these galaxies have high [Mg/Fe] abundances, from $\sim$0.3 to 0.5 dex, indicating short star formation time-scales early in the Universe. Hence, the galaxy sample studied here comprises low-redshift, very massive galaxies corresponding to the extreme high-mass end of ETGs, located at the centres of galaxy clusters.

4.3 Stacking spectra

Massive galaxies, such as those in our sample, are known to be dominated by very old stellar populations. Therefore, detecting the contribution of the youngest stars in their optical spectra is difficult. As we have seen in Figure 2.2, NUV indices are sensitive to young stellar populations, but require higher S/N spectra than bluer indices. Unfortunately, obtaining high S/N spectroscopy in the NUV is not an easy task, mostly due to the faint flux level of ETGs in this spectral range, and also because of the significant absorption from the atmosphere. Despite the very high-quality of the data presented here, the individual galaxy spectra for our sample still have relatively low S/N in the NUV range. The S/N is, on average, 13 Å^{-1} for the innermost galaxy spectra, which is sufficient for detecting the presence of small amounts of young stars from the NUV spectral indices. However, at the outermost galactocentric distances it is much lower ($\sim 3\,\text{Å}^{-1}$). Therefore, we take advantage of the fact that all the galaxies in our sample are massive, with very similar central velocity dispersions, to increase the S/N by stacking the spectra according to their physical radial distance to the galaxy centre within 4.2 kpc.

In order to explore the behaviour of the young stellar component with distance from the galaxy centre, the individual spectra are grouped into five bins according to their galactocentric distances. These bins cover 0 – 0.8, 0.8 – 1.2, 1.2 – 1.7, 1.7 – 2.4 and 2.4 – 4.2 kpc radial ranges. The individual galaxy spectra are stacked together in each bin so that all galaxies from our sample contribute to each radial bin. Note that the outermost radial bin has slightly larger size in order to ensure a S/N > 13 per Å in the NUV range in the final stack, necessary to measure certain spectral indices. Before the stacking procedure, we performed gaussian smoothing in both models and individual galaxy spectra at a common velocity dispersion of 350 kms^{-1}. This is the highest velocity dispersion of all galaxy spectra (see Table 4.1), which were measured in the optical with the `pPXF` software (Cappellari & Emsellem, 2004).

We create the stacks by bringing each individual galaxy spectrum to rest-frame wavelength and taking the median flux at each common wavelength as the stacked flux value. The error on the flux comes from the standard deviation of the individual galaxy fluxes at each wavelength. This way, we have five spectra of high S/N at different radial distances representative of very massive central galaxies. The final stacked spectra with their corresponding S/N are shown in Figure 4.1. The central wavelengths of the spectral indices used in the analysis are identified by vertical dashed lines. The stacked spectra have high S/N, above ~ 13 at wavelengths larger than 3300 Å and several hundreds in the optical. In particular, the central bins have higher S/N than the outermost ones. This permits us to increase the number of absorption spectral lines usable for the analysis of the innermost bins. All spectra exhibit relatively modest NUV fluxes compared to the optical range and no strong emission lines are clearly seen, indicative of the presence, on average, of quiescent stellar populations in our galaxies. Although some of our targets show some emission contamination in their individual spectra (see appendix F in LB19 for a detailed analysis) the final stacked spectra are not corrected for the emission, since our index sample of interest is not affected by the emission contamination.

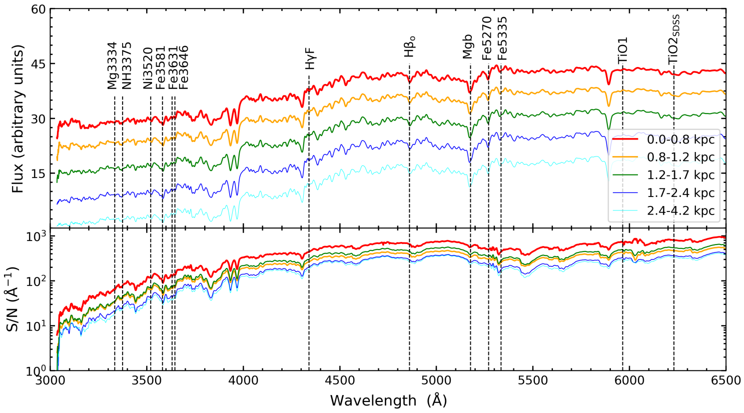

FIGURE 4.1— **Stacked spectra and S/N of each radial bin.** In the upper panel we show the stacked spectra in the range of interest of this work, 3000 – 6500 Å. The lower panel shows the S/N per Å of each spectrum. Both panels are colour coded according to their radial bin. Dashed lines indicate the central wavelength of the spectral indices used in the analysis.

4.4 Line-strength index measurements

Thanks to the wide spectral range of the X-Shooter spectrograph, we are able to use spectral indices from NUV (>3000 Å in this case) to optical wavelengths. This allows us to constrain the various stellar components that contribute with different proportions to these spectral ranges. In this study, we use features in the NUV range that are sensitive to very small mass fractions of young stars (Vazdekis et al., 2016) that allow us to constrain the youngest stellar populations of massive old galaxies.

The set of indices used in this study differ at each radial bin and are listed in Table 4.2. We note that wavelengths larger than 3000 Å are less sensitive to young stars in comparison to bluer wavelengths (see Figure 2.2), given the low level of star formation rates in massive ellipticals. Fortunately, with sufficient S/N, indices from this spectral range can also trace the youngest stellar populations. Thus, indices in the NUV spectral range are selected in order to have a large sensitivity to small fractions of young stars (<1 Gyr).

Particularly, we choose NUV indices that are most sensitive to these young components in comparison to other effects such as alpha-element enhancement, which is observed in these galaxies. For this purpose, we have explored how each

Bin (kpc) (1)	Γ_b (2)	Set of indices used (3)
0.0 – 0.8	3.0	Mg3334, NH3375, Ni3520, Fe3631, Fe3646, HγF, [MgFe]$'$, TiO1, TiO2$_{\rm SDSS}$
0.8 – 1.2	2.8	Same as first bin
1.2 – 1.7	2.5	Same as first bin but w/o Mg3334
1.7 – 2.4	1.8	Same as first bin but w/o Mg3334
2.4 – 4.2	1.3	Same as first bin but w/o Mg3334, Fe3631 and Fe3646

TABLE 4.2— **Set of indices used at each radial stacked spectrum.** Col. 1 indicates the galactocentric distance range of each bin. Col. 2 lists the average logarithmic IMF slope of each radial bin from LB19. Col. 3 summarises the index sample used in the fitting process in each bin for constraining the young stellar component.

index in the NUV spectral range is influenced by the presence of a small mass fraction (0.1%; see Figure 2.2) of a young stellar population on top of an old component, and by an alpha-enhancement of [Mg/Fe] = 0.4. For the latter we employ the Vazdekis et al. (2015) and Conroy & van Dokkum (2012) SSP models, which both use the MILES stellar library (Sánchez-Blázquez et al., 2006b) and differential corrections from theoretical star spectra. Although Mg3334, NH3375 and Ni3520 indices are outside the wavelength range where these models are defined and provide safe predictions, we include them in our index set since they are the bluest indices defined in the spectral range of our spectra and, therefore, the most sensitive to the youngest stars.

We exclude Fe3581, Fe3619, Fe3683 and Fe3706 indices because models suggest that they are strongly affected by the [Mg/Fe] abundance, which leads to variations of similar magnitude (or larger) to those from the young component. The Fe3741 absorption line is excluded for being affected by the oxygen emission line in 3727 Å, whose impact, despite being small, is not completely negligible. We include the Fe3631 and Fe3646 indices which appear to be more sensitive to the presence of young stars than to Mg abundance.

We also include indices defined within the optical range that trace the bulk of the stellar population. We use age-sensitive Balmer lines and particularly, Hβ_o, which provides better constraints on the age than the classical Lick index Hβ (Cervantes & Vazdekis, 2009). We include [MgFe]$'$ index defined to be insensitive to variations of [Mg/Fe] abundance ratio (Thomas et al., 2003) but sensitive to the total metallicity. We also include the TiO1 and TiO2$_{\rm SDSS}$ indices for being strongly sensitive to the IMF slope, as our galaxies have been shown to have a strong IMF gradient. All these optical indices have been widely used in a large number of stellar population studies of massive galaxies.

Since the S/N in the NUV range decreases with increasing radius, some indices are excluded in the outer radial bins during the analysis because of their S/N requirements. Mg3334 can only be used in the two central bins, since it requires S/N > 40 per Å for being able to disentangle small fractions ($< 1\%$) of young stars on top of old stellar populations. Similarly, the Fe3631 and Fe3646 indices are not used in the outermost bin. Therefore, the set of spectral indices used in our analysis changes with each galactocentric distance bin as summarised in Table 4.2. However, to make sure that our results are robust, we have checked that the omission of these indices does not introduce any systematic effects in our results. This has been assessed by deriving the young stellar component by including (and excluding) these indices during the fitting process in all radial bins, and finding that the best-fitting solution does not change and thus, neither does the obtained trend with galactocentric distance.

The error associated with the index measurements comes from two different sources. First, from the Poissonian noise, which is smaller for the optical indices as a result of the higher S/N of the stacked spectra in this wavelength range. Secondly, the error on the stacked spectra is measured by stacking the errors on the fluxes of the individual galaxy spectra. This error is included in order to account for the variations among the six galaxies in a given stack, since the Poissonian noise is very small and does not represent the individual galaxy indices. Finally, the adopted index uncertainties come from the Poissonian noise added in quadrature to the noise from the individual galaxy flux errors.

Note that we have not corrected the spectra for internal dust extinction in these galaxies. Our targets have been selected to have low internal extinction, as detailed in La Barbera et al. (2017) and LB19. Additionally, as explained in Chapter 2, the effect on the index measurements due to dust reddening is expected to be negligible.

4.5 Constraints on the age and metallicity

An integrated galaxy spectrum from predominantly old stellar systems such as BCGs can be approximated with one SSP in the optical range. We initially derive the mean luminosity-weighted ages and metallicities of the stellar population in the stacked spectra using two optical indices. Results from the optical range (LB19) show that the bulk of the stars of these massive BCGs was formed in early epochs, so the dominant stellar population is very old. Left panel of figure 4.2 shows the widely used index-index plot in the visible with the age-sensitive index Hβ_o versus the total metallicity indicator [MgFe]$'$. SSP model predictions are shown for different ages and metallicities for two grids with two different bimodal IMFs. We show the predictions corresponding to a logarithmic standard slope 1.3 in black, which is representative of the outer bins, and for a bottom-heavy IMF with slope 3.0 in grey representative of the inner bins. We overplot the measurements of the stacked spectra (star symbols) that indicate old ages and metal-rich ([M/H] >0.0) stellar populations in all galactocentric distances. The inner regions have higher [MgFe]′ values, revealing more metal-rich stellar populations towards the galaxy centre. We also see that the two innermost bins fall outside the standard IMF slope grid, which indicates a bottom-heavy (dwarf-enhanced) IMF as shown in LB19. For this reason, we included IMF-sensitive indices in the analysis to ensure that our results are self-consistent. We note that the highest metallicity of both SSP model grids is not enough to match the value of the central bin, which requires [M/H] >0.22.

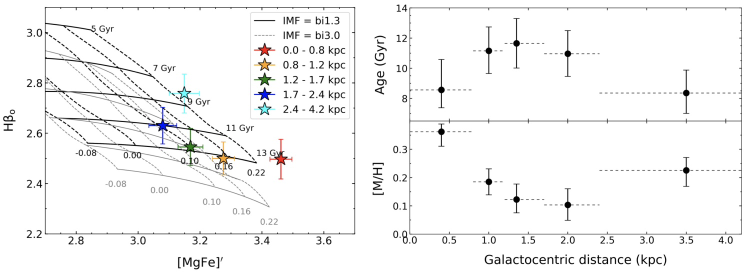

FIGURE 4.2— **Estimates of the mean ages and metallicities of the BCGs stacked spectra.** Left panel: Age-sensitive Hβ_o index is plotted versus the total metallicity-sensitive indicator [MgFe]′. Grids show the E-MILES model predictions for a standard IMF (black) and a bottom-heavy IMF (grey) for different ages (solid lines), increasing from top to bottom, and metallicities (dashed lines), which increase from left to right. Stars show values measured in each stacked spectrum, following the same colour code used in Figure 4.1. Data and models have been smoothed to the same spectral resolution of $\sigma = 350\,\mathrm{km\,s^{-1}}$. Right panel: Mean luminosity-weighted ages and metallicities of each radial bin as a function of the distance to galaxy centre, derived by fitting the observed optical Hβ_o and [MgFe]′ spectral indices with SSP model predictions. Horizontal dashed lines indicate the galactocentric distance range covered by each bin.

We use these two indices to infer the MLWA and metallicity for each radial stacked spectrum shown in the right plot of Figure 4.2. Here we assume a different IMF slope for each bin according to the LB19 results. Our derived stellar population parameters are in general agreement with the values derived in LB19 for these galaxies. The age-sensitive index Hβ_o reveals very old stellar ages indicating that the bulk of stars in those regions were formed early.

The age gradient is very shallow, in agreement with Brough et al. (2007) and Loubser et al. (2009) from optical spectroscopy analysis of BCGs. We note that the median MLWA is 11.0 ± 1.2 Gyr (the uncertainty comes from the standard deviation of the MLWAs). We derive a steep negative metallicity gradient with all values showing super-solar metallicities. This metallicity trend is in good agreement with what previous studies have reported for very massive galaxies (Kuntschner et al. 2010; La Barbera et al. 2012; González Delgado et al. 2015; Goddard et al. 2017; Martín-Navarro et al. 2018b; Ferreras et al. 2019; Zibetti et al. 2020). The outermost bin shows a "jump" in both age and metallicity. This stack has the largest scatter in both indices measured in the individual galaxy spectra. However, importantly for this work given the overlap in the error bars in both age and metallicity we do not consider this statistically significant.

4.5.1 Observed versus model indices

In order to characterise the behaviour of the NUV and optical indices, we show the dependence of the SSP model predictions for each index with respect to the stellar population age, metallicity and IMF slope in Figure 4.3. Measured indices at varying radial bins are shown with different colours. The lines represent the SSP model predictions as a function of the age for a standard ($\Gamma_b = 1.3$, black) and bottom-heavy ($\Gamma_b = 3.0$, grey) IMFs, and for three different metallicities: solar ([M/H] = 0.0, solid line), highest metallicity value from SSP models ([M/H] = 0.22, dashed line) and extrapolated metallicity ([M/H] = 0.36, dot-dashed line). The latter is plotted in order to represent the innermost bin for which we find a mean luminosity-weighted metallicity of [M/H] = 0.36. Some indices show strong sensitivity to the age, such as the Balmer lines Hβ_o or HγF, whereas, as expected, the [MgFe]$'$ indicator is more sensitive to the metallicity. Note the strong IMF dependence of the TiO1 and TiO2$_{\rm SDSS}$ indices.

The most remarkable aspect is that a single old SSP, while matching the optical indices, provides an unsatisfactory match to the observed NUV indices and suggests a more complex SFH than one star formation burst. These indices require an additional component to be matched. The departure of the observed NUV values with respect to an old SSP needs to come from a very hot stellar population. As previous studies have found recent star formation in some samples of BCGs, we interpret this departure as being due to the presence of young stars in these massive central galaxies. If any other hot stellar components are contributing to this departure of NUV indices, such as the PAGB stars, these are sub-dominant contributions as has been discussed in Chapter 3 and as it is predicted by the stellar evolution theory (Buzzoni 1989; Charlot & Bruzual A

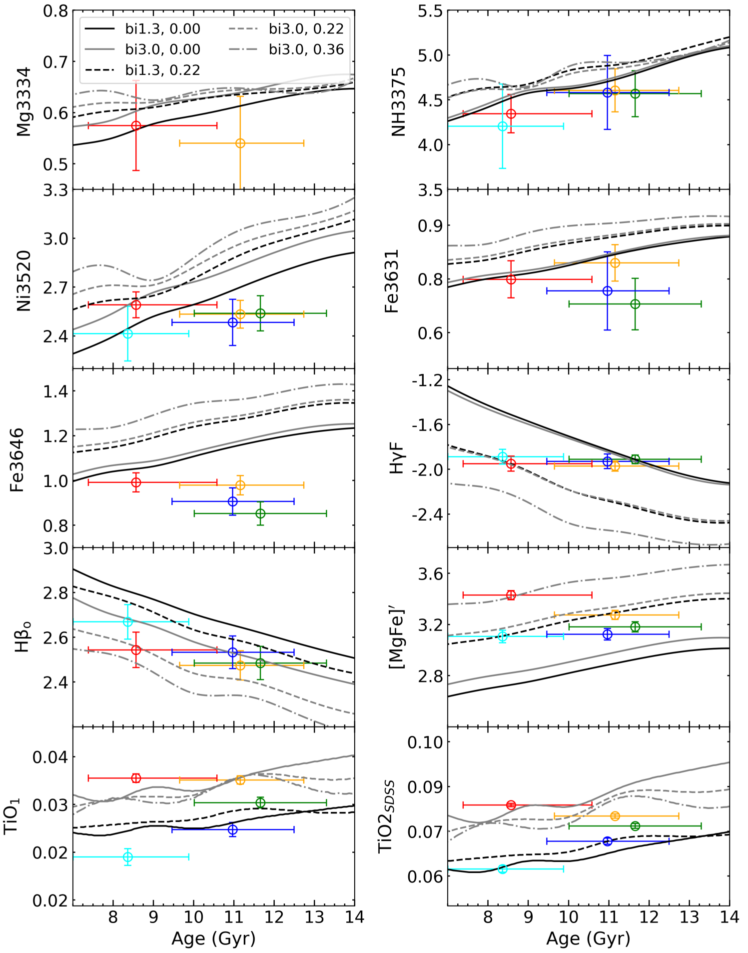

FIGURE 4.3— **NUV and optical line-strength measurements.** Observed and predicted SSP line-strengths are shown as a function of age for three different metallicities $[M/H] = 0.0$ (solid line), $[M/H] = 0.22$ (dashed line) and $[M/H] = 0.36$ (dot-dashed line), and two IMFs, bimodal Γ_b=1.3 in black and a bottom heavy bimodal IMF $\Gamma_b = 3.0$ in grey. Note that predictions for $[M/H] = 0.36$ come from an extrapolation of the SSP models (see the text) and are plotted only for $\Gamma_b = 3.0$, to represent the innermost bin. Observed indices are overplotted as a function of their MLWA and colour coded as in Figure 4.1. Both SSP models and data are at the same spectral resolution of $350\,\mathrm{km\,s^{-1}}$.

1991; Conroy 2013).

4.6 Fitting methods

To characterise the young component, our method consists of fitting the observed spectral lines with stellar population synthesis model predictions that are derived from a simple modelling of the SFH for very massive galaxies, which in this case is the *1SSP+cSFR* model described in Chapter 2. For the old stellar component – described by a SSP – we assume prior distributions of ages from 1 to 13 Gyr and metallicities from –0.40 to 0.45 dex. The young component is parametrised by assuming a constant SFR in the last 1 Gyr to estimate the relative fraction of stars formed during that period.

Each MCMC simulation consist of 40 walkers exploring the parameter space over 40000 steps. We fit the observed line-strengths of each radial bin to obtain the best-fitting model parameters via MCMC chains. For the IMF we do not perform a continuous coverage and, instead, we use SSP models with IMF slopes 1.0, 1.3, 1.5, 1.8, 2.0, 2.3, 2.5, 2.8, 3.0, 3.3 and 3.5 and obtain the best-fitted IMF via minimization of the χ^2. This process gives the best-fitting values for the set of model parameters of each spectrum: the age and metallicity of the old stellar component, $\mathrm{age_{old}}$ and $\mathrm{[M/H]_{old}}$, respectively, the mass fraction of the stars formed in the last 1 Gyr ($\mathrm{f_{young}}$) and the IMF slope.

Note that we adopt 2 Gyr in Chapter 3, where we employ bluer indices with greater sensitivities to the young stellar components. Our present choice of indices here is aimed at maximising the sensitivity to the youngest stellar components. Thus, since spectral indices above 3000 Å are less sensitive to small fractions of young components (see Figure 2.2 in Chapter 2), we shorten to 1 Gyr the period of time corresponding to these populations where we assume a constant SFR. Nevertheless, in Section 4.7.5 we compare our results to those obtained for BOSS by extending the upper age limit of the young component to 2 (rather than 1) Gyr, finding consistent results.

The young component may be represented by different SFH parametrizations. Certainly, one infers different young mass fractions depending on the parametrization of the SFH, but the main goal of this work is to assess the spatial distribution of young stars in massive central galaxies by constraining all the contributions within the last Gyr. If one considers a two-stellar population (*2SSPs*) model as SFH approach, i.e., one old stellar burst plus one young stellar burst, this might be representative for some specific massive galaxies, where they formed the bulk of their stars in a high-redshift star formation burst, and some little accretion later may produce a second burst at lower redshift, forming new stars in the centre. However, this secondary star-forming epoch would be very unlikely to be the same for different BCGs, as the environment would randomly determine this star formation process. Therefore, since in this work we are averaging the spectra of six different galaxies, a constant SFH representing the young stellar component goes a step further with respect to the *2SSPs*, in order to account for the stars formed in a given period of time (1 Gyr in this work) in our galaxy sample. It is true that the "exact" SFH of our BCGs it is unknown, since we cannot obtain information about their resolved stellar populations. However, we still can estimate stellar population formed in the last 1 Gyr following our modelling approach. Note that the best-fitting solution age of the *2SSPs* approach would be representative of the mean luminosity-weighted age of the young component for the constant star formation approach.

4.7 Results

In this section, we present the stellar population parameters obtained with the method described above. Figure 4.3 shows the mismatch between the observed and the model NUV indices for a single old SSP, which provides good fits to the optical indices. This mismatch can be resolved by adding a small amount of recent star formation on top of an old stellar population. We derive the young stellar population mass fraction in the last 1 Gyr for each radial stacked spectrum. We also infer this fraction for the innermost spectrum of each individual galaxy to detect possible differences among the six galaxies.

4.7.1 Young stellar population gradients

Results for the young stellar component for each radial stacked spectrum are provided in Figure 4.4. We measure mass fractions for the young stellar component f_{young} below 1% at all galactocentric distances. There is a larger contribution of young stellar populations in the innermost regions with a mass fraction of $\sim 0.7\%$ in the central bin decreasing to $\sim 0.3\%$ at 1 kpc distance. Beyond that, the gradient becomes shallower with virtually no contribution from young stars outwards of 2 kpc. Therefore, the young component is mostly concentrated in the galaxy cores (< 2 kpc) of our sample of massive central cluster galaxies.

Best-fitting values for the other fitted parameters are summarised in Table 4.3. The old component shows metal-rich metallicities decreasing with galactocentric distance, in agreement with previous studies for massive ETGs. Note that the metallicity for the innermost bin is $[M/H] = 0.32$, which comes from a linear extrapolation of the SSP models. The best-fitting metallicity of the innermost bin before the extrapolation was the highest value allowed in the E-MILES models, i.e. $[M/H] = 0.22$, giving $f_{young} = 0.42\%$. This extrapolation

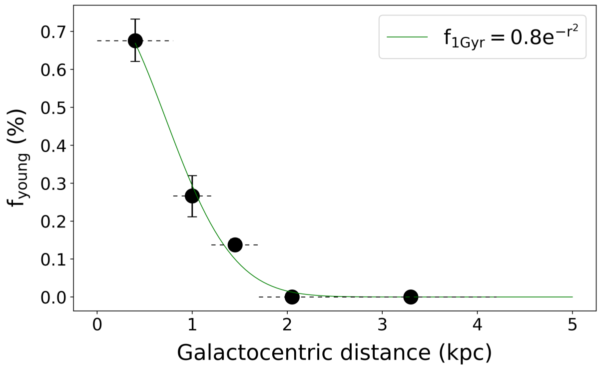

FIGURE 4.4— **Young stellar population gradient.** The mass fractions of stars formed in the last 1 Gyr (f_{young}) are plotted as a function of the galactocentric distance in units of kpc. Black symbols are the best-fitting values from the index fitting analysis. Horizontal dashed lines indicate the galactocentric region covered by each bin. Green solid line indicates the polynomial fit (in the inset) to the best-fitted values up to 5 kpc.

Bin (kpc) (1)	IMF (2)	age_{old} (Gyr) (3)	$[M/H]_{old}$ (4)	f_{young} (%) (5)
0.0 – 0.8	3.0	$11.6^{+0.2}_{-0.3}$	0.32±0.01	$0.67^{+0.06}_{-0.05}$
0.8 – 1.2	2.8	$12.0^{+0.4}_{-0.3}$	0.19±0.02	0.27±0.06
1.2 – 1.7	2.5	$12.2^{+0.2}_{-0.3}$	0.15±0.01	$0.14^{+0.02}_{-0.01}$
1.7 – 2.4	1.8	$11.4^{+0.7}_{-0.5}$	0.14±0.03	0
2.4 – 4.2	1.3	$9.0^{+2.0}_{-1.0}$	0.20±0.05	0

TABLE 4.3— **Best-fitting values of the stellar population parameters.** For each radial bin listed in Col. 1 we have obtained the best-fitting IMF slope (Col. 2), and age and metallicity for the old stellar component (Col. 3 and 4, respectively). The young fraction is shown in Col. 5. Note that the metallicity of the old component in the first bin exceeds the upper limit of the E-MILES SSP models ($[M/H]_{old} = 0.22$).

to higher metallicities improves the fits to constrain properly the young component for this radial bin. In the case of the two outermost bins, the best-fitting f_{young} of our modelling approach is zero, i.e. consistent with a single, old SSP. Hence, the age and metallicity derived in Figure 4.2 are a good representation of the stellar population in these two bins.

We find that by including the IMF-sensitive TiO spectral indices (La Barbera et al. 2013; Martín-Navarro et al. 2018b; Eftekhari et al. 2019), we infer IMF values as a function of radius consistent with those derived in LB19 for the same set of galaxies, which is based on a larger set of IMF-sensitive indices. This variation of the IMF with radius in massive ETGs is in agreement with previous studies (Martín-Navarro et al. 2015a; La Barbera et al. 2016; Vaughan et al. 2018; Sarzi et al. 2018; Meyer et al. 2019; La Barbera et al. 2019).

We show in Figure 4.5 the observed (black) and best-fitting (blue) model indices as a function of galactocentric distance. Some indices show a clear trend with distance to galaxy centre, such as the negative gradients for the Fe and Ni NUV indices, and the optical [MgFe]′ and the TiO indices, as expected. Balmer lines present slightly positive gradients. The best-fits show very good agreement with the observed indices. The NUV indices are well fitted, except for the Fe3646 line. This could be due to the fact that this index is still affected by alpha-element abundance, despite the fact that we have selected indices that are more sensitive to small fractions of young stars than alpha abundance. However, the alpha-enhancement may produce a larger effect on this index than in the other NUV indices that we are not taking into account with the SSP models used. The impact of alpha-elements on SSP models is more uncertain in the UV than is the case for the optical. Therefore, both effects could be contributing to the Fe3646 index, but in this work we are only constraining the young stellar component. We have checked that the exclusion of this index does not affect the results. The optical best-fitting indices are in agreement with the observations.

4.7.2 Impact of varying index selection on results

The derived fractions of young stars are only meaningful if accompanied with a comprehensive analysis of the errors associated with the obtained fractions. As the Balmer lines are the main age indicators in the optical range we investigate the impact of removing these indices from the fitting process on the derived fractions. In Figure 4.6 we see that the removal of the Balmer lines lead to higher young mass fractions at all the radial bins with respect to those obtained with all the index set. This is not surprising given the fact that in this case the age constraints come from the NUV indices, which are mostly contributed by the youngest populations. However, the trend with galactocentric distance is maintained. Interestingly, small fractions of young components in massive ETGs can be derived also by using extremely high S/N spectra in the optical range (Loubser et al. 2009; Martín-Navarro et al. 2018b). If only fitting the optical indices, we obtain rather similar results as shown in the figure, albeit

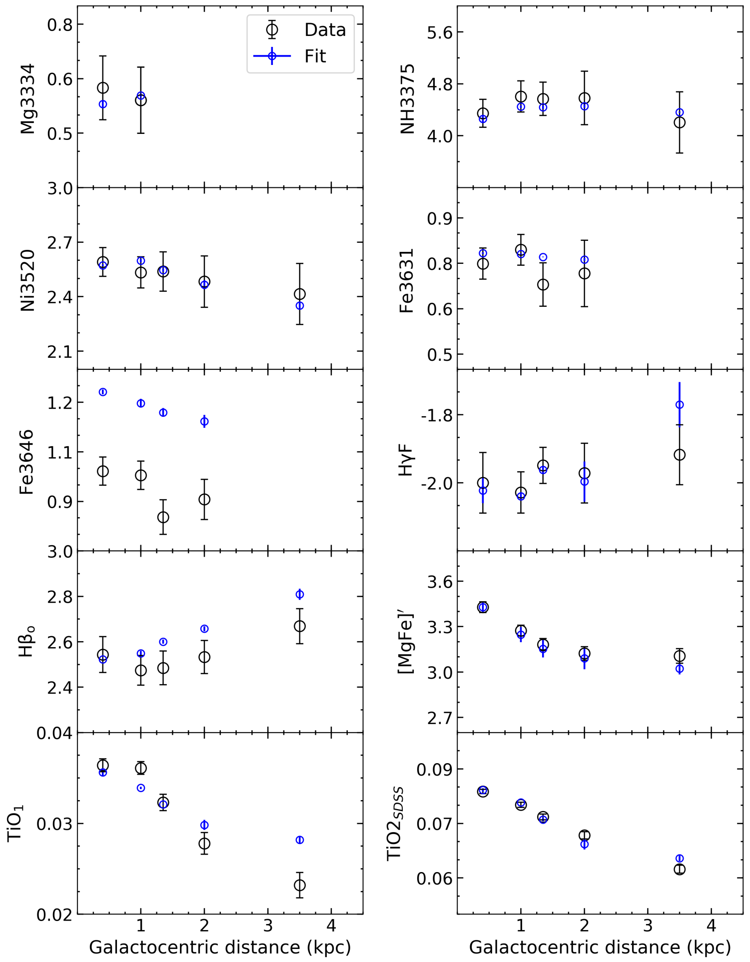

FIGURE 4.5— **Best-fitting indices of the BCG's stacked spectra.** The best-fitting spectral indices as a function of the galactocentric distance of each radial bin are plotted in blue. Measurements on the observed spectra are shown in black. Note that different sets of indices are used at each radial bin during the fitting process to obtain the best-fitting parameters indicated in Table 4.3.

with slightly lower young star fractions and larger uncertainties. The agreement found in the solutions between the optical and the optical plus the NUV indices shows that our results are very robust, as we are getting fully consistent results across the UV and optical spectral ranges.

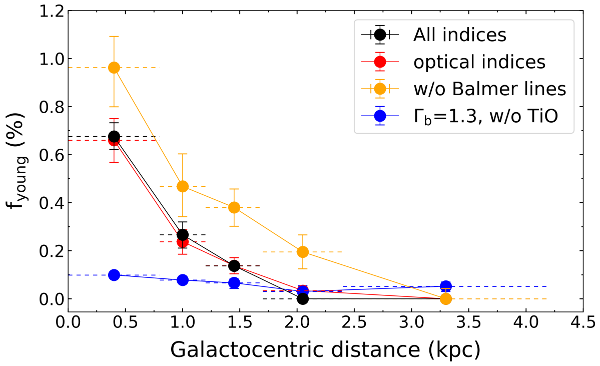

FIGURE 4.6— **Best-fitting results when testing different sets of indices.** The panel shows the fractions of young stars when using the full set of indices used in the fitting process listed in Table 4.2 (black) and when excluding the optical age-sensitive Balmer lines (orange) and the NUV indices (red). Also shown are the results when fixing the IMF as Γ_b ~1.3 for all the radial bins (blue) and removing the TiO IMF-sensitive indices in the fitting process.

4.7.3 Impact of IMF on results

We also investigated how the derived parameters are affected when using a standard bimodal IMF slope of Γ_b ~1.3 for all radial bins. This is a conservative approach that departs from what LB19 and this work find: an IMF gradient from bottom-heavy IMF slope in the central regions of our BCGs and a rapid decrease to Milky Way like IMF at larger radii. As TiO indices cannot be fit with a standard IMF we have excluded TiO1 and $TiO2_{SDSS}$ in the fitting process, thus avoiding biasing significantly the results. This is particularly evident for the two innermost bins where the IMF deviates significantly from a standard distribution. Figure 4.6 shows smaller fractions of young stars ($f_{young} < 0.1\%$) with a shallower trend with galactocentric distance in the case of $\Gamma_b \sim 1.3$, than when the IMF is set as a free parameter. This is an indirect effect of the larger age estimate obtained for the old stellar component that, by being fainter, it requires a smaller young fraction to provide the observed departure in the NUV indices. Note that in Figure 4.2, the two innermost bins have ages older than 13 Gyr if $\Gamma_b \sim 1.3$, which are older than when considering a bottom-heavy IMF. Therefore, the effect of the IMF is to change the radial gradient of the age of the old component and, as a consequence, the gradient of the fractions of young stars. This highlights the importance of considering the IMF by including IMF-sensitive indices in the analysis of stellar populations in galaxy cores of extremely massive galaxies, which are characterised by extremely bottom-heavy IMFs.

4.7.4 Young stellar populations in BCG's cores

We also quantify the young mass fractions in the innermost regions for each individual galaxy in order to detect possible variations among the six galaxy cores. This can only be achieved for the innermost individual galaxy spectra (0 – 0.8 kpc) due to their sufficiently high S/N in the NUV spectral range. For each spectrum, the Hβ_o line is corrected for nebular emission contamination as detailed in LB19. The contamination is significant only for XSG1, XSG6 and XSG8 galaxies. We consider a bottom-heavy IMF slope for each galaxy according to the LB19 estimates. The derived parameters are presented in Table 4.4. All our galaxies present signs of young stars in their central regions. The stellar populations younger than 1 Gyr contribute less than one percent in all galaxies. The median value for our sample of 6 BCGs is 0.70±0.24%, in agreement with our estimate of the innermost stacked spectrum (Table 4.3). Note that the metallicity of the old component for all galaxies is higher than the maximum value allowed by the E-MILES models ([M/H] = 0.22), so we have performed a linear extrapolation of the metallicity up to [M/H] = 0.45.

As explained in appendix. A of LB19, XSG1, XSG6, XSG8, XSG9, and XSG10 are central group galaxies, according to the updated SDSS-DR7 group catalogue of Wang et al. (2014). XSG7 shares the central position of a galaxy group with another galaxy of similar luminosity. Also, XSG1, XSG6 and XSG8 have more prominent emission lines. In particular XSG6 is the galaxy with strongest emission in this work, being apparent at all the galactocentric distances. Based on these results, if one assumes that environment enhances the levels of star formation, one may expect galaxies like XSG6 to have the highest fractions of young stars, while XSG2 – not located at its cluster galaxy core – to have lowest f_{young} (see Section 4.7.6). However, we obtain that the young stellar contribution in XSG6 is the lowest. Moreover, we cannot establish a clear link between the young stellar populations in massive galaxies and their surrounding environment. Although it is remarkable that our sample of BCGs show quite similar young mass fractions smaller than 1% – with the exception

ID	$\mathrm{age_{old}}$ (Gyr)	$\mathrm{[M/H]_{old}}$	$\mathrm{f_{young}}$
(1)	(2)	(3)	(4)
XSG1	10.88±0.06	0.28±0.01	0.77±0.02
XSG6	10.73±0.06	0.25±0.01	0.14±0.03
XSG7	$11.75^{+0.05}_{-0.02}$	0.28±0.01	$0.84^{+0.04}_{-0.02}$
XSG8	10.63±0.05	0.41±0.01	0.62±0.03
XSG9	10.2±0.1	0.36±0.01	0.48±0.03
XSG10	>13.0	0.24±0.01	0.77±0.02

TABLE 4.4— **Best-fitting stellar population parameters for each BCG at the innermost regions (<0.8 kpc)**. For each galaxy listed in Col. 1 we obtain the best-fitting ages and metallicities for the old component reported in Col. 2 and 3, respectively. Col. 4 reports the best-fitting fraction of young stars of each galaxy.

of XSG6 for which we obtain less than 0.2% – we are aware that our sample is small.

4.7.5 Comparison with the young mass fractions obtained for massive galaxies at z∼0.4

We compare our results with the fraction of young stars found for the general ETG population in Chapter 3 for which we employed a similar methodology to stacked spectra from thousands of very massive ETGs at average redshift z∼0.4. At this redshift, the aperture $\phi_{\rm R}$ of the SDSS fibers corresponds to a radius of R = 5 kpc. For ETGs whose central velocity dispersion is larger than 300 kms^{-1} – similar to the BCG sample used here –, we derive mass fractions of stars formed in the last 2 Gyr of ∼0.48±0.01%. To perform a fair comparison with the present study, it is necessary to compute the young mass fractions in the same way as described in Section 2.3, i.e. for a 2 Gyr instead of 1 Gyr period of the young stellar component and integrate these fractions within an aperture $\phi_{\rm R} = 5$ kpc.

To be able to integrate the amount of young stars within 5 kpc, first we need to know the stellar mass of the young component $\mathrm{M_{young}}$ within that radius. Since the IMF slope is known at each radial distance, we follow the equation written in Figure 6 from LB19 to derive the stellar mass density Σ as a function of radius from the IMF slope Γ, written as:

$$\Sigma = -0.24\ln\left(-1 + \frac{1.84}{\Gamma - 1.3}\right) \tag{4.1}$$

The stellar mass density is multiplied by the area covered in each radial bin to derive the total stellar mass ($M_\star$) in each stack. Then, we fit an exponential function to the young mass fractions to extrapolate them out to 5 kpc. We multiply those fractions by the total stellar mass derived before, in order to obtain M_{young} as a function of radius. Finally, the fraction of young stars within a given aperture f_{ϕ_R} can be computed with:

$$f_{\phi_R} = \frac{\sum_{r=0kpc}^{r=R} M_{young}}{\sum_{r=0kpc}^{r=R} M_\star} \tag{4.2}$$

We obtain a f_{ϕ_R} ∼0.42% of young stars within an aperture of $\phi_R = 5$ kpc. Interestingly, the mass fraction of young stars within 5 kpc is slightly lower than the fraction derived in Chapter 3. Note that our BCGs are nearby galaxies located at the centre of a galaxy cluster or group. From abundance matching methods, at least half of the BOSS galaxies used are located in galaxy clusters with mass larger than $10^{14}\,M_\odot$. However, whether they are central or satellite galaxies remains unknown. Therefore, we need to have in mind that we are not comparing exactly the same class of objects, but very massive galaxies at different redshifts with an early-type morphology and very high central velocity dispersions. If we assume that our objects are similar to the galaxies in the most massive bin (central velocity dispersion of 300 – 340 kms^{-1}) but at different epochs we may conclude that these lower young mass fractions within the central 5 kpc regions are consistent with passive evolution. Lower contributions of young stars are expected at lower redshifts as a consequence of the decrease of gas available to form new stars. Moreover, if the required gas is contributed by mergers, it would be also expected to decrease at lower redshift, similar to the expected merger rate (Lotz et al. 2011; López-Sanjuan et al. 2015).

4.7.6 Young stellar components of the satellite galaxy XSG2

We analyse the young stellar contribution of galaxy XSG2, which is the only target of the sample used in LB19 classified as a satellite. Named J002819.3-001446.7 according to the SDSS, this galaxy is very similar to the other galaxies: a very massive early-type system with high central velocity dispersion. However, we exclude XSG2 from the main analysis of this work since it is the only galaxy that is not located in the centre of its parent cluster.

We have explored how the best-fitting parameters differ when including the XSG2 galaxy in the stacked spectra. Results are shown in Table 4.5. Overall, we find similar stellar population properties. Among the differences we obtain $f_{young} = 0.75\%$ for the innermost bin, which is slightly higher than the value obtained when this galaxy is excluded (see Table 4.3). Therefore, XSG2 has a slightly larger young stellar component in its centre compared to our main sample. The young component decreases to 0.07% for the second outermost bin. Without XSG2, this bin shows no fraction of young stars, which indicates that this galaxy also has a larger contribution of young stars at larger radii.

We also investigate the young stellar component from the individual galaxy spectrum of its central region. XSG2 hosts a $f_{young} = 1.1\%$. within its 0.8 kpc, which is larger than the fractions derived for our main sample (see Table 4.4).

Bin (kpc)	age$_{old}$ (Gyr)	[M/H]$_{old}$	f_{young}
(1)	(2)	(3)	(4)
0.0 – 0.8	$11.6^{+0.5}_{-0.3}$	0.30±0.02	$0.75^{+0.09}_{-0.10}$
0.8 – 1.2	$11.9^{+0.4}_{-0.3}$	0.20±0.02	0.27±0.05
1.2 – 1.7	$12.6^{+0.5}_{-0.4}$	0.14±0.03	0.17±0.03
1.7 – 2.4	$11.4^{+0.6}_{-0.5}$	0.14±0.03	0.07±0.03
2.4 – 4.2	$10.5^{+2.0}_{-1.0}$	0.13±0.05	0
XSG2 (centre)	$11.75^{+0.06}_{-0.03}$	0.22±0.01	1.10±0.02

Table 4.5— **Best-fitting values when XSG2 is included.** Each column shows the best-fitting stellar population parameters for each galactocentric distance bin when the massive satellite galaxy XSG2 studied in detailed in LB19 is included in the final stacks. Last row shows the estimates for the XSG2 galaxy of the individual spectrum at the innermost region (< 0.8 kpc). Ages and metallicities for the old stellar component are listed in the Col. 2 and 3, respectively, and fraction of young stars in Col. 4.

4.8 Discussion

A 0.7% fraction of young stars implies that the SFR in the last 1 Gyr of their SFHs (i.e. redshifts $z < 0.1$) in the galaxy cores of our galaxy sample is, on average, $2.2\,M_{\odot}yr^{-1}$. Such a level of star formation activity is possible due to the existence of reservoirs of cold gas in their central regions. The source of this gas supply to form new stars remains unclear. It could be associated with intrinsic processes such as pristine gas not yet transformed into stars or recycled gas from stellar evolution, or extrinsic processes such as a modest accretion of gas-rich galaxies or the intracluster medium that reach the galaxy cores. BCGs are thought to experience a large number of galaxy mergers and interactions with the satellite galaxies surrounding them. Recent numerical simulations have shown that the inner galaxy regions are dominated by *in-situ* stars, i.e., stars formed within the host galaxy, whereas the outer regions are mostly populated with *ex-situ* stars accreted during mergers with smaller galaxies (Oser et al. 2010; Navarro-González et al. 2013; Shankar et al. 2013; Cooper et al. 2015).

The accreted material dominates the outer galaxy regions, but whether the accreted gas reaches the central regions of central cluster galaxies and cools down to be able to form these new stars remains unknown. With the methodology and data used in this work we are not able to constrain the metallicity of the young component. This would give hints on the origin of the gas employed to form such new stars.

A related issue concerns the IMF, which imposes further constraints on the available budget of gas. The IMF regulates the amount of gas returned to the ISM due to stellar evolution. A bottom-heavy IMF is dominated by low-mass dwarf stars with longer lifetimes than the Hubble time, which lock-up most of this gas making it unavailable for star formation. For example, according to the E-MILES models, a Kroupa-like IMF $\Gamma_b = 1.3$ returns a gas fraction of $f_{gas} \sim 36.7\%$ into the ISM after 10.5 Gyr (i.e., the age of the old stellar population before the 1 Gyr period that we consider for constraining the young component). However, a stellar population with a bottom-heavy IMF $\Gamma_b = 3.0$ returns an order of magnitude less gas: $f_{gas} \sim 3.3\%$. From equation (4.1), we infer that the stellar mass of the old stellar population in the innermost bin (< 0.8 kpc) is $3.2{\times}10^{11}\,M_{\odot}$. Since for this bin $\Gamma_b = 3.0$, this implies that the amount of gas returned to the ISM from this population is $\sim 1{\times}10^{10}\,M_{\odot}$. Interestingly, the stellar mass of the young stellar component in this region is $2.2{\times}10^{9}\,M_{\odot}$. Therefore, this amount of gas could be responsible for producing the young stars we observe if this gas is able to cool. In this case, the star formation efficiency (SFE), i.e, the star formation rate per unit gas mass, would be 2.1×10^{-10} yr^{-1} within the last 1 Gyr. However, this SFE is one order of magnitude lower than the Kokusho et al. (2017) estimates for nearby ETGs of similar stellar masses. Therefore, only 10% of this gas would be required to cool down and form stars in order to match their SFE estimates. If the innermost bin, instead, was populated by a Kroupa-like IMF stellar population, as considered in Section 4.7.3, the SFE would be 3 orders of magnitude lower than the Kokusho et al. (2017) results and only 0.1% of the gas returned into the ISM would be required to cool down to form new stars. Additionally, from the equation shown in Figure 5 of Martig et al. (2013), which establishes a correlation between the SFR and the gas surface densities for a sample of ETGs and LTGs, we infer a SFR surface density in good agreement with our estimates.

Our results suggest that the young stellar populations found in the central regions of our BCGs may be the result of star formation fueled by gas returned from the evolution of the old stellar populations that dominate the bulk of these galaxies. However, due to the particular location of these objects in their host clusters, BCGs constantly interact with and are shaped by their surrounding

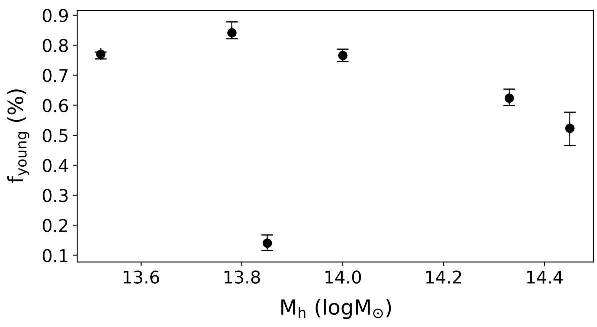

FIGURE 4.7— **Correlation between young stellar populations with halo mass.** Young stellar mass fraction in the centre of each individual BCG as a function of its halo mass values from in Table A1 in LB19.

environment. Several studies observed a trend with the fraction of star-forming BCGs and halo mass, where this fraction decreases with the halo mass (Oliva-Altamirano et al. 2014; Cerulo et al. 2019). With the values provided by LB19, we find that, with the exception of the XSG6 galaxy, BCGs with higher fraction of young stars in their central regions tend to be located in lower halo mass clusters (see Figure 4.7). There is no clear reason why XSG6, which has the lowest fraction of young stars, should be different than the other galaxies for this particular trend. Thus, our galaxy sample is too small to study this trend with the halo mass accurately, and therefore a larger sample should be used.

Galaxy cores are where larger amounts of available gas are accumulated due to their deep gravitational potential wells, which are expected to retain gas more efficiently than in the outer regions. Moving outwards, the star formation activity produces increasingly smaller fractions of young stars, so that beyond 2 kpc no new stars are being formed. Note, however, that these results are average estimates for our sample of six BCGs. Given that the sample studied in this work is small, it is not possible to draw more statistically meaningful conclusions about the existence of young stellar population gradients in the BCG population as a whole.

While this study is not able to answer which is the main mechanism that fuels the late star formation in BCGs, these young stellar gradients are in agreement with those works that associate the ”blue-core” in some sample of BCGs to the presence of active star formation with young stellar mass fractions lower than 1% (Bildfell et al. 2008; Pipino et al. 2009). More recently, Cerulo et al. (2019) reported that the star formation in BCGs is more frequent at higher redshifts and decreases with cluster mass and galaxy stellar mass. Since more massive BCGs lie in the centre of more massive clusters the young stellar gradients should be further investigated by a larger sample of individual BCGs so we can determine whether the star formation is affected by the surrounding environment in each galaxy cluster. Very important constraints to the SFH of BCGs should also come from studying how the young stellar gradients of massive central galaxies evolve with redshift.

4.9 Conclusions

Central galaxies in clusters are very special places to study galaxy formation and evolution. Line-strength indices of their integrated spectra provide important insights on their stellar populations. In this Chapter, we analyse the average radial distribution of the young stellar component of six massive BCGs (with central velocity dispersions $\sigma > 300$ kms^{-1}). We divide the individual galaxy spectra in five radial bins and stack them to obtain representative spectra with high S/N. The set of NUV indices have been selected so that they are highly sensitive to young stars, and the optical indices sensitive to the bulk of the stellar population. The latter include indices sensitive to the age, metallicity and IMF slope. We show that the measured NUV indices in our stacked spectra are not well represented by a single, old SSP model, as is the case if only the optical indices are fitted. The NUV indices of our BCGs show significantly lower strengths in comparison to the SSP models. We interpret this departure as evidence for a young stellar component. We investigated the young stellar gradients with an index-fitting approach, by comparing the observed values with the model predictions that come from a simple model of the SFH of a massive galaxy. This model consists of a superposition of a single burst representing the old stellar component, and a young component that is characterised by assuming constant SFR in the last 1 Gyr. The main results are summarised below.

From Hβ_o and [MgFe]$'$ we measured the mean luminosity-weighted ages, metallicities and IMF slopes of each radial bin. We find old ages with an average MLWA of 11.8 Gyr. The best-fitting metallicities present a negative gradient with super-solar values at all radial bins. The stacked NUV index values show, however, a mismatch with respect to the old stellar population model predictions of their MLWAs, suggesting that a SSP is not the optimal representation so that an additional component is required, which is mainly contributing to bluer wavelengths.

Thanks to the highly IMF-sensitive indices included in the set of indices, TiO1 and $TiO2_{SDSS}$, we have been able to fit the IMF slope Γ_b. The obtained values are in good agreement with those derived by LB19. As it has already been studied by previous authors, there is a clear IMF variation with radius, from bottom heavy at the central regions to a standard IMF at larger radii. We find that it is crucial to account for the radially varying IMF in massive galaxies in order to correctly determine the young stellar gradients via the NUV.

The key finding in this study is a negative gradient of the young stellar contribution in our stacked spectra of BCGs. The results show that young stars ($<$ 1 Gyr) are localised in the cores of massive central cluster galaxies, where we measure a young mass fraction of f_{young} $\sim$0.7% at $<$ 0.8 kpc. At larger radii this decreases rapidly to virtually an absence of young stars beyond 2 kpc. With these small components of young stars on top of a dominant old population we are able to match the observed indices of each radial bin as shown in Figure 4.5.

The analysis of the innermost regions of the individual BCGs, shows that all galaxies exhibit fractions of young stars smaller than 1% within 0.8 kpc. However, given the small sample size, we are not able to derive general properties about the young contributions of the BCG population compared to those from non-central cluster galaxies. Further investigations should be performed along this line including a wider variety of environments of the most massive galaxies in the Universe.

5

Young stars in the relic galaxy NGC 1277

My wish is to stay always like this
living quietly in a corner of nature.

Claude Monet

Relic galaxies are thought to be the progenitors of the cores of present-day massive ellipticals where successive mergers and interactions act to increase their sizes and stellar masses to form the local ETG population. However, given the stochastic nature of galaxy evolution processes, a few of these progenitors survive without interacting with other galaxies keeping their compactness from high-redshift. These galaxies are known as ”relic galaxies” (also sometimes called massive ultra-compact galaxies). Therefore the relic galaxies we see in the nearby Universe are composed of mainly old stellar populations. On one hand, this is the result of a passive evolution of long-lived stars that are born at $z > 2$, during this first stage in a two-phase galaxy formation scenario. Also, on the other hand, the lack of more recent star formation events arises due to the lack of accreted material that characterise a second, frustrated, phase, which extends over a much longer time scale until the present time.

The study of young stellar components in relic galaxies has not been investigated in detail and such results would provide key insights regarding the evolution of massive galaxies. If these galaxies have not been interacting since their initial epoch of formation but they are still forming new stars at low-redshift, this would suggest that the star formation activity found in the cores of our samples of massive ETGs analysed in the two previous chapters, could be mainly triggered by intrinsic galaxy processes.

In this chapter we investigate the young stellar components in the central region of NGC 1277, which is regarded as the best representative of these relic galaxies. We follow the same methodology applied before, i.e. by fitting its observed NUV and optical indices with model predictions from a SFH parameterisation. NGC 1277 is a particularly well studied galaxy and identified as a relic from different stellar population analysis. Observational evidences pointed out that NGC 1277 has very old stellar population and, therefore, if a young (<1 Gyr) stellar component is present, it would be clearly detectable by analysing the NUV range.

5.1 The relic galaxy NGC 1277

In the early Universe, the cores of present-day ETGs form dissipatively (Larson, 1974), creating massive, compact objects termed "red nuggets" (Damjanov et al., 2009). NGC 1277 is a low-redshift galaxy (z ∼ 0.0169) that closely resembles a red nugget: it is compact, rapidly rotating, and its internal structure matches compact galaxies at z ∼ 2 (Trujillo et al., 2014). NGC 1277 has been studied in extensive detail (Trujillo et al. 2014; Ferré-Mateu et al. 2015, 2017; Martín-Navarro et al. 2015b; Yıldırım et al. 2017) and has been identified as a relic galaxy (Beasley et al., 2018). Therefore, the properties of NGC 1277 at z ∼ 0 are very similar to those of massive galaxies at z ∼ 2, which make this relic galaxy a key target to study as it holds information unaltered since high-redshift.

NGC 1277 is a massive compact galaxy located in the Perseus cluster. A remarkable aspect of NGC 1277 is that it has a mass of $1.2 \times 10^{11}\,M_{\odot}$ and effective radius of only 1.2 kpc (Trujillo et al. 2014; Yıldırım et al. 2017). Normal ETGs of the same mass are on average five times larger. Therefore, NGC 1277 is considerably more compact and dense than mass-matched ETGs. This indicates that it has evolved until the present-day Universe preserving its size and remaining untouched since its initial epoch of formation. It contains old and metal-rich stellar populations enhanced in [Mg/Fe] (Trujillo et al. 2014; Martín-Navarro et al. 2015b; Ferré-Mateu et al. 2017), indicating that most of its stars were formed in a extremely short and intense star formation burst at z > 2, followed by passive evolution. Martín-Navarro et al. (2015b) showed that this galaxy has a extremely bottom-heavy IMF at all radii, in sharp contrast with massive ETGs, which show negative radial IMF profiles, with bottom-heavy IMFs in the centre and reaching Milky Way-like shapes beyond their half effective radii. NGC 1277 has the most massive central black hole known so far (van den Bosch et al., 2012). Beasley et al. (2018) showed that the lack of blue globular clusters correlates with an unusually uneventful merger history. According to these results, at most only 10% of its mass has been accreted. On the contrary, the accreted mass fraction of massive ETGs is typically 50 – 60%. Therefore, quantifying the contribution of young stars in NGC 1277 emerges as a key observational constraint for understanding the origins of recent star formation in massive galaxies.

5.2 Observations and data reduction

5.2.1 NUV data

We performed long-slit spectroscopic observations of the relic galaxy NGC 1277, carried out at the 2.5 m Isaac Newton Telescope (INT), located at the Observatory del Roque de los Muchachos on La Palma (Spain). Observations were carried out in visitor mode during an observing run on December 2018 under proposal program ID: 149-INT12/18B (PI: NSR). We employed the IDS spectograph using the R1200B grating centered at 3600 Å – to acquire the bluest wavelength possible with the instrument 3100 Å – with a x2 binning in both spatial and spectral direction, which corresponds to a spatial resolution of 0.8 arcsec/pixel. The INT slit is 3.3 arcmin long. We opened the slit width 2 arcsec and positioned along the major axis of NGC 1277, as shown in Figure 5.1. NGC 1277 is located in the Perseus cluster, which is one of the most massive nearby structures. The image shows that our target is close to the massive elliptical NGC1278.

We took 24 exposures of 30 minutes. Two individual exposures had to be removed since clouds covered the target during most of the exposure and the signal was too low. The total useful exposure time and other galaxy properties are listed at Table 5.1. The exposures were acquired during three different nights.

We followed the standard procedure for reducing the INT spectroscopic data using IRAF + python packages. We summarise below some important data reduction steps that needed to be performed for each observing night:

- *Bias subtraction.* This step removes the zero-level counts introduced by the instrumental configuration that can vary at each pixel. With our configuration this level is on average 2100 counts per pixel. These images were taken without any exposure time and just reading the CCD. We take the mean of 15 bias (with an average standard deviation of 1.5 counts) and subtracted from the rest of the images.

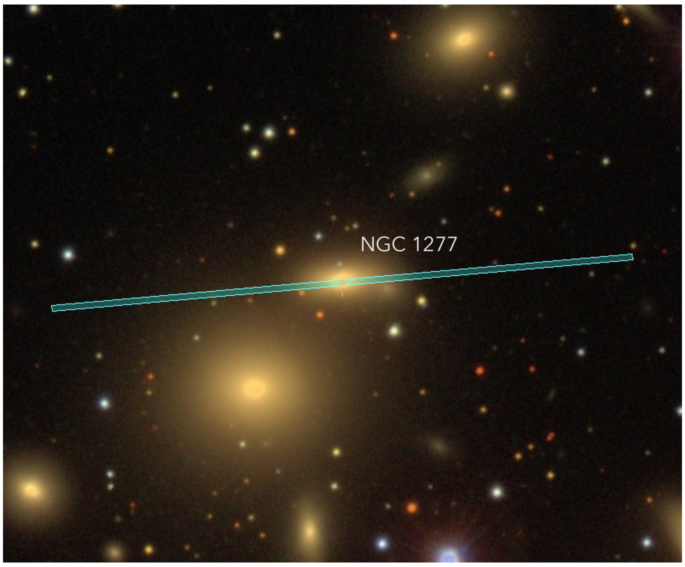

FIGURE 5.1— True colour image of a region of a Perseus cluster centered at NGC 1277 galaxy. Blue rectangle represents the slit of 2 arcsec width positioned along the major axis of the galaxy used at the INT observation runs. The field of view of this image is 4×3.1 arcmin. This composition image is obtained with Aladin (Bonnarel et al., 2000).

Galaxy	NGC 1277
RA	03 19 51
DEC	+41 34 24
Exposure time	11 h
PA	95 deg
redshift	0.0169
grating	R1200B
pixel scale	0.8 arcsec/pix
wavelength range	3100 – 4100 Å
spectral resolution	3.5 Å
spectral dispersion	0.97 Å/pix
seeing	0.6 – 1.0 arcsec

TABLE 5.1— **NGC 1277 observation properties.** The table summarises the main observing characteristics with the instrumental configuration at the INT.

- *Cosmic rays removal.* High-energy particles impact to the CCD and saturate some pixels. Cosmic rays have been removed with the python version of LA-cosmic package (van Dokkum, 2001), which detects pixels damaged by cosmic rays, and removes them by making an interpolation from the surrounding pixels.

- *Flat-fielding.* Pixels of the CCD do not respond in the same way when they are illuminated with the same amount of light. This sensitivity pattern needs to be corrected to the science images. We took 11 dome flats of 60 seconds exposure each, which take an image of a uniformly illuminated screen in the dome. The average image represents the sensitivity pixel-to-pixel and is used to remove the illumination patterns by dividing the science images by the normalised flat-field.

- *Wavelength calibration.* A CuAr+CuNe lamp was used for wavelength calibration. A 5th order polynomial fitted 20 arc lines that led to a typical *rms* of 0.04 Å. This polynomial is used in the spectral direction to convert each pixel to a specific wavelength. The bluest arc line of this lamp is positioned at 3247.54 Å, which is redder than the bluest observed wavelength. Therefore, given the few arc lines in the blue, this calibration was verified via fourier cross-correlation against MILES model templates.

- *Sky subtraction.* The sky subtraction is performed when extracting the final one-dimension spectrum using the APALL routine. During this step, a polynomial from both sides of the galaxy spectrum is fitted and then subtracted to the extracted spectrum. The removed sky is at 10 kpc distance from the centre of the galaxy, which is sufficient given that the effective radius of this galaxy is Re = 1.2 kpc.

Before sky subtraction, all the individual exposures have been added to obtain the final added two-dimensional (2D) spectrum. We show in Figure 5.2 the 11 h 2D spectrum. Since the exposures were taken with different weather and atmospheric conditions, the individual exposures are added according to a weight w_i (where $\sum w_i = 1$) that depends basically on the seeing and the airmass at the moment of the observation. In this way, exposures with better observing conditions have relatively more weight in the final spectrum, allowing us to increase the final S/N of the added 2D spectrum. A spectrum of NGC 1277 was extracted within an aperture of 1 kpc radius, that is, 3.6 pixels aperture radius. The extracted spectrum with useful information covers the spectral range 3100 – 4100 Å in the rest-frame and is shown in Figure 5.3.

Before measuring NUV indices and comparing them with E-MILES model predictions, we need to smooth the observed spectrum and the SSP models to the same spectral resolution. However, we take into account the instrumental resolution of 3.5 Å to obtain the kinematics using `pPXF` program. This code is based on a penalized likelihood approach, fitting each pixel of the spectrum. We use as templates the E-MILES SSP models and convolve the data to match the spectral resolution of the model template. The kinematics was derived using the wavelength range 3500 – 3950 Å in rest-frame. We derive a stellar velocity dispersion of 350±8 km/s, which indicates that this is a very massive galaxy, and a redshift z ∼ 0.0169, consistent with Yıldırım et al. (2017) and Martín-Navarro et al. (2015b).

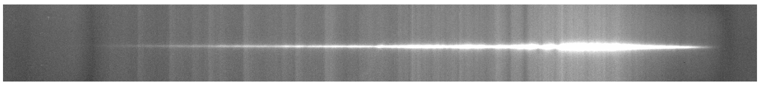

FIGURE 5.2— **Two dimensional INT spectrum of NGC 1277.** The image shows the 11 hours two-dimensional spectrum of NGC 1277. It has 175×2100 pixels. The spatial direction is the vertical axis and the spectral direction is the horizontal axis.

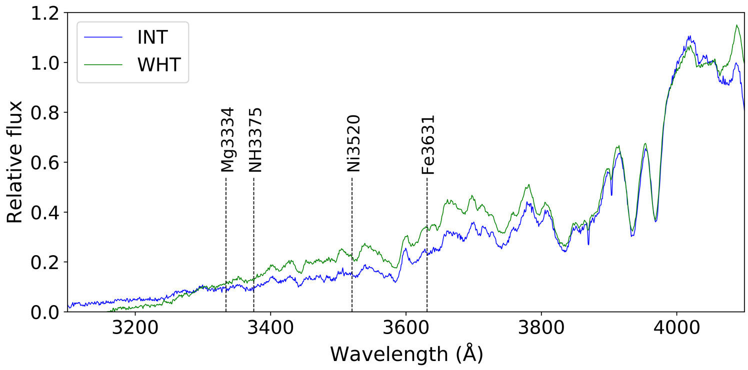

FIGURE 5.3— **NUV spectrum of NGC 1277.** One-dimensional spectra of NGC 1277 in the NUV spectral range extracted within 1 kpc from INT (blue) and WHT (red). Vertical lines indicate the set of NUV indices used during the fitting process in Section 5.5.

5.2.2 Optical data

In the spectral range covered by the INT we miss information from the optical spectral range. We have used long-slit optical data obtained with the ISIS spectrograph on the 4.2m William Herschel Telescope (WHT) by previous authors. A detailed description of the observations and data reduction of the optical data of NGC 1277 is described in Trujillo et al. (2014). Briefly, a blue grating R300B was centered at 5300 Å with a x2 binning in the spatial direction. The 1 arcsec slit was placed along NGC 1277's major axis. The target was observed with good sky conditions with a seeing of 0.7 arcsec. The total exposure time on source was 3 hours split into exposures of 30 minutes. This configuration provided a spectral resolution of 3.4 Å. The extracted spectrum covers the wavelength range 3400 – 6200 Å and has very high quality. We use the spectrum extracted within 1 kpc as we have done with the INT spectrum and measure indices from the same galaxy region. The stellar velocity dispersion measured of this optical spectrum is $380{\pm}6\,\mathrm{km\,s^{-1}}$, slightly higher than the one we obtain from the INT data. The difference found in velocity dispersion between the NUV and optical spectra ($\Delta\sigma = 30\,\mathrm{km\,s^{-1}}$) has a negligible effect in our measured NUV indices. This difference is mainly because of the different wavelength ranges used. The stellar velocity dispersion of galaxies has been tipically derived from the optical range, which contains a larger amount of absorption features.

5.2.3 Variation of the NUV indices without flux calibration

We have checked how the NUV indices used in this work are affected by flux calibration. We could not calibrate the INT data to convert the number of counts into flux and correct for the variation of the CCD response with wavelength. We obtained a bad CCD response calibration with the observed standard stars and the response function could not be applied to our observations. Our inability to flux calibrate well these data was not unexpected, given the extremely blue nature of the spectra, which essentially reach the atmospheric cut-off at 3000 Å. This makes them very sensitive to small variations in airmass and other observing conditions that changed between the observation of the galaxy and the standard star. Fortunately, between 3100 and 4100 Å the instrumental sensitivity is quite flat. We address this issue to evaluate how this may affect the measured indices. We measure the NUV indices in the flux and non flux-calibrated spectra of WHT within 1 kpc aperture, which are shown in the top panel of Figure 5.4, both normalised around 4000 Å.

The right panel shows the measured NUV line-strengths. There is a virtually negligible difference of the non-flux calibrated NUV indices with respect to the measurements on the flux calibrated spectrum, which reasure our index measurements. The indices used here cover a narrow spectral range that include two pseudo-continua defined locally at both sides of each absorption feature, minimising the effect of a change in the continuum level. Therefore, the change of the slope of the spectral continuum due to flux calibration does not have a significant impact on the NUV line-strength indices. We compare the INT and WHT non-flux calibrated spectra in Figure 5.3.

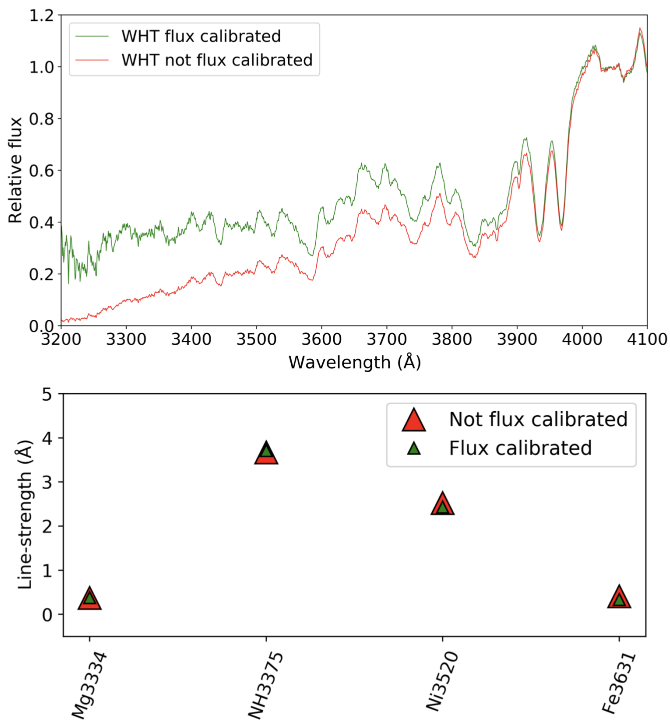

FIGURE 5.4— **Effect on the NUV indices due to flux calibration.** The top panel shows the WHT spectra flux-calibrated (red) and non-flux calibrated (green). The bottom panel shows the indices measured in both spectra following the same colour-code.

5.3 Constraints on the age and metallicity of NGC 1277

The stellar populations of relic galaxies are characterised by being very old and metal-rich. Single old SSP models would be good representations of their spectra, or at least in the optical range, representing the bulk of their stars. Therefore, we estimate the average stellar population properties by fitting the widely used Hβ_o and [MgFe]$'$ optical indicators, sensitive to the MLWA and mean metallicity, respectively.

The spectrum may include some nebular emission, revealing the presence of ionised gas due to a modest level of star formation activity. The age-sensitive index Hβ_o may be thus affected and as a consequence, it would lead to an overestimate of the inferred MLWA. To address this issue, we subtract a best-fitting SSP model spectrum around Hβ_o from the observed spectrum. We obtain a residual of ΔH$\beta_o \sim 0.2$ Å, which is added to the observed index before deriving the MLWA the age.

The observed strengths indicate an overall old and metal-rich stellar population as shown in the grid of Figure 5.5. The grid shows the SSP model values for a bottom-heavy IMF with slope $\Gamma_b = 3.0$ and for varying age and metallicity. The two observed indices are fitted with the SSP model predictions by minimising the χ^2. We derive an old age of 14 Gyr and a metal-rich stellar poulation with metallicity [M/H]=0.23. Note that the estimated age is the upper age limit of the E-MILES SSP models, indicating that NGC 1277 was formed in early epochs when the first galaxies started to form. Our results are in good agreement with Trujillo et al. (2014) that derived a nearly constant age with radius of 13.5 Gyr and a strong negative metallicity gradient with super-solar values up to 1.5 kpc.

5.4 NGC 1277 line-strength indices

Given the spectral range of the INT and WHT spectra, we focus on 8 absorption line indices defined within the NUV and optical ranges. In this study, we use those NUV indices that show larger sensitivity to small fractions of young stars as we did in Chapter 4. Figure 5.6 shows the variation of the indices used for the fitting process as a function of the age of a single SSP for a bottom-heavy IMF $\Gamma_b = 3.0$ and for three different metallicities: solar metallicity [M/H] = 0 (solid line), super-solar metallicity [M/H] = +0.22 (dashed line), and super metal-rich [M/H] = +0.36 (dot-dashed line). The latter predictions come from a linear extrapolation of the SSP models. The observed indices in the relic galaxy NGC 1277 within 1 kpc are shown as orange stars with 1 σ level uncertainties. There is a clear mismatch between the observed data and old SSP model predictions in the NUV indices, which is not found in the optical

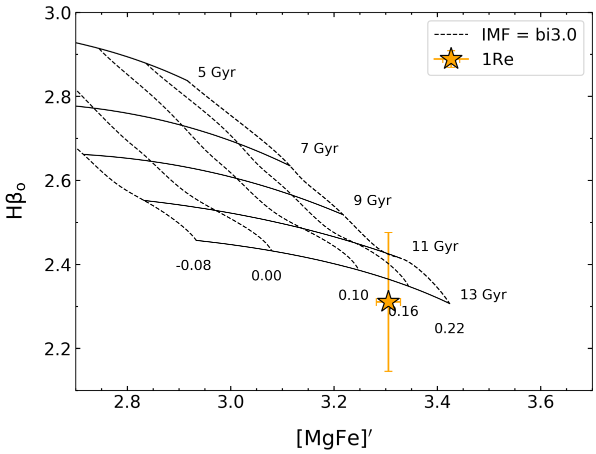

FIGURE 5.5— **Optical index-index grid.** Measurements of the age-sensitive spectral index Hβ_o are plotted as a function of the total metallicity sensitive index [MgFe]′. The grid covers a range of SSP ages (solid lines) and metallicities (dashed lines). The orange star is the observed NGC 1277 index measurement. Observed data and model grid are smoothed to match a common velocity dispersion of 380 km s^{-1}.

indices. This suggests that an old SSP is not compatible as a representation of the SFH of the relic galaxy and calls for an additional component. Here we aim to quantify the mass fraction of very young stellar populations that decreases the strength of the NUV features.

As a reference, the figure also shows in black dots the measurements on the most massive BOSS ETG stack of Chapter 3, as it has a similar velocity dispersion to our target. Note, however, that it represents the index values measured within a larger aperture (5 kpc) than NGC 1277. The index values from the innermost bin (0.8 kpc) from the BCGs studied in Chapter 4 are represented as triangles. All NUV measurements show a deviation with respect to a old SSP of its MLWA and its metallicity. Note that, as expected, NGC 1277 is clearly older than the other two galaxies since the BOSS stack is at z ∼ 0.4 and the BCG stack, in contrast to our relic, has experienced a large amount of mergers that have slightly rejuvenated on average its mean stellar populations.

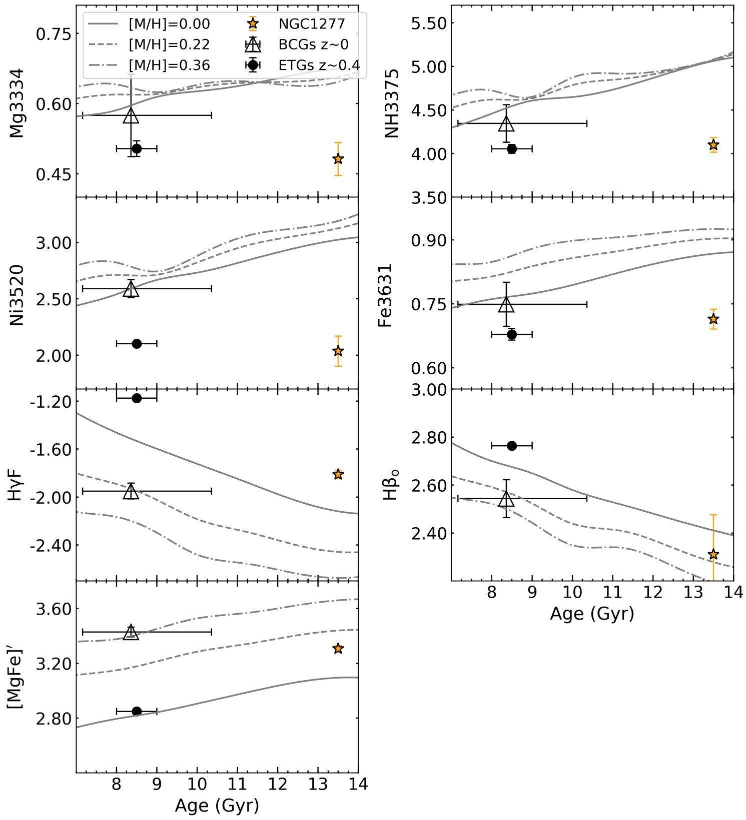

FIGURE 5.6— **NUV and optical line-strength indices.** Each panel shows the selected NUV and optical SSP model indices as a function of age, for three different metallicities (solar, [M/H] = 0.00 solid lines; [M/H] = 0.22 dashed lines; [M/H] = 0.36 dashed-dotted lines) for a bottom heavy bimodal IMF $\Gamma_b = 3.0$. The observed measurements of NGC 1277 are plotted as orange stars as a function of the MLWA. SSP models and data are at the same spectral resolution of 380 km s^{-1}. Measurements on the most massive ETG bin of Chapter 3 are plotted as black dots and values from the innermost bin from the BCGs studied in Chapter 4 are represented as triangles all smoothed to match the same resolution.

5.5 Fitting methods

The method employed here consists of fitting the observed line-strengths with model predictions derived from a simple modelling of the SFH for very massive galaxies, which in this case is the *1SSP+cSFR* model described in Chapter 2. For the old stellar component – described by a SSP – we assume prior distributions of ages from 1 to 14 Gyr and metallicities from – 0.40 to 0.40 dex. The young component is parametrised by assuming a constant SFR in the last 1 Gyr. We assume a bottom-heavy IMF of $\Gamma_b = 3.0$, following Martín-Navarro et al. (2015b). These authors derived an IMF radial profile for this galaxy up to 1.5 R_e, which smoothly decreases from $\Gamma_b = 3.0$ at the innermost regions to $\Gamma_b = 2.5$ at 1.5 R_e. The fitted stellar population parameters are the age and metallicity of the old stellar component, Age_{old} and $[M/H]_{old}$, respectively, and the relative mass fraction of young stars formed during the most recent period (f_{young}).

For this case, each MCMC fitting process consists of 20 walkers exploring the parameter space over 20000 steps. We fit the observed line-strengths to obtain the best-fitting model parameters via MCMC chains. This process gives the best-fitting values for the set of model parameters described above.

5.6 Results

Figure 5.6 shows the discrepancy between the observed and the model NUV indices for a single old SSP. This mismatch is resolved by adding a small amount of recent star formation on top of an old stellar population.

- **Fits with NUV indices**

In the spectral range covered by the INT we miss information from the optical spectral range. We have investigated how our results could be potentially affected if only fitting the NUV indices with central wavelengths redder than 3100 Å. We explore this effect by using the stacked spectra from BOSS (studied in Chapter 3), which covers a wider spectral range. We repeat the fitting process to see if we retrieve the obtained amount of young stars but in this case by using only the indices defined within the spectral range of our INT data, which are Mg3334, NH3375, Ni3520, Fe3631 and Fe3646. We find that these five indices alone are not able to constrain small amounts of young stellar components. This indicates that they require optical indices to be also sensitive to the bulk of old stellar populations. We do not use other indices defined in the NUV spectral region since they are highly affected by the alpha-element abundance present in massive galaxies, as discussed in Chapter 4.

As found in Chapter 3 (see Figure 3.11), without optical indices but using bluer indices down to Fe2609, we are able to infer small amounts of young stellar populations on top of an old component. Note, however, that lower young mass fractions are obtained than when optical indices are fitted simultaneously. Indices bluer than 3000 Å are much more sensitive to small fractions of young stars (see Figure 2.2 in Chapter 2) and can be used, with enough S/N, without the optical to study the recent star formation. On the contrary, NUV indices within the wavelength range 3100 – 3700 Å not only are less sensitive to young components than bluer ones, but also they are less sensitive to the old stellar populations than the optical ones. This means that indices defined within this intermediate spectral range require the optical indices to infer the young stellar components.

- **Fits with each NUV index**

We have tested how each NUV index is affected by the young stellar component to see if there is any particular index that has any particular behaviour. We fit the optical indices, HγF, Hβ_o and [MgFe]$'$ simultaneously with each NUV index, one by one. The results are summarised in Table 5.3. Almost all the indices provide similar best-fitting solutions, with a very old and metal-rich old stellar component and a nearly similar contribution from young stars that ranges from 0.72% to 0.88%, in mass. Interestingly, indices with larger χ^2_ν are the ones we discarded in the previous Chapter due to their sensitivity not only to the young stellar component, but also to the alpha-element abundances to an even greater degree. Fe3646 was not discarded in Chapter 4 but was the only index that was not well fitted (see Figure 4.5), probably due to its sensitivity to the alpha-enhancement. This suggests that it has a high sensitivity to the alpha-enhancement that is not well reproduced by the alpha-enhanced SSP models and, for this reason, we exclude it here. Therefore, we base the following analysis on the remaining indices, i.e. Mg3334, NH3360, NH3375, Ni3520 and Fe3631.

- **Fits with NUV + optical indices**

We fit the selected NUV and optical features simultaneously. We do not use NH3360 since this feature is represented in part by the NH3375 index. The best-fitting indices following our *1SSP+cSFR* modelling approach are shown in Figure 5.8. We measure mass fractions for the young stellar component within the 1 kpc aperture of $f_{young} \sim 0.8\%$. This means that the relic galaxy NGC 1277 experience a low level of recent star formation in its central regions compatible

index	Age_{old} (Gyr)	$[M/H]_{old}$ (dex)	f_{young} (%)	χ^2_ν
Mg3334	12	0.25	0.75	1.1
NH3360	14	0.23	0.75	0.4
NH3375	10	0.3	0.72	1.0
Ni3520	9	0.27	0.76	3.2
Fe3581	11	0.38	0.88	28
Fe3619	14	0.22	0.86	6.5
Fe3631	14	0.27	0.73	1.9
Fe3646	<4	>0.4	>1.2	82

TABLE 5.2— **Fits to each NUV index individually.** Each index listed in column 1 fitted with the optical indices simultaneously gives the best-fitting age and metallicity of the old component of Col. 2 and 3, respectively, and the best-fitting young stellar mass fraction of Col. 4. The reduced χ^2 of the fit is shown in the last column.

with a specific SFR of $\sim 8\,x\,10^{-12}\,yr^{-1}$ within the last 1 Gyr. These best-fitting line-strengths provide a better agreement with the observations with a combination of a small mass fraction in stars younger than 1 Gyr, on top of an overwhelming dominating old component.

	Age_{old} (Gyr)	$[M/H]_{old}$ (dex)	f_{young} (%)	χ^2_ν
NGC 1277	$12.6^{+0.6}_{-0.7}$	$0.23^{+0.02}_{-0.01}$	0.80±0.06	2.4

TABLE 5.3— **Young stellar populations in NGC 1277.** The table summarises the best-fitting stellar population parameters. The best-fitting age and metallicity of the old component are shown in Col. 2 and 3, respectively, and the best-fitting young stellar mass fraction of Col. 4. The reduced χ^2 of the best-fitting model is shown in the last column.

In Figure 5.7 we show the sampled probability distribution functions as histograms and the two-dimensional contours between each pair of fitted parameters that result from the MCMC fitting process, which represent the joint PDFs between a given pair of parameters.

5.7 Discussion and conclusions

The star formation in massive galaxies was efficiently ceased at earlier times. The majority of these high-redshift massive galaxies experienced a growth both in mass and size at later times. This growth was through successive mergers and interactions originating the massive and large ETGs we see in the present-day Universe. Therefore, it gets more difficult to disentangle whether the young stellar population found in lower-redshift massive ETGs is due to intrinsic prop-

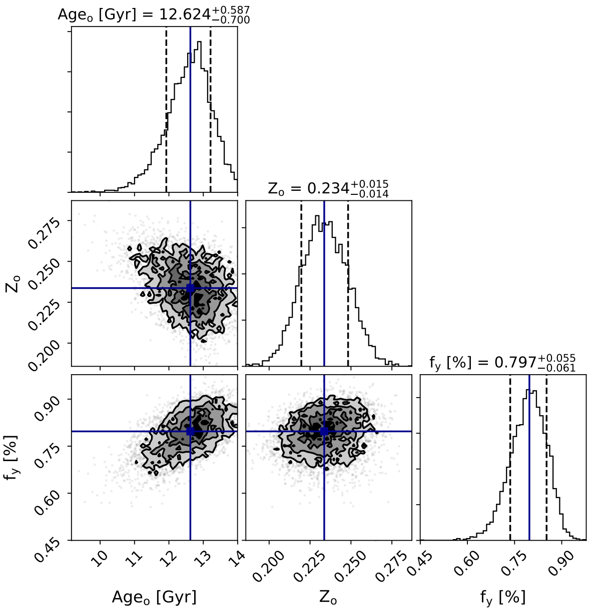

FIGURE 5.7— **MCMC probability distribution functions.** Each panel shows the PDF of the fitting parameters. From the top to the bottom: age and metallicity for the old component, and mass fraction of the young stellar component. Upper panels show the PDF for each parameter marginalised over the other parameters. Contours show the two-dimensional projections between all parameters. The solid lines indicate the medians of each distribution.

erties derived from their initial formation or due to the experienced disruptions with surrounding galaxies and environment.

Fortunately, without contamination from recent accretion (Beasley et al., 2018), relic galaxies are the perfect targets to study the intrinsic regulation of star formation in massive galaxies. They are characterised for being extremely old, so the majority of their stellar populations was formed at their initial epoch of formation. The absence of major interactions has prevented their growth in size and they evolved as massive compact systems until the local Universe. They represent the local progenitors of the cores of massive ETGs. Therefore, they are ideal laboratories for studying the mechanisms that regulate the evolution

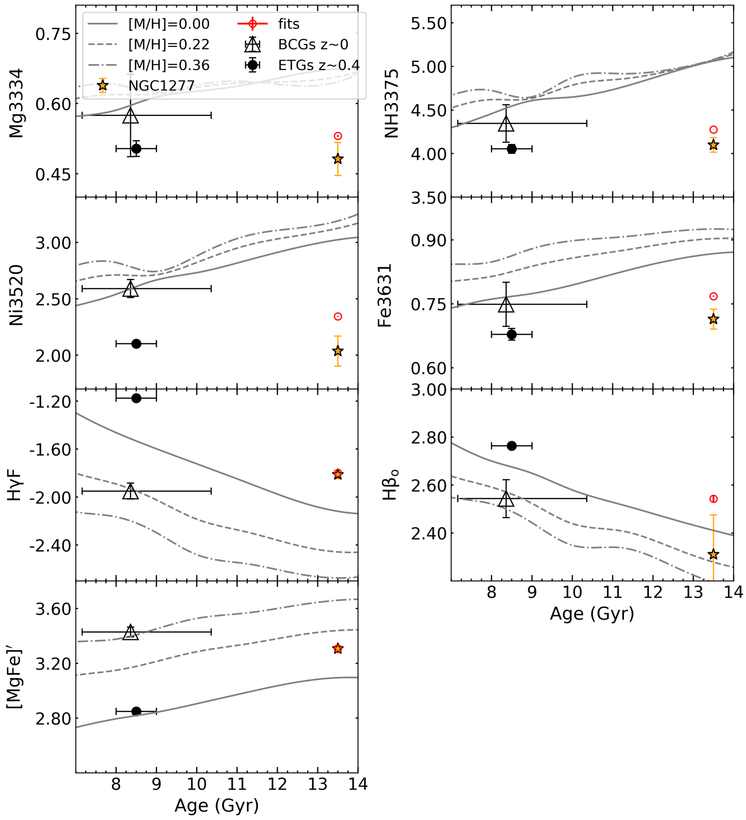

Figure 5.8— **NUV and optical best-fitting line-strength indices.** Each panel shows the selected NUV and optical SSP model indices as a function of age, following the same colour-code as in Figure 5.6. The best-fitting indices are plotted in red.

of the stellar populations in the cores of massive ETGs.

We have performed the first study concerning the recent star formation in a prototype relic galaxy, NGC 1277. Optical observations of NGC 1277 are biased towards old stellar populations and the effect of young stars becomes more relevant at bluer wavelengths. We have measured the NUV indices and found that the line-strengths deviate significantly with respect to the model predictions for an old SSP. This mismatch is resolved by adding a small fraction of young stellar populations. The best-fitting solutions estimate that a 0.8% in mass of stars within 1 kpc is formed in the most recent 1 Gyr of its star formation history.

This relic galaxy is exceptionally interesting for hosting one of the most-massive black holes known (van den Bosch et al. 2012; Ferré-Mateu et al. 2015). AGN suppression of the star formation is invoked in almost every state-of-the-art numerical simulation. Feedback from energetic jets of AGN in massive galaxies heats and expells the available cold gas, preventing the star formation at high redshift. Observationally, Martín-Navarro et al. (2018b) suggested that this quenching is strongly linked to the mass of the black hole. Thus, the overly massive black hole of NGC 1277 makes it one of the most AGN-dominated galaxies in the nearby Universe.

The AGN feedback took place mainly at high-redshift ($z > 2$) but which are the mechanisms that keep massive galaxies quenched from earlier times to the local Universe remains unknown. The results of this work show that feedback mechanisms are not able to completely stop star formation in the relic galaxy NGC 1277. NGC 1277 is located in the Perseus cluster, a very dense galaxy cluster. One possibility would be that the hot halo structures surrounding the galaxy prevents gas to get sufficiently cold for triggering the star formation. In addition, NGC 1277 is likely a satellite of the large and massive BCG NGC 1275, which is presently accreting large amounts of gas (Conselice et al. 2001; Lim et al. 2008) and possibly acts as an attractor preventing accretion onto NGC 1277. Therefore, studying the young stellar populations in relic galaxies located in lower-density environments, i.e. more isolated, like the massive compact galaxies MRK 1216 and PGC 32872 (Ferré-Mateu et al., 2017), would be relevant for disentangling quenching mechanisms at low-redshifts.

Massive galaxies underwent an early collapse phase but, unlike the general ETG population, relics failed to evolve by accreting smaller satellite galaxies. ETGs and BCGs such as the ones analysed in the previous two chapters also have a sub-one percent level of young stars like NGC 1277. BCGs, with a huge influence by their surrounding cluster, host some young stellar populations within their 0.8 kpc of 0.7% in mass. Interestingly, this amount is very similar to the value found in the relic for a similar aperture, suggesting that these low levels of recent star formation in the cores of BCGs are self-regulated. The study of young stellar populations in relic galaxies gives unique insights into the formation and evolutionary processes of the most massive galaxies.

As discussed in Chapter 4, the amount of gas returned into the interstellar medium from dying stars is mostly regulated by the IMF. For the present work, relic galaxies seem to have a nearly constant IMF with rather bottom-heavy shape at all radii. According to the numbers made in the previous chapter, a bottom heavy IMF would produce an amount of gas from stellar evolution that would be sufficient to form the estimated mass fraction of young stars in NCG1277. It would be highly interesting to explore how these young stars distribute within relic galaxies, and see if we also find that they are concentrated in the innermost regions as we see for the BCG case. Such a scenario would imply that the cores of massive galaxies – ETGs and BCGs – evolve in an almost identical way as the relic galaxies do.

6

Conclusions

My eyes were finally opened and I understood nature.
I learned at the same time to love it.

Claude Monet

More than one decade ago, the NUV photometry of some samples of ETGs was found to be consistent with young stars contributing with less than 1% in mass. In this thesis we have constrained the amount of young stars in massive early-type galaxies to gain additional insights into their recent star formation activity. We have explored the information contained within the NUV spectra of different samples of massive ETGs. Particularly, we analysed their NUV absorption line-strengths, which are significantly influenced by the presence of sub-one percent fractions of young stars.

Line-strength indices from massive ETGs had been usually measured only in the optical to derive stellar population parameters from the bulk of stars, concluding that they nearly resemble a coeval old and metal-rich stellar population. However, we find that all the ETGs analysed throughout this work show a discrepancy between the observed NUV indices and those predicted from a purely old stellar population. This mismatch can be addressed by adding small fractions of young stellar populations. One of the novelties of this thesis is that the best-fitting solutions are in agreement with indices measured in both NUV and optical spectral ranges.

Specifically, we first studied a large sample of BOSS galaxies to get a general view of recent star formation in massive ETGs. We then focused on a small sample of BCGs to explore the spatial distribution of this star formation. Finally, we investigated the special case of a "relic galaxy" in order to determine whether the origin of the star formating gas is *in-situ* or *ex-situ*.

In Chapter 3, we obtained seven stacked spectra from thousands of individual SDSS/BOSS galaxy spectra as a function of their velocity dispersion (i.e. tracking the mass). The final added spectra represent an average population of massive ETGs at the mean redshift $z \sim 0.4$. The stacks have very high S/N ($>200\,\text{Å}^{-1}$ in the visible and $>20\,\text{Å}^{-1}$ in the NUV) and their stellar velocity dispersions range from 220 to 340 $\mathrm{km\,s^{-1}}$ (i.e. from $\sim 10^{11.3}$ to $10^{11.5}\,\mathrm{M_\odot}$). From this study of young stellar components in the general population of ETGs:

- We have derived mean old ages and metal-rich metallicities from optical indices, which are older and more metal-rich towards the most massive stack. Particularly, the obtained mean age of the most massive stack is consistent with the age of the Universe at the average redshift of the sample, i.e. 9.4 Gyr. This suggests that these galaxies formed at high-redshift while lower mass galaxies peak their star formation activity at lower-redshifts.

- The measured NUV indices are not well represented by a single SSP of an age equal to the derived mean age. This discrepancy is larger towards bluer indices.

- From the fits to NUV indices with our modelling approaches, the young stellar component always contributes less than 1% in the seven mass bins, consistent with what was already claimed from NUV photometry. With this small amount in young stars, the mismatch in the NUV indices disappears. This result suggests that, on average, massive ETGs at an intermediate redshift are still forming new stars.

- The amount of young stars increases for less massive galaxies. The 1SSP+cSFR approach has revealed that the fraction in mass of stars formed within the last 2 Gyr ranges from 0.48 to 0.56% in ETGs with velocity dispersions of 220 – 230 and 300 – 340 $\mathrm{km\,s^{-1}}$, respectively. This trend with mass might be an evidence of the more extended timescales of star formation of lower mass galaxies, in which we expected a larger fraction of young stars than for more massive galaxies.

- We tested the robustness of the results shown here by performing the analysis with models composed by two bursts and exponentially declining SFHs. From these different modelling approaches, we always derive sub-one percent young mass fractions and a negative trend with velocity dispersion, which indicates that our methodology applied for deriving the young stellar component is very robust.

- Our fits of galaxy spectral indices at intermediate redshifts provide the most stringent limits on recent star formation in massive ETGs to date. Simulated galaxies from the EAGLE cosmological simulation produce far more extended SFHs than is observed in the galaxy stacks. Only two galaxies are found to match the colour criteria applied to the observations for removing the late-type galaxy contamination, indicating that simulated massive galaxies are in general too blue.

The sample studied in Chapter 4 consists of extremely massive brightest cluster galaxies with high central velocity dispersions ($\sigma_0 > 300\,\mathrm{kms}^{-1}$). We have estimated their young stellar components and how they are spatially distributed. We stacked the individual galaxy spectra in five bins according to the radial distance to increase the S/N in the outermost regions. Since the spectral range of the spectra does not reach short wavelengths as in the previous work, we are less sensitive to the youngest stars. Therefore, we have employed an optimised set of NUV indices (namely in the U-band), which are maximally sensitive to young stars, while at the same time minimises their sensitivity to alpha-enhancement. From the analysis of the NUV and optical indices of BCGs as a function of distance to galaxy centre:

- From optical indices we have obtained mean old ages and metal-rich stellar populations. Ages are found to be approximately constant with radius, whereas the metallicity decreases with distance to the galaxy centre.
- NUV indices from the innermost spectra show a deviation with respect to the predictions of an old SSP. This clearly indicates that an old SSP does not fully represent the indices from innermost bins and an additional component should be considered.
- From the fits of NUV and optical line-strength indices we have found that our sample of 6 BCGs are presently forming new stars in small quantities. On average, the contribution of stars younger than 1 Gyr is less than 1% in mass.
- We found that these young components are located in the innermost regions of our BCGs. A 0.7% of the total galaxy mass within the innermost 0.8 kpc belongs to stellar populations younger than 1 Gyr. Beyond 2 kpc

we do not detect newly formed stars. Therefore, our BCG sample is actively forming stars in their cores, whereas the outskirts remain entirely old.

- In the innermost regions the amount of gas returned from the stellar evolution is sufficient to form the obtained amount of young stars. This suggests that intrinsic galaxy processes such as recycled gas from dying stars could trigger the star formation in the cores of BCGs.
- The IMF varies with radius in such a way that a much higher amount of gas would be returned to the galaxy from dying stars beyond 4 kpc. However, our findings show that in those outer regions there are no young stars. This indicates that, on one hand, that this gas is not able to reach the optimal conditions to trigger the star formation in the outer regions or, on the other hand, that this gas falls towards the galaxy cores where new stars are being formed.

Although in the BOSS sample we do not differentiate the galaxies according to their environment, given their high velocity dispersion, galaxies from the most massive stack would be preferently located in high-density environments or even in the centre of a group or galaxy cluster similar to the BCGs analysed. We have found that the amount of young stars in the nearby BCGs is smaller than that one found at higher redshift for the most massive stack. This suggests that the amount of gas available to form new stars decreases at lower redshifts, consistent with a purely passive evolution in the cores of massive galaxies.

In Chapter 5, we have performed long-slit observations to obtain 11h exposure time spectral data of the relic galaxy NGC 1277. We have reduced the data to get a NUV spectrum within 1 kpc aperture. From the study of the indices of NGC 1277:

- We have obtained from optical indicators that the bulk of the stellar populations of NGC 1277 is extremely old and metal-rich. The derived age is the maximum value allowed by the SSP models, suggesting that the galaxy was formed at early epochs. Our findings are consistent with those derived by previous authors.
- The measured NUV indices are not well represented by a single old SSP of an age equal to the derived mean age and show a discrepancy that suggests that an additional component should be taken into account.
- We found that 0.8% of the total galaxy mass within 1 kpc has been formed within the last 1 Gyr. Therefore, the relic galaxy NGC 1277 has experienced low levels of recent star formation in its core during the most recent

period of its SFH. This amount of young stars is able to match the observed NUV indices.

- Due to the limited accretion history of this galaxy, the most likely origin for the formation of these new stars is from gas that comes solely from intrinsic processes.

The work presented here is one of the most detailed studies performed so far on the young stellar components in massive ETGs from NUV absorption lines. The fact that ETGs are so massive and present rather old and metal-rich stellar populations make them ideal to study galaxy evolution. From NUV-optical spectroscopy, this thesis claims that massive ETGs at intermediate-low redshifts are not completely quenched and are still forming new stars at very low levels. Relic galaxies undergo little interaction with other galaxies since their initial formation of the bulk of their stars. As a consequence, the recent star formation found in NGC 1277 suggests that the star formation found within the cores of our samples of massive ETGs and BCGs is self-regulated. Therefore, the formation of new stars in the cores of massive galaxies is likely to be triggered by intrinsic galaxy processes such as gas returned from stellar evolution. Future studies of individual ETGs and other relic galaxies should be performed if we want to constrain how massive galaxies evolve and whether their star formation activity is influenced or not by their surrounding environment.

7

Future work

We need to rediscover how to be sustainable.
To move from being apart from nature,
to becoming a part of nature once again.
David Attenborough in *A life on our planet* (2020)

This thesis has shown the power of analysing NUV line-strength indices in massive galaxies, as they are significantly influenced by the presence of small fractions of young stars. Our approach provides additional clues to be able to properly track the most likely channel for the build-up and assembly of massive galaxies. The findings of this thesis have opened new horizons that need to be properly addressed:

- **How does the amount of young stellar components in massive ETGs evolve with redshift?**

  In Chapter 3 we inferred the level of recent star formation of the general ETG population at the average redshift of $z \sim 0.4$. An interesting study with potential key constraints on galaxy evolution is to investigate how the amount of young stellar components in massive ETGs evolve with lookback time. We know that the star formation activity in massive galaxies have been quenched at $z > 2$, but some residual star formation at very low levels has survived until the present in the ETG population as a whole. Thus, it would be interesting to consider the SDSS/BOSS spectra of massive galaxies as we did in Chapter 3 but, in this case, by stacking them in bins of redshift and, if the final S/N permits, in bins of velocity dispersion. Since we found in Chapter 4 that even from indices redder than 3000 Å small fractions of young stellar components can be derived, there is no need to move to the redshift we did in Chapter 3. BOSS spectra with wavelengths larger than 3000 Å are achieved from $z > 0.2$. The redshift bin size would depend on the final S/N. For a study at higher redshifts, since BOSS survey only targets up to $z \sim 0.7$, we can use data from eBOSS and LEGA-C surveys, that observed massive galaxies from redshift 0.6 to 1.0, and process stacked spectra in redshift bins and galaxy mass to increase the S/N. If purely passive evolution is the main regime dominating the evolution of the star formation in massive ETGs, we should measure larger amounts of young stellar populations with progressively increasing redshift.

- **Is the amount of young stellar populations larger in lower density environments?**

  What remains to be understood is how much of the galaxy evolution is due to "nature", i.e. galaxy mass, or "nurture", i.e. the role of the galaxy environment. ETGs in isolation are claimed to have relatively more extended SFHs, as well as those in low-density galaxy clusters. That is, higher density regions exhibit on average older galaxies for a given galaxy mass. As discussed in Chapter 4, it has been recently shown that the amount of BCGs with recent star formation is larger in clusters with lower halo masses. BCGs are good candidates to study the influence of high-density environments. It is worth studying the recent tail of star formation in massive ETGs as a function of the environmental density. An observational campaign to compare massive ETGs in clusters and in lower density regions would be very useful and would provide important clues to discuss the *in-situ* vs. *ex-situ* origins of the star formation in massive galaxies.

- **What are the main differences of the young stellar populations between massive ETGs and relic galaxies?**

  In this thesis we measure the young stellar components in massive galaxies in a global context, i.e. from stacked spectra but not from individual ETGs. Our results show that the ETG population at $z \sim 0.4$ hosts, on average, recent star formation at low levels, with a fraction of 0.5% of the stars formed in the last 2 Gyr. However, this value may change galaxy-to-galaxy to be able to assess the origin of these differences. In this thesis, the spectra of individual targets has been only analysed for one relic galaxy at their innermost regions (<1 kpc) and in the cores of 6 BCGs, but nothing has been done for non central galaxies of the same mass of relics but larger sizes (i.e. massive ellipticals). As has been extensively shown by observations and theoretical models, local ETGs have grown both in mass and size from z$\sim$2 to the present, but some of these massive compact galaxies at high redshift have had little interaction with other galaxies and remained unaltered until redshift 0. It will be useful to investigate the young stellar populations in the cores of massive ETGs and how they differ to those from relic galaxies. We have obtained long-slit spectroscopy for a set of ETGs and relic galaxies located at similar redshifts (and similar to the relic investigated in Chapter 5). The spectra were obtained during different observing runs at the INT telescope, but the optical spectra required to properly constrain the young stars is missed. Our plan is to get oberving time to obtain their optical spectra.

- **Where are the young stars in ETGs located?**

  In Chapter 4 we find that our sample of BCGs show young stellar populations in the innermost regions but nothing is found at distances larger than 2 kpc. The evolution of these stellar systems is thought to be largely influenced by their environment, so that why their young stars are distributed in such way may be hard to interpret. In view of this, it is therefore important to know the distribution of the youngest stars in massive ETGs. For this purpose we have obtained long slit spectra of NGC3115, an isolated large lenticular galaxy located at z$\sim$0.00361. We integrated 2 hours in the 4.5 m SOAR telescope in Cerro Pachón (Chile), so we obtain very high S/N spectra from 3000 to 5500 Å at different galactocentric distances. In Figure 7.1 we show a two-dimensional spectrum of 30 minutes exposure before the data reduction process. The two strong absorption lines in the left side of the image are the Ca H+K lines before the 4000 Å break. With our data we will be able to study the distribution of the young stars in a nearby ETG individually. Due to its proximity, this is the first ETG where hot gas has been observed flowing toward its supermassive black hole that may be triggering the formation of new stars in the centre. Such observations can explore the link between the central young stellar populations and the influence of the AGN.

- **Are our findings consistent to those from fitting the full spectral range?**

  The methodology employed in this thesis to derive stellar population parameters is based on comparing the observed NUV and optical line-

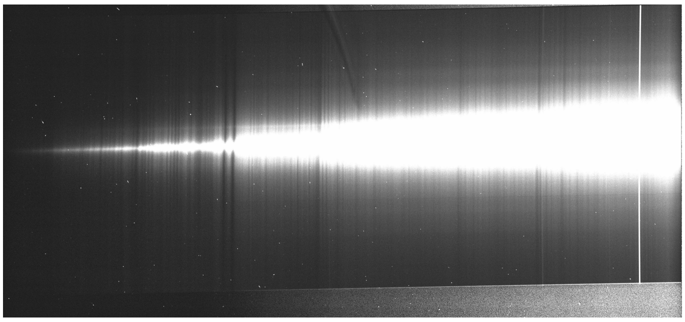

FIGURE 7.1— **2D spectrum of the elliptical NGC3113.** The image show the 2D spectrum of NGC3115 obtained during a exposure of 30 minutes with the 4.5 m SOAR telescope. The spectral range cover from 3000 to 5500 Å.

strength indices with model predictions. However, a galaxy spectrum can also be explored by analysing its shape and the information contained pixel-to-pixel. The full spectrum fitting technique has been applied so far in the optical range, but not much has been done in the NUV spectra. It would be interesting to explore the best-fitting solutions with this method. Therefore it is worth exploring this approach.

- **What are the predictions from numerical simulations?**

  Our comparison to EAGLE simulated galaxies shown in Chapter 3 suggests that these models are unable to match observational constraints, calling for a revision of how feedback mechanisms are currently implemented in numerical methods. Important insights are expected from comparing the observed SFHs from BOSS stacked spectra with the predicted SFHs from other sets of simulations (e.g., C-EAGLE, IllustrisTNG, MASCLET), as a function of galaxy mass and the environment where galaxies reside. For this purpose, the SFHs of simulated galaxies will be derived following two different approaches. First, by using the actual line-of-sight age and metallicity distribution of star particles, within a projected aperture similar to that of the BOSS stacked spectra. Second, by attaching to each star particle of a simulated galaxy an EMILES SSP model SED, with suitable age and metallicity, in order to produce an integrated spectrum that will be analyzed with the same methodology as performed throughout this thesis. This analysis will tell us if feedback in simulations is able to capture the overall physics involved to the star formation processes or some revision of feedback mechanisms in numerical methods is actually still required. Moreover, such comparisons will let us know whether these simulations follow the observed young mass fractions with mass, environment and redshift, which will add further constrains to improve these models.

- **Are our solutions compatible with other spectral ranges?**

  It is challenging to extend this UV-optical study to the NIR (JHK bands) to further constrain the obtained solutions. This is particularly relevant for contributions from intermediate-aged components that are dominated by AGB stars in these red wavelengths. Note that these stellar populations also show significant contributions in the blue.

Bibliography

Asa'd, R. S., Vazdekis, A., Cerviño, M., et al. 2017, MNRAS, 471, 3599

Baldry, I. K., Balogh, M. L., Bower, R. G., et al. 2006, MNRAS, 373, 469

Baldry, I. K., Sullivan, T., Rani, R., & Turner, S. 2021, MNRAS, 500, 1557

Barbosa, C. E., Arnaboldi, M., Coccato, L., et al. 2016, A&A, 589, A139

Barnes, J. E. 1992, ApJ, 393, 484

Beasley, M. A., Trujillo, I., Leaman, R., & Montes, M. 2018, , 555, 483

Bédorf, J. & Portegies Zwart, S. 2013, MNRAS, 431, 767

Behroozi, P. S., Conroy, C., & Wechsler, R. H. 2010, ApJ, 717, 379

Belli, S., Newman, A. B., & Ellis, R. S. 2014, ApJ, 783, 117

Bernardi, M., Sheth, R. K., Nichol, R. C., Schneider, D. P., & Brinkmann, J. 2005, , 129, 61

Bezanson, R., van Dokkum, P. G., Tal, T., et al. 2009, ApJ, 697, 1290

Bildfell, C., Hoekstra, H., Babul, A., & Mahdavi, A. 2008, MNRAS, 389, 1637

Binney, J. & Tabor, G. 1995, MNRAS, 276, 663

Blakeslee, J. P., Franx, M., Postman, M., et al. 2003, ApJL, 596, L143

Bonnarel, F., Fernique, P., Bienaymé, O., et al. 2000, A&AS, 143, 33

Bower, R. G., Lucey, J. R., & Ellis, R. S. 1992, MNRAS, 254, 601

Brough, S., Couch, W. J., Collins, C. A., et al. 2008, MNRAS, 385, L103

Brough, S., Proctor, R., Forbes, D. A., et al. 2007, MNRAS, 378, 1507

Buitrago, F., Trujillo, I., Conselice, C. J., et al. 2008, ApJL, 687, L61

Buzzoni, A. 1989, ApJS, 71, 817

Buzzoni, A., Bertone, E., Carraro, G., & Buson, L. 2012, ApJ, 749, 35

Capak, P., Aussel, H., Ajiki, M., et al. 2007, ApJS, 172, 99

Cappellari, M., Bacon, R., Bureau, M., et al. 2006, MNRAS, 366, 1126

Cappellari, M. & Emsellem, E. 2004, , 116, 138

Cappellari, M., Emsellem, E., Krajnović, D., et al. 2011, MNRAS, 413, 813

Cappellari, M., McDermid, R. M., Alatalo, K., et al. 2012, , 484, 485

Cardelli, J. A., Clayton, G. C., & Mathis, J. S. 1989, ApJ, 345, 245

Cardiel, N., Gorgas, J., & Aragon-Salamanca, A. 1998, MNRAS, 298, 977

Cenarro, A. J., Cardiel, N., Gorgas, J., et al. 2001, MNRAS, 326, 959

Cenarro, A. J., Gorgas, J., Vazdekis, A., Cardiel, N., & Peletier, R. F. 2003, MNRAS, 339, L12

Cerulo, P., Orellana, G. A., & Covone, G. 2019, MNRAS, 487, 3759

Cervantes, J. L. & Vazdekis, A. 2009, MNRAS, 392, 691

Charlot, S. & Bruzual A, G. 1991, ApJ, 367, 126

Chauke, P., van der Wel, A., Pacifici, C., et al. 2018, ApJ, 861, 13

Chavez, M., Bertone, E., Buzzoni, A., et al. 2007, ApJ, 657, 1046

Chen, Y.-M., Kauffmann, G., Tremonti, C. A., et al. 2012, MNRAS, 421, 314

Choi, J., Conroy, C., Moustakas, J., et al. 2014, ApJ, 792, 95

Cimatti, A., Cassata, P., Pozzetti, L., et al. 2008, A&A, 482, 21

Cimatti, A., Daddi, E., & Renzini, A. 2006, A&A, 453, L29

Citro, A., Pozzetti, L., Moresco, M., & Cimatti, A. 2016, A&A, 592, A19

Cole, S., Lacey, C. G., Baugh, C. M., & Frenk, C. S. 2000, MNRAS, 319, 168

Conroy, C. 2013, , 51, 393

Conroy, C. & van Dokkum, P. 2012, ApJ, 747, 69

Conselice, C. J., Gallagher, John S., I., & Wyse, R. F. G. 2001, , 122, 2281

Cooke, K. C., Kartaltepe, J. S., Tyler, K. D., et al. 2019, ApJ, 881, 150

Cooke, K. C., O'Dea, C. P., Baum, S. A., et al. 2016, ApJ, 833, 224

Cooper, A. P., Gao, L., Guo, Q., et al. 2015, MNRAS, 451, 2703

Cowie, L. L., Songaila, A., Hu, E. M., & Cohen, J. G. 1996, , 112, 839

Crain, R. A., Schaye, J., Bower, R. G., et al. 2015, MNRAS, 450, 1937

Crawford, C. S., Allen, S. W., Ebeling, H., Edge, A. C., & Fabian, A. C. 1999, MNRAS, 306, 857

Crawford, C. S. & Fabian, A. C. 1993, MNRAS, 265, 431

Cushing, M. C., Rayner, J. T., & Vacca, W. D. 2005, ApJ, 623, 1115

Daddi, E., Renzini, A., Pirzkal, N., et al. 2005, ApJ, 626, 680

Dalla Vecchia, C. & Schaye, J. 2012, MNRAS, 426, 140

Damjanov, I., Abraham, R. G., Glazebrook, K., et al. 2011, ApJL, 739, L44

Damjanov, I., McCarthy, P. J., Abraham, R. G., et al. 2009, ApJ, 695, 101

Dawson, K. S., Schlegel, D. J., Ahn, C. P., et al. 2013, , 145, 10

de La Rosa, I. G., La Barbera, F., Ferreras, I., & de Carvalho, R. R. 2011, MNRAS, 418, L74

De Lucia, G. & Blaizot, J. 2007, MNRAS, 375, 2

Djorgovski, S. & Davis, M. 1987, ApJ, 313, 59

Domínguez Sánchez, H., Bernardi, M., Brownstein, J. R., Drory, N., & Sheth, R. K. 2019, MNRAS, 489, 5612

Donahue, M., Bruch, S., Wang, E., et al. 2010, ApJ, 715, 881

Donas, J., Deharveng, J.-M., Rich, R. M., et al. 2007, ApJS, 173, 597

Dorman, B., O'Connell, R. W., & Rood, R. T. 1995, ApJ, 442, 105

Dressler, A. 1980, ApJ, 236, 351

Dressler, A., Lynden-Bell, D., Burstein, D., et al. 1987, ApJ, 313, 42

Dubinski, J. 1998, ApJ, 502, 141

Dubois, Y., Gavazzi, R., Peirani, S., & Silk, J. 2013, MNRAS, 433, 3297

Edge, A. C. 2001, MNRAS, 328, 762

Edwards, L. O. V. & Patton, D. R. 2012, MNRAS, 425, 287

Edwards, L. O. V., Salinas, M., Stanley, S., et al. 2020, MNRAS, 491, 2617

Eftekhari, E., Mosleh, M., Vazdekis, A., & Tavasoli, S. 2019, MNRAS, 486, 3788

Eggen, O. J., Lynden-Bell, D., & Sandage, A. R. 1962, ApJ, 136, 748

Faber, S. M., Friel, E. D., Burstein, D., & Gaskell, C. M. 1985, ApJS, 57, 711

Faber, S. M. & Jackson, R. E. 1976, ApJ, 204, 668

Fan, L., Chen, Y., Er, X., et al. 2013, MNRAS, 431, L15

Fan, L., Lapi, A., Bressan, A., et al. 2010, ApJ, 718, 1460

Fanelli, M. N., O'Connell, R. W., Burstein, D., & Wu, C.-C. 1990, ApJ, 364, 272

Ferré-Mateu, A., Mezcua, M., Trujillo, I., Balcells, M., & van den Bosch, R. C. E. 2015, ApJ, 808, 79

Ferré-Mateu, A., Sánchez-Blázquez, P., Vazdekis, A., & de la Rosa, I. G. 2014, ApJ, 797, 136

Ferré-Mateu, A., Trujillo, I., Martín-Navarro, I., et al. 2017, MNRAS, 467, 1929

Ferreras, I., La Barbera, F., de La Rosa, I. G., et al. 2013, MNRAS, 429, L15

Ferreras, I., Scott, N., La Barbera, F., et al. 2019, MNRAS, 489, 608

Ferreras, I. & Silk, J. 2000, ApJL, 541, L37

Foreman-Mackey, D., Hogg, D. W., Lang, D., & Goodman, J. 2013, , 125, 306

François, P., Morelli, L., Pizzella, A., et al. 2019, A&A, 621, A60

Fraser-McKelvie, A., Brown, M. J. I., & Pimbblet, K. A. 2014, MNRAS, 444, L63

Fukugita, M., Hogan, C. J., & Peebles, P. J. E. 1998, ApJ, 503, 518

Gabor, J. M., Davé, R., Finlator, K., & Oppenheimer, B. D. 2010, MNRAS, 407, 749

Gallazzi, A., Charlot, S., Brinchmann, J., & White, S. D. M. 2006, MNRAS, 370, 1106

Gao, Y. & Fan, L.-L. 2020, Research in Astronomy and Astrophysics, 20, 106

George, K. 2017, A&A, 598, A45

Girardi, L., Bressan, A., Bertelli, G., & Chiosi, C. 2000, A&AS, 141, 371

Goddard, D., Thomas, D., Maraston, C., et al. 2017, MNRAS, 465, 688

González, J. J. 1993, PhD thesis, -

González Delgado, R. M., García-Benito, R., Pérez, E., et al. 2015, A&A, 581, A103

Goodman, J. & Weare, J. 2010, Communications in Applied Mathematics and Computational Science, 5, 65

Gorgas, J., Pedraz, S., Guzmán, R., Cardiel, N., & González, J. J. 1997, ApJL, 481, L19

Gregg, M. D. 1994, , 108, 2164

Gregg, M. D., Silva, D., Rayner, J., et al. 2006, in The 2005 HST Calibration Workshop: Hubble After the Transition to Two-Gyro Mode, ed. A. M. Koekemoer, P. Goudfrooij, & L. L. Dressel, 209

Groenewald, D. N. & Loubser, S. I. 2014, MNRAS, 444, 808

Guo, Q., White, S., Li, C., & Boylan-Kolchin, M. 2010, MNRAS, 404, 1111

Harrison, C. D., Colless, M., Kuntschner, H., et al. 2010, MNRAS, 409, 1455

Hausman, M. A. & Ostriker, J. P. 1978, ApJ, 224, 320

Hernández-Pérez, F. & Bruzual, G. 2014, MNRAS, 444, 2571

Hicks, A. K., Mushotzky, R., & Donahue, M. 2010, ApJ, 719, 1844

Hill, A. R., Muzzin, A., Franx, M., & Marchesini, D. 2017, ApJL, 849, L26

Hilz, M., Naab, T., & Ostriker, J. P. 2013, MNRAS, 429, 2924

Hilz, M., Naab, T., Ostriker, J. P., et al. 2012, MNRAS, 425, 3119

Hoffer, A. S., Donahue, M., Hicks, A., & Barthelemy, R. S. 2012, ApJS, 199, 23

Hopkins, P. F., Bundy, K., Murray, N., et al. 2009, MNRAS, 398, 898

Jackson, T. M., Pasquali, A., Pacifici, C., et al. 2020, MNRAS, 497, 4262

Jeong, H., Bureau, M., Yi, S. K., Krajnović, D., & Davies, R. L. 2007, MNRAS, 376, 1021

Jeong, H., Yi, S. K., Bureau, M., et al. 2009, MNRAS, 398, 2028

Kauffmann, G., White, S. D. M., Heckman, T. M., et al. 2004, MNRAS, 353, 713

Kaviraj, S., Peirani, S., Khochfar, S., Silk, J., & Kay, S. 2009, MNRAS, 394, 1713

Kaviraj, S., Schawinski, K., Devriendt, J. E. G., et al. 2007, ApJS, 173, 619

Kokusho, T., Kaneda, H., Bureau, M., et al. 2017, A&A, 605, A74

Kriek, M., van der Wel, A., van Dokkum, P. G., Franx, M., & Illingworth, G. D. 2008, ApJ, 682, 896

Kroupa, P. 2001, MNRAS, 322, 231

Kubo, M., Yamada, T., Ichikawa, T., et al. 2017, MNRAS, 469, 2235

Kuntschner, H., Emsellem, E., Bacon, R., et al. 2010, MNRAS, 408, 97

Kuntschner, H., Smith, R. J., Colless, M., et al. 2002, MNRAS, 337, 172

La Barbera, F., de Carvalho, R. R., de La Rosa, I. G., et al. 2010a, MNRAS, 408, 1313

La Barbera, F., Ferreras, I., de Carvalho, R. R., et al. 2012, MNRAS, 426, 2300

La Barbera, F., Ferreras, I., Vazdekis, A., et al. 2013, MNRAS, 433, 3017

La Barbera, F., Lopes, P. A. A., de Carvalho, R. R., de La Rosa, I. G., & Berlind, A. A. 2010b, MNRAS, 408, 1361

La Barbera, F., Vazdekis, A., Ferreras, I., et al. 2019, MNRAS, 489, 4090

La Barbera, F., Vazdekis, A., Ferreras, I., et al. 2017, MNRAS, 464, 3597

La Barbera, F., Vazdekis, A., Ferreras, I., et al. 2016, MNRAS, 457, 1468

Larson, R. B. 1974, MNRAS, 169, 229

Larson, R. B. 1975, MNRAS, 173, 671

Lavoie, S., Willis, J. P., Démoclès, J., et al. 2016, MNRAS, 462, 4141

Le Cras, C., Maraston, C., Thomas, D., & York, D. G. 2016, MNRAS, 461, 766

Leonardi, A. J. & Rose, J. A. 1996, , 111, 182

Lidman, C., Iacobuta, G., Bauer, A. E., et al. 2013, MNRAS, 433, 825

Lidman, C., Suherli, J., Muzzin, A., et al. 2012, MNRAS, 427, 550

Lim, J., Ao, Y., & Dinh-V-Trung. 2008, ApJ, 672, 252

Liu, F. S., Mao, S., & Meng, X. M. 2012, MNRAS, 423, 422

Longhetti, M., Saracco, P., Severgnini, P., et al. 2007, MNRAS, 374, 614

López-Sanjuan, C., Cenarro, A. J., Varela, J., et al. 2015, A&A, 576, A53

Lotz, J. M., Jonsson, P., Cox, T. J., et al. 2011, ApJ, 742, 103

Loubser, S. I., Babul, A., Hoekstra, H., et al. 2016, MNRAS, 456, 1565

Loubser, S. I. & Sánchez-Blázquez, P. 2012, MNRAS, 425, 841

Loubser, S. I., Sánchez-Blázquez, P., Sansom, A. E., & Soechting, I. K. 2009, MNRAS, 398, 133

MacArthur, L. A. 2005, ApJ, 623, 795

Maraston, C., Nieves Colmenárez, L., Bender, R., & Thomas, D. 2009, A&A, 493, 425

Maraston, C., Pforr, J., Henriques, B. M., et al. 2013, MNRAS, 435, 2764

Martig, M., Crocker, A. F., Bournaud, F., et al. 2013, MNRAS, 432, 1914

Martin, D. C., Fanson, J., Schiminovich, D., et al. 2005, ApJL, 619, L1

Martín-Navarro, I., Brodie, J. P., Romanowsky, A. J., Ruiz-Lara, T., & van de Ven, G. 2018a, , 553, 307

Martín-Navarro, I., La Barbera, F., Vazdekis, A., Falcón-Barroso, J., & Ferreras, I. 2015a, MNRAS, 447, 1033

Martín-Navarro, I., La Barbera, F., Vazdekis, A., et al. 2015b, MNRAS, 451, 1081

Martín-Navarro, I., Vazdekis, A., Falcón-Barroso, J., et al. 2018b, MNRAS, 475, 3700

Masters, K. L., Maraston, C., Nichol, R. C., et al. 2011, MNRAS, 418, 1055

McAlpine, S., Helly, J. C., Schaller, M., et al. 2016, Astronomy and Computing, 15, 72

McDermid, R. M., Alatalo, K., Blitz, L., et al. 2015, MNRAS, 448, 3484

McIntosh, D. H., Bell, E. F., Rix, H.-W., et al. 2005, ApJ, 632, 191

Meyer, R. E., Sivanandam, S., & Moon, D.-S. 2019, ApJ, 875, 151

Miller, G. E. & Scalo, J. M. 1979, ApJS, 41, 513

Morton, D. C. 1991, ApJS, 77, 119

Moster, B. P., Somerville, R. S., Maulbetsch, C., et al. 2010, ApJ, 710, 903

Naab, T., Johansson, P. H., & Ostriker, J. P. 2009, ApJL, 699, L178

Navarro-González, J., Ricciardelli, E., Quilis, V., & Vazdekis, A. 2013, MNRAS, 436, 3507

O'Dea, C. P., Baum, S. A., Privon, G., et al. 2008, ApJ, 681, 1035

O'Dea, K. P., Quillen, A. C., O'Dea, C. P., et al. 2010, ApJ, 719, 1619

Oliva-Altamirano, P., Brough, S., Lidman, C., et al. 2014, MNRAS, 440, 762

Oser, L., Naab, T., Ostriker, J. P., & Johansson, P. H. 2012, ApJ, 744, 63

Oser, L., Ostriker, J. P., Naab, T., Johansson, P. H., & Burkert, A. 2010, ApJ, 725, 2312

Ostriker, J. P. & Tremaine, S. D. 1975, ApJL, 202, L113

Papovich, C., Dickinson, M., Giavalisco, M., Conselice, C. J., & Ferguson, H. C. 2005, ApJ, 631, 101

Patel, S. G., van Dokkum, P. G., Franx, M., et al. 2013, ApJ, 766, 15

Patil, M. K., Pandey, S. K., Sahu, D. K., & Kembhavi, A. 2007, A&A, 461, 103

Peletier, R. F., Falcón-Barroso, J., Bacon, R., et al. 2007, MNRAS, 379, 445

Pérez, E., Cid Fernandes, R., González Delgado, R. M., et al. 2013, ApJL, 764, L1

Pipino, A., Kaviraj, S., Bildfell, C., et al. 2009, MNRAS, 395, 462

Postman, M. & Lauer, T. R. 1995, ApJ, 440, 28

Rafferty, D. A., McNamara, B. R., & Nulsen, P. E. J. 2008, ApJ, 687, 899

Rayner, J. T., Cushing, M. C., & Vacca, W. D. 2009, ApJS, 185, 289

Renzini, A. 2006, , 44, 141

Rosas-Guevara, Y. M., Bower, R. G., Schaye, J., et al. 2015, MNRAS, 454, 1038

Runge, J. & Yan, H. 2018, ApJ, 853, 47

Salim, S. & Rich, R. M. 2010, ApJL, 714, L290

Salpeter, E. E. 1955, ApJ, 121, 161

Sánchez-Blázquez, P., Gorgas, J., Cardiel, N., & González, J. J. 2006a, A&A, 457, 787

Sánchez-Blázquez, P., Peletier, R. F., Jiménez-Vicente, J., et al. 2006b, MNRAS, 371, 703

Saracco, P., Longhetti, M., & Andreon, S. 2009, MNRAS, 392, 718

Sarzi, M., Spiniello, C., La Barbera, F., Krajnović, D., & van den Bosch, R. 2018, MNRAS, 478, 4084

Schaller, M., Dalla Vecchia, C., Schaye, J., et al. 2015, MNRAS, 454, 2277

Schawinski, K., Khochfar, S., Kaviraj, S., et al. 2006, , 442, 888

Schawinski, K., Thomas, D., Sarzi, M., et al. 2007, MNRAS, 382, 1415

Schaye, J., Crain, R. A., Bower, R. G., et al. 2015, MNRAS, 446, 521

Schaye, J. & Dalla Vecchia, C. 2008, MNRAS, 383, 1210

Scholtz, J., Alexander, D. M., Harrison, C. M., et al. 2018, MNRAS, 475, 1288

Schwarz, G. 1978, Annals of Statistics, 6, 461

Serven, J., Worthey, G., Toloba, E., & Sánchez-Blázquez, P. 2011, , 141, 184

Shankar, F., Marulli, F., Bernardi, M., et al. 2013, MNRAS, 428, 109

Sheen, Y.-K., Yi, S. K., Ree, C. H., et al. 2016, ApJ, 827, 32

Somerville, R. S. & Primack, J. R. 1999, MNRAS, 310, 1087

Spiniello, C., Trager, S., Koopmans, L. V. E., & Conroy, C. 2014, MNRAS, 438, 1483

Springel, V., Di Matteo, T., & Hernquist, L. 2005, ApJL, 620, L79

Stockmann, M., Toft, S., Gallazzi, A., et al. 2020, ApJ, 888, 4

Stoughton, C., Lupton, R. H., Bernardi, M., et al. 2002, , 123, 485

Stringer, M., Trujillo, I., Dalla Vecchia, C., & Martinez-Valpuesta, I. 2015, MNRAS, 449, 2396

Thomas, D., Greggio, L., & Bender, R. 1999, MNRAS, 302, 537

Thomas, D., Maraston, C., & Bender, R. 2003, MNRAS, 339, 897

Thomas, D., Maraston, C., Bender, R., & Mendes de Oliveira, C. 2005, ApJ, 621, 673

Thomas, D., Steele, O., Maraston, C., et al. 2013, MNRAS, 431, 1383

Thomas, R., Le Fèvre, O., Zamorani, G., et al. 2019, A&A, 630, A145

Toft, S., van Dokkum, P., Franx, M., et al. 2007, ApJ, 671, 285

Tojeiro, R., Percival, W. J., Wake, D. A., et al. 2012, MNRAS, 424, 136

Toomre, A. 1977, , 15, 437

Toomre, A. & Toomre, J. 1972, ApJ, 178, 623

Trager, S. C., Faber, S. M., Worthey, G., & González, J. J. 2000, , 119, 1645

Tran, K.-V. H., Moustakas, J., Gonzalez, A. H., et al. 2008, ApJL, 683, L17

Trayford, J. W., Theuns, T., Bower, R. G., et al. 2015, MNRAS, 452, 2879

Trujillo, I. & Aguerri, J. A. L. 2004, MNRAS, 355, 82

Trujillo, I., Conselice, C. J., Bundy, K., et al. 2007, MNRAS, 382, 109

Trujillo, I., Ferré-Mateu, A., Balcells, M., Vazdekis, A., & Sánchez-Blázquez, P. 2014, ApJL, 780, L20

Trujillo, I., Feulner, G., Goranova, Y., et al. 2006, MNRAS, 373, L36

Trujillo, I., Rudnick, G., Rix, H.-W., et al. 2004, ApJ, 604, 521

Twite, J. W., Conselice, C. J., Buitrago, F., et al. 2012, MNRAS, 420, 1061

Valdes, F., Gupta, R., Rose, J. A., Singh, H. P., & Bell, D. J. 2004, ApJS, 152, 251

van de Sande, J., Kriek, M., Franx, M., Bezanson, R., & van Dokkum, P. G. 2014, ApJL, 793, L31

van de Sande, J., Kriek, M., Franx, M., et al. 2013, ApJ, 771, 85

van den Bosch, R. C. E., Gebhardt, K., Gültekin, K., et al. 2012, , 491, 729

van der Wel, A., Franx, M., van Dokkum, P. G., et al. 2005, ApJ, 631, 145

van der Wel, A., Holden, B. P., Zirm, A. W., et al. 2008, ApJ, 688, 48

van der Wel, A., Noeske, K., Bezanson, R., et al. 2016, ApJS, 223, 29

van Dokkum, P., Conroy, C., Villaume, A., Brodie, J., & Romanowsky, A. J. 2017, ApJ, 841, 68

van Dokkum, P. G. 2001, , 113, 1420

van Dokkum, P. G. & Conroy, C. 2010, , 468, 940

van Dokkum, P. G., Franx, M., Kriek, M., et al. 2008, ApJL, 677, L5

Vaughan, S. P., Davies, R. L., Zieleniewski, S., & Houghton, R. C. W. 2018, MNRAS, 479, 2443

Vazdekis, A., Casuso, E., Peletier, R. F., & Beckman, J. E. 1996, ApJS, 106, 307

Vazdekis, A., Coelho, P., Cassisi, S., et al. 2015, MNRAS, 449, 1177

Vazdekis, A., Koleva, M., Ricciardelli, E., Röck, B., & Falcón-Barroso, J. 2016, MNRAS, 463, 3409

Vazdekis, A., Peletier, R. F., Beckman, J. E., & Casuso, E. 1997, ApJS, 111, 203

Vazdekis, A., Trujillo, I., & Yamada, Y. 2004, ApJL, 601, L33

Vernet, J., Dekker, H., D'Odorico, S., et al. 2011, A&A, 536, A105

Vidal-García, A., Charlot, S., Bruzual, G., & Hubeny, I. 2017, MNRAS, 470, 3532

Wang, L., Yang, X., Shen, S., et al. 2014, MNRAS, 439, 611

Weinberger, R., Springel, V., Hernquist, L., et al. 2017, MNRAS, 465, 3291

Welch, G. A., Sage, L. J., & Young, L. M. 2010, ApJ, 725, 100

Wellons, S., Torrey, P., Ma, C.-P., et al. 2016, MNRAS, 456, 1030

Werle, A., Cid Fernandes, R., Vale Asari, N., et al. 2020, MNRAS, 497, 3251

White, S. D. M. & Frenk, C. S. 1991, ApJ, 379, 52

Wiersma, R. P. C., Schaye, J., & Smith, B. D. 2009a, MNRAS, 393, 99

Wiersma, R. P. C., Schaye, J., Theuns, T., Dalla Vecchia, C., & Tornatore, L. 2009b, MNRAS, 399, 574

Worthey, G., Faber, S. M., Gonzalez, J. J., & Burstein, D. 1994, ApJS, 94, 687

Worthey, G. & Ottaviani, D. L. 1997, ApJS, 111, 377

Wu, P.-F., van der Wel, A., Gallazzi, A., et al. 2018, ApJ, 855, 85

Yi, S., Demarque, P., & Oemler, Augustus, J. 1997, ApJ, 486, 201

Yi, S. K., Kaviraj, S., Schawinski, K., & Khochfar, S. 2007, in Astronomical Society of the Pacific Conference Series, Vol. 374, From Stars to Galaxies: Building the Pieces to Build Up the Universe, ed. A. Vallenari, R. Tantalo, L. Portinari, & A. Moretti, 463

Yi, S. K., Yoon, S. J., Kaviraj, S., et al. 2005, ApJL, 619, L111

Yıldırım, A., van den Bosch, R. C. E., van de Ven, G., et al. 2017, MNRAS, 468, 4216

Young, L. M., Scott, N., Serra, P., et al. 2014, MNRAS, 444, 3408

Zahid, H. J., Geller, M. J., Fabricant, D. G., & Hwang, H. S. 2016, ApJ, 832, 203

Zhu, G., Blanton, M. R., & Moustakas, J. 2010, ApJ, 722, 491

Zibetti, S., Gallazzi, A. R., Hirschmann, M., et al. 2020, MNRAS, 491, 3562